
TÜRKİYE CUMHURİYETİ'NİN YÜZÜNCÜ YILI
Various Applications of Physics: Past, Present and Future
Editor
Özgül KARATAŞ
BİDGE

BIDGE Publications

Various Applications of Physics: Past, Present and Future

Editor: Dr. Öğr. Üyesi Özgül KARATAŞ

ISBN: 978-625-372-422-1

Page Layout: Gözde YÜCEL

1st Edition:

Publication Date: 25.12.2024

BIDGE Publications,

Certificate No: 71374

www.bidgeyayinlari.com.tr - bidgeyayinlari@gmail.com

Krc Bilişim Ticaret ve Organizasyon Ltd. Şti.

Güzeltepe Mahallesi Abidin Daver Sokak Sefer Apartmanı No: 7/9 Çankaya / Ankara

Content

CHAPTER I

Newton's Laws of Motion: Basic Principles and Universal Truth

Cem Cüneyt ERSANLI [1]
Ercümend ERSANLI[2]

Introduction

Isaac Newton is considered one of the important scientists who made revolutionary studies in the field of physics in the 17th century and pioneered the foundations of science with the laws of motion. These rules, known today as Newton's laws of motion, were obtained as a result of very careful and long observations examining motion and its changes. Newton is especially known for the three laws of motion he put forward to understand the nature of motion, and Newton's laws of motion are among the most fundamental

[1] Prof. Dr., Sinop University, Faculty of Arts and Sciences, Department of Physics, Sinop/Turkey, Orcid: 0000-0002-8113-5091, ccersanli@sinop.edu.tr, ccersanli@gmail.com
[2] Prof. Dr., Ondokuz Mayıs University, Faculty of Health Sciences, Department of Social Work, Samsun/Turkey, Orcid: 0000-0003-4840-3629, eersanli@omu.edu.tr, eersanli@gmail.com

concepts of physics. These laws are universal truths that reveal how objects move and how they are affected by forces. Although Newton's laws of motion are limited, they are widely used not only in physics but also in many fields of science, from engineering to astronomy, from biology to chemistry, due to their simplicity and breadth of validity. These basic rules of motion help us understand the phenomena that are frequently seen in our daily lives. Newton's laws of motion have been used in the examination of the motion of many systems we encounter in our daily lives, from celestial bodies to fluids and springs, from cannonballs to electric charges. While these laws help us understand the basic principles of the physical world, they also have indirect effects on psychological processes and human relationships. The work Philosophiae Naturalis Principia Mathematica, published by the English scientist Isaac Newton in 1687, contains these laws (Newton, 1687).

Newton's First Laws of Motion

Newton's laws of motion consist of three basic laws:

Newton's First Law of Motion: Principle of Inertia

Sir Isaac Newton (1642-1727) put forward the principle of inertia by making use of the ideas and results put forward by Galileo. Newton's first law of motion is also known as the **principle of inertia**. It states that the state of rest of an object is a special case of an object moving at a constant speed.

"*An object, unless acted upon by a net force, continues to move in a straight line at its current speed if it is at rest, and continues to move in a straight line at its current speed if it is in motion. In short, it continues to move at a constant speed.*"

The mathematical expression of Newton's first law of motion is; $\mathbf{v}$ = constant, $\sum \mathbf{F} = 0$ and $d\mathbf{v}/dt = 0$. Here $\mathbf{v}$ represents speed, $\mathbf{F}$ represents force, and t represents time.

This law states that an external force is required for the moving parts of an object to change. Inertia is a natural feature of the object, and this feature means that the object maintains its state of motion. In other words, if there is a change in the state of motion of objects, the objects have the ability to resist this change. An object at rest does not move unless an external force is applied; Similarly, an object in motion continues to move at a constant speed unless it is forced to stop or accelerated by a force (URL 1, 2024). In other words, inertia is the ability of an object to preserve its current motion records. We encounter this law very often in our daily lives. For example, when a car is moving and the driver brakes suddenly, the passengers in the car are thrown forward. We have all encountered in our daily lives that if a stopped car moves forward suddenly, the passengers in the car are forced to move backwards. This is a result of inertia. Similarly, an object that is stopped does not move unless a force is applied to it. Therefore, if a ball is at rest before being thrown, a force is required to start it in motion. Inertia can be observed not only in the physical world but also in human behavior. When people act in a certain routine for a long time, they have difficulty breaking out of this routine. This also appears as behavioral inertia. It also has a significant effect on human psychology. People may have difficulty changing existing situations and this situation is called psychological inertia. For example, when an individual is asked to change an existing skill or routine the individual may encounter difficulties arising from this change. In

this process, the person needs to improve himself. The change in the current situation usually creates a feeling of discomfort. This leads the individual to resist the change process. Psychological inertia is related to the resistance they show against the changes that will be encountered in the lives they will live. Since people maintain their stability, they may have difficulty transitioning to a new situation. For example, an individual who wants to switch to a healthy lifestyle may have difficulty giving up old habits. Even if the individual has motivations to change his current situation, the feeling of inertia may prevent this motivation. The principle of inertia can also be observed at the societal level. In the transition to a new system at work, it is possible for people to remain attached to the current system. In such a case, it may be difficult for the individual to adapt to the change. Therefore, effective communication and training are important during the change process. In this case, informing employees about the new system process can help overcome inertia. This law of Newton provides an important metaphor for understanding social behavior and the dynamics of change.

Another important dimension of the first law is related to the condition of the moving parts. If a moving bus brakes suddenly, the passengers continue their own movements despite the condition of the bus. In such a case, there are seat belts on the buses that passengers must wear for safe transportation. These belts prevent passengers from being thrown forward during sudden stops and minimize possible negative situations. This is one of the simple but beautiful examples we come across in our daily lives.

Newton's Second Law of Motion: The Relationship Between Force and Acceleration (Fundamental Principle of Dynamics)

"*A system or an object under the influence of an unbalanced constant force (i.e. net force) makes a constant acceleration movement. Mathematically, this is basically explained by* $\boldsymbol{F_{net}}$ *=* $mx\boldsymbol{a}$ *(net force = mass x acceleration).*"

Newton's second law of motion, the **fundamental principle of dynamics**, states that the acceleration of an object is directly proportional to the resultant force (or net force, $\sum\mathbf{F}$) applied to that object and inversely proportional to its mass. This law is expressed with the formula $\mathbf{F_{net}} = mx\mathbf{a}$; where $\mathbf{F_{net}}$ represents the force, m represents the mass, and **a** represents the acceleration. The resistance of the object opposes slowing down when in motion and moving when at rest. For this reason, the mass mentioned in Newton's second law of motion is often called the inertial mass. Let's consider a simple example of how this law is applied in daily life. Imagine that you have a soccer ball in your hand. When you apply force to this ball, it moves forward at the highest speed. However, when you apply force to a larger and heavier basketball with the same force, it accelerates more slowly than the football. This is because a larger mass (basketball) accelerates less with the same force. Similarly, when we try to accelerate a bicycle and a motorcycle by pushing them with the same force, the bicycle accelerates faster than the motorcycle. This is because the bicycle has less mass than the motorcycle. This clearly shows the proportionality between mass and acceleration.

Newton's second law of motion measures the force under different compressions and tensions by regulating the mass.

Newton's first law of motion defines all other forces. Once these forces are known, the second law gives the equations of motion of an object with a known mass. Neither the first nor the second Newton's law can determine which of two separate observers in different reference frames is moving and which is at rest.

Another interesting application of Newton's second law is space exploration. For example, during the launch of a spacecraft, the rocket engines produce a large amount of force. This force releases the spacecraft from the effects of gravity and launches it into space. If the rocket is heavier, more force will be required to get off the ground. In this case, this is an important issue that space engineers should pay attention to when launching a spacecraft.

The thing to pay attention to in the equation $\mathbf{F}_{net}$=mx**a** is the net force, or $\mathbf{F}_{net}$, which is a vector quantity. Vectors have both magnitude and direction. In other words, if we want to accelerate in a certain direction, then the magnitude of the force we apply and the direction of this force will make a difference. In other words, efficiency is not only related to how much work you do (magnitude), but also to where the work is applied (direction). This applies to all the big and small decisions we make as individuals. As you can see, it is not enough for humans to get rid of inertia just to do something. We also need a direction, a direction, to accelerate.

Internal attraction is a powerful factor that guides and motivates people. People tend to different goals depending on various internal and external factors and exhibit various characteristics in an effort to achieve these goals. In this context, maintaining motivation is proportional to the energy and effort they

spend to achieve it. This process can help us better understand the motivation and behavioral dynamics of people with Newton's physical laws. The formula $\mathbf{F_{net}}$=mx**a** (net force = mass × acceleration) plays an important role by basing it on the dynamics of motivation and power. Here, "force" may represent the things individuals want, "mass" may represent the current existence of individuals, and "acceleration" may represent the individual's effort to achieve this goal. Motivation is defined as the effort spent to achieve a goal. This effort can be directly achieved with the belief and motivation of the individual. For example, if a student wants to be successful in an exam, the effort he/she will spend to achieve this goal depends on his/her motivation. The effort applied to achieve this goal shows that the force is working in a way. This is possible with the basic principle of dynamics. The stability of motivation determines the magnitude of the force required to achieve. An individual with high motivation increases his/her momentum by spending more energy and effort to achieve. However, the individual's current situation and capacity (mass) are another factor in this process. If the individual's current situation is positive and the goal is clearly determined, the level of motivation increases and the individual gains momentum faster. Otherwise, motivation decreases and energy decreases. Intrinsic motivation is a force that is directed by a sense of inner satisfaction and curiosity. This type of motivation contributes to the individual's discovery of his/her potential and personal development. The presence of intrinsic motivation enables the individual to be more determined and determined to stand tall. For example, while an artist feeds his/her intrinsic motivation with the desire to perform his/her art, this motivation is strengthened with

the student's desire to learn. This allows him/her to gain more momentum thanks to this internal attraction. Extrinsic motivation can be provided through external rewards. For example, an employee may spend more effort for external rewards such as a promotion or salary increase. However, external motivation is usually not as sustainable as intrinsic motivation. Long-term, persistent intrinsic motivations create a stronger, lasting impact, while extrinsic motivations provide a temporary source of energy.

Newton's Third Law of Motion: Action-Reaction Principle

Newton's third law of motion describes the mutual interactions of objects. Newton's third law of motion is known as the **action-reaction principle** and is expressed as follows:

"*If two objects interact, the force* $\boldsymbol{F_{12}}$ *exerted by object 1 on object 2 is equal to, in the same direction and opposite to the force* $\boldsymbol{F_{21}}$ *exerted by object 2 on object 1.*"

This expression is mathematically expressed as;

$$\boldsymbol{F_{12} = -F_{21}}$$

According to this law, when a force is applied to an object, the other object applies a force of the same magnitude but in the opposite direction. The force applied by object 1 on object 2 is called the "action" force, and the force applied by object 2 on object 1 is called the "reaction" force. This is basically an event that we can observe frequently in our lives. For example, the propellant gases coming out of the engines at the bottom of rockets exert a force towards the ground, and the opposite reaction of this force causes the rocket to move upward. Again, while the Earth exerts a force on the Moon, causing it to rotate around it, the Moon also exerts a gravitational

force on the Earth. In fact, ocean tides are a result of the gravitational force that the Moon exerts on the Earth. The Earth and the Moon exert a gravitational force on each other. This law explains why an ice skater moves backwards when he pushes another skater forward. Again, according to this law, the force that an apple exerts on the Earth is the same magnitude but in the opposite direction as the force that the Earth exerts on the apple. Force does not act directly on an object, but rather acts between two objects or between the object and its surroundings. When forces are active between objects, the objects interact with each other. This effect does not depend on the inertial reference system of the observer. When hammering a nail into a surface, the force exerted by the hammer on the nail is equal to the reaction force exerted by the nail on the hammer.

This law is not limited to physical events; it also manifests itself in social interactions. The applicability of this law is important for human dynamics to continue. Our level of productivity, like Newton's third law of motion, is generally the balance of forces that increase and inhibit productivity in our lives (Johnson & Miller, 2018). The action-reaction principle also manifests itself in social relations and human behavior (Jones & White, 2013). Communication and interactions between people are similar to this principle. For example, when you help someone, we usually receive a thank you or a positive reaction in return (Brown, 2018). Similarly, a negative reaction usually occurs in a negative behavior. Such social dynamics show how Newton's third law of motion can be associated with the human dimension.

In daily life, this action-reaction situation will also affect people's interactions with their social environment. For example,

when a certain behavior becomes the norm in a group, group members adopt an attitude towards adopting this behavior. This helps us understand how social norms and social rules are formed. People exhibit similar behaviors in order to conform to the expectations of their social environment, and this determines the basic dynamics of interactions.

Social media and digital interactions are also a modern fusion of the action-reaction principle. Sharing and liking over the internet accelerates the interactions shown to each other. When a person shares positive content on a social media platform, the positive reactions to this sharing can increase the individual's desire to share more similar content. At the same time, negative reactions can occur and the sharing can be withdrawn. This situation shows how social media plays a role in interpersonal interactions and how group dynamics are affected.

The Historical Importance of Newton's Laws of Motion and Their Place in Daily Life

Newton announced these three basic laws of motion in his work Philosophiae Naturalis Principia Mathematica (Mathematical Principles of Natural Philosophy) published in 1687 (Newton, 1687). This work is considered a turning point in the history of science. Because Newton managed to create an integrated model by combining many theories known until then about motion and force. Newton's laws of motion provide basic principles for many events we observe in our daily lives. The motion, force and acceleration relationships in our daily lives show how universal and applicable these laws are. These laws are not only valid for elements on Earth, but also for all components in the universe. Newton's laws of motion

allow us to better communicate with the physical world. Athletes' training programs are usually planned based on Newton's laws of motion. Strength is an important exercise that athletes apply to increase muscle strength. Activities such as weightlifting are a perfect example to demonstrate Newton's laws. This type of training allows the muscles to strengthen and also to train. Muscles develop with the applied forces; therefore, athletes try to achieve the best results by organizing their training according to these principles.

Although these laws were developed within the framework of theoretical physics, we all use these methods and live according to these principles without realizing it. These laws provide an understanding of how an object needs to apply force to continue its motion, change its direction or direction. Countless examples such as traveling in our car, throwing a ball, riding a bicycle or lifting an object reveal the reflection of Newton's laws of motion in daily life. This perspective of Newton provided a very broad perspective to people who spread the physical world and accepted the existence of universal life in motion. These laws play a vital role in many fields from engineering to architecture, from the automotive sector to sports sciences. In addition, Newton's laws of motion are not limited to the physical world; these laws also provide a valuable metaphor for human growth and social relations.

Inertia in Daily Life

Newton's laws also manifest themselves in activities at home. For example, when a broom is running, the brushes of the broom interact with the ground. The force applied to the ground during the movement of the broom ensures that dust and dirt are swept away. If we move the broom fast and smoothly enough, we can collect more

dirt. Inertia also comes into play in this process; because in order for the broom to move, it needs to be pushed. The fan continuing to run for a while after a power outage, the function of an airbag (when a vehicle equipped with an airbag is involved in an accident, the sudden deceleration in its speed causes the electric switch to operate, which initiates a chemical reaction that produces a gaseous substance that fills the airbag and protects the driver's head) can be given as examples of the principle of inertia in our daily lives (URL 1, 2024).

Inertia exists as a metaphor not only for physical objects but also for human life and psychological processes. People often maintain their current state, and this can occur as psychological inertia. Such inertia is accompanied by variations, resistance, or fear of change.

Habits help people organize their lives in a certain way. In this order, the repetition of continuity that will continue automatically occurs and these behaviors become a part of the person's identity. However, when these competencies are tried to be changed, individuals may encounter a state of inertia. When people enter a certain behavioral model, they show a strong tendency towards this continuity. For example, someone who exercises regularly does not have difficulty maintaining this habit, while someone who does not exercise at all may have difficulty gaining this habit. An external force (motivation, encouragement or pressure) is required for the individual to be in the current situation and to be regulated with this system. In this case, the process of changing habits, motivation and support systems are of great importance. The support that people receive from their environment causes them to manage the change

processes more easily. Family, friends or professional support play a critical role in the growth of new capacities. A supportive environment can increase their motivation and help overcome inertia. For example, this professional support that an individual will receive from an expert to achieve healthy nutrition can help them maintain their individual motivation and gain healthy competencies. Another important factor for changing habits is goal setting. In order to achieve success, goal setting allows them to adapt better to the change processes. Goals can help them overcome inertia by increasing their motivation. For example, if a person sets a goal of doing sports three days a week, this goal can increase their ability to take action. The goal setting process, ensuring that the goal is clear and realized, is important in terms of maintaining their motivation.

Procrastination is a common example of human inertia. Many people find it difficult to act when they do not have external pressure or motivation to start a task. Just as an existing object needs a force to move, people need an internal or external force to take action. This force can be a deadline for a given task, a goal, or a reward. People often resist change because it disrupts the status quo. Psychological inertia causes them to maintain their status quo. Inertia is often related to comfort zones. People want to stay in the situation they are used to because it gives them confidence. Change disrupts, and this can make people uncomfortable. For this reason, many people prefer to stay where they are rather than change their current situation. However, like physical inertia, this psychological inertia can be overcome. People can act and make changes because of external motivations, goals, or new experiences. There are many parallels between inertia at the international level and inertia in humans. In

both cases, a system or person appears to be in a state of being and needs an external force to change this state. However, while in physical inertia these external forces are usually clear, in psychological inertia these forces can be more abstract. Motivation, goals, education, social pressure or internal drives can be ways of overcoming psychological inertia. The important thing is that in both the physical and psychological worlds, these forces need to be present in order for a system or individual to show change.

The Basic Principle of Dynamics in Daily Life

The basic principle of dynamics is seen in many physical events frequently encountered in daily life. The acceleration or deceleration of a car can be given as an example of the basic principle of dynamics. A car accelerates forward with a force generated by its engine. The larger the parts of the car, the more force is required to achieve the same acceleration. Similarly, in braking movements, the braking system applies a force opposite to the direction of motion of the car and the car slows down. When trying to push a heavy table, no matter how hard we push, we cannot notice that the table is moving faster. However, when we use the same force on a light chair, we see that the chair accelerates faster. Here, the difference between the masses of the table and the chair causes the same force to produce different results. With the same force, a light weight moves more easily than a heavy weight. Because a light weight has less mass and accelerates faster. If one of two people walking is heavier than the other, the one with the heavier weight walks slower. Because the acceleration of the one with the lighter weight is greater. This is where Newton’s second law of motion

comes into play; that is, we can say that there is a direct relationship between the applied force and the acceleration.

When we apply the basic principle of dynamics to human life and social changes by abstracting it from the physical world, we see that this information gains a broad metaphorical meaning. People and societies show changes under external influences. People usually react to changes in their lives with an external force. These forces can be various factors such as motivation, external pressure, opportunities or crises. A kind of "force" is required for people to change. The greater the external influence on a person, the faster and more pronounced the change that person experiences due to this influence can be. For example, if there is a great motivation (force) to achieve a goal, this situation quickly affects the person's movements and increases their actions towards it. Societies have a dynamic structure and change with external forces. Social movements, revolutions or social reforms can be examined in this way. The magnitude of the force applied for a social change determines the rates and depth of change. For example, major social changes such as war, economic crises etc. can lead to rapid changes. A great force is formed on society. As a result, this force leads to the rapid progress of social structures.

When a person or group makes a decision, the forces that affect the collection of this decision also play a role in the process. When a leader or manager wants the organization to be directed in a certain direction, they must provide the necessary motivation and support for the implementation of their decisions. If the individuals in the organization show great resistance (mass), that is, if the force applied by the leader (determination, motivation) is not sufficient, the

decision cannot be implemented or the process may be delayed. However, if the force is great enough, the organization quickly adapts to these new behaviors. The basic principle of dynamics is the net force, mass and acceleration in the formula $\mathbf{F_{net}} = mx\mathbf{a}$, and in the same way, external influences determine the reactions of people and societies in human behavior and social dynamics. People and societies maintain their current situations. A force is required for a change to occur. The greater the mass of individuals or societies, that is, their resistance, to change, the greater the force required for this change to occur. This resistance usually appears as the beliefs or social norms that people live by. As in the basic principle of dynamics, a greater force is required against a greater mass (resistance). As a result, the elements or societies of this force move with greater acceleration.

The Action-Reaction Principle in Daily Life

Isaac Newton, one of the important scientists of the 17th century, helped formulate the fundamental laws that help us understand the entire universe. Newton's laws of motion constitute one of the foundations of classical physics and today play a major role in physics. The third of these laws, the "action-reaction principle", is not limited to physical events, but can also be used as a metaphor in very different areas such as human relations, society and psychology. When we step on the ground while walking, our feet apply a force to the ground. This force is a pushing force towards the ground. However, due to the existence of action-reaction, it applies a force of the same magnitude but in the opposite direction, in the same direction on the ground. This force provides forward movement. When we push the water back with our hands while

swimming in water, the water applies a forward force to us and this force supports us and enables us to move. Helicopters create a lifting force by pushing the air downwards. Thus, the air is exposed to an upward reaction force. In all sports competitions, the dominant force is in one direction, and the reaction force is in the opposite direction (URL 1, 2024). When we sit on a chair, we apply a force to the chair with our weight. The chair, in turn, applies a force of the same magnitude but in the opposite direction. Again, when a washing machine rotates, it uses the power of transformation to throw the water out of the laundry. In this process, we see that Newton's third law of motion comes into play in the examples mentioned above, such as the movement of the laundry and the throwing of water out, that is, it is a result of the action-reaction principle.

Newton's action-reaction principle does not only apply to physical events. People usually produce a reaction in response to a reaction and can often contribute to this effect directly or indirectly. Interactions between people can be explained with action-reaction principles. For example, when we encounter a positive attitude from a person, we usually give positive feedback. However, when we are approached with a negative attitude, we are likely to encounter a similarly negative reaction. This can be seen as a manifestation of the action-reaction principle. Change in a society usually triggers a reaction specific to it. For example, a group of people demanding independence on a social issue may cause another group to form in the opposite direction. Here, we can observe the continuation of the action-reaction relationship in social dynamics. The reactions they give to the events they experience are usually shaped by the experiences they have experienced. An individual who encounters a

stressful event may react to this event with stress. However, when they have a positive experience, this individual's mood is usually good. All these conditions reveal the course of action-reaction development in people's emotional relationships.

Family dynamics are also an important part of social interactions. Interactions between family members affect emotional and psychological development. The love, support and understanding that reside within the family help individuals feel secure. For example, when a family member supports another family member, this support strengthens family ties and increases their commitment to each other. This also contributes to the learning of social norms and the improvement of values.

The increase in social energy has positive effects on the individual's permanent health. Thanks to healthy social relationships, the individual's stress decreases and they feel happier. People receive emotional support through social interactions and this support helps them cope with difficult times. The increase in the strength of social ties allows the life they will live to expand and social solidarity to be strengthened. However, positive results are not always obtained in social interactions. Sometimes, disruptions and negative reactions can also occur between individuals. For example, if an individual's failure to help another is misunderstood, unexpected negative reactions can be encountered. Such conditions can cause damage to social components and the formation of a sense of insecurity between individuals. Therefore, effective and clear communication in social interactions is of critical importance in terms of achieving positive results.

The realization of social interaction is also shaped by the characteristics and past experiences of the person. While some people are more social and open, others may be more introverted and shy. In this case, it negatively affects the effects of social interactions. Being sensitive to freedoms in social environments, expanding empathy and ensuring effective communication help to develop social opportunities. In this way, the effort to develop social developments ensures the establishment of healthy social interactions.

Another striking aspect of the action-reaction principle is that human beings use their reactions in some situations in a hidden way. Especially when making decisions, people take time-dependent steps by considering how an action they take will cause a reaction. Balance is also needed in human and social issues. The actions taken between people and the reactions given to these actions determine the balance between individuals and groups. Failure to achieve this balance can lead to divisions, misunderstandings and ruptures in relationships.

The Role of Newton's Laws in the Modern World

Technology and Engineering

Newton's laws of motion are the basic principles offered by modern technology. These rules allow engineers and designers to develop various systems and structures safely, effectively and efficiently. From transportation vehicles to civil engineering, these principles enable engineering applications in many areas and lead to innovations that make human life easier. Engineers can develop faster and more efficient vehicles by using these laws. Aerodynamic design is another important area where Newton's laws are valid.

Aerodynamic forms are designed to minimize air resistance, especially in air and water vehicles. Civil engineering also makes great use of Newton's laws. In the design of buildings and other structural systems, how forces are distributed is of critical importance. For example, in the design of a bridge, the loads that the bridge must carry and how these loads will affect the structures are determined. These programs are essential for safe construction. Also, the design of the machines and equipment used in the construction process is equally important. Cranes use Newton's laws to program the power required to carry and move loads. These laws help engineers design cranes that can operate safely and effectively. In the field of technology, for example, an electrical energy production study is based on the interaction of electric current with a magnetic field and the creation of physical forces by this interaction. These laws are also used in automotive engineering. In addition, sports technology provides innovations to increase performance using these laws. For example, sports equipment is designed based on aerodynamic and physical principles to optimize the movements of athletes. In the design of a bicycle or running shoe, studies are carried out to reduce air resistance and minimize growth using Newton's laws. This allows athletes to perform faster and more effectively.

Education and Training

In the field of education, teaching Newton's laws of motion to students helps students better understand the physical world. Learning this information not only helps physical events emerge; it also contributes to the development of analytical thinking skills. This process allows them to question and observe the world around them.

For example, Newton's first law of inertia helps to understand the differences between moving and stationary objects. Teaching this principle allows children to better model the situations they encounter in their daily lives.

Newton's second law, the differences between force, mass and acceleration emerge. This law helps them analyze physical events digitally. It helps them develop their skills in the subjects of how the force applied to an object will continue to accelerate the object.

Newton's third law, the action-reaction principle, helps us understand the balance in social interactions. The behaviors people show to each other receive similar reactions from the other party. In this case, it contributes to the understanding of the dynamics in social relationships. By presenting such examples in educational programs, it allows for a better understanding of the relationship between social sciences and physics.

In education, it is important to spread a permanent understanding of how Newton's laws can be applied in daily life. In this way, learning is made more effective. Another important issue in education is the reflections of Newton's laws in social sciences. Thanks to these reflections, students' interest in social sciences increases and allows students to build bridges between different disciplines.

Conclusion

Newton's three fundamental laws of motion represent the most fundamental laws of the universe and have universal validity. Because these laws exist not only in the universal world but also in

daily life. Thanks to these laws, we can understand how objects move, why they accelerate, slow down or change direction.

The first law, inertia, can be observed both in the physical world and in human behavior. Whether objects and people remain stationary or maintain their current state of motion shows how widespread and continuous this information is. In our daily lives, we constantly experience these developments while driving a car or pushing an object. Newton's first law, inertia, has an important place in psychology. It is a critical step to help people have healthier abilities.

The second law helps us understand the relationship between force and acceleration. The power required for an object to move is directly related to its data. This law can be applied in many areas in daily life; it is valid in a wide range from sports activities to engineering designs. In addition, the comprehensiveness of Newton's second law provides a better understanding of both physical and social dynamics. The third law, action-reaction, states that there is a reaction in response to movement. This principle can be applied not only in the physical world but also in social and psychological processes (Williams, 2020). The behaviors people display are shaped by mutual reactions, and this determines the dynamics of human relations. The formation of social norms in daily life, personal information and social changes reveal the details of this principle. For this reason, the prevalence of the action-reaction principle can help better understand and use communications with social environments in a healthier way. Therefore, this principle is one of the cornerstones of social life and helps us understand the depth of human relations.

Newton’s laws of motion play a critical role in modern engineering and technology. These laws help engineers and designers improve various systems safely, effectively and efficiently. In many areas, from transportation vehicles to civil engineering, these principles lead to the emergence of innovations that make human life easier.

It is seen that Newton’s laws of motion are not just theories, but rather fundamental truths that shape our lives. Every day, we act, interact and make decisions under the guidance of these laws. From our relationships with the world to our individual lives, these laws allow us to understand our movements and changes. As a result, Newton’s laws of motion guide us at every moment of our lives. These universal rules provide a powerful guide in understanding the nature and communication of people. These laws are present in our daily lives and allow us to look at both the world and our own movements with a deeper understanding.

As a result; knowing these physical laws allows us to both develop our practical skills and contribute to improving our quality of life. Therefore, Newton’s ideas are important principles that are valid in every area of our lives, beyond just physical rules.

References

Brown, T. (2018). Digital interactions and their impact on social dynamics. Journal of Digital Sociology, 45(2), 123-137.

Johnson, K. & Miller, R. (2018). Physics in Daily Life: Applications of Newton's Laws. Oxford University Press.

Jones, P. & White, A. (2013). Group norms and human behavior: A sociological perspective. London: Social Science Publications.

Newton, I. (1687). Philosophiae naturalis principia mathematica. University of Cambridge Digital Library. https://cudl.lib.cam.ac.uk/view/PR-ADV-B-00039-00001/1.

URL 1 (2024). (Retrieved on 03/08/2024 from https://praxilabs.com /en/blog/2021/02/24/applications-of-newtons-laws-of-motion-in-daily-life/#Overview_of_Newtons_Laws_of_ Motion).

Williams, R. (2020). Social norms and change: Physics as a metaphor for human interaction. Journal of Sociology, 32(4), 209-225.

CHAPTER II

Uses and Applications of X-rays in Industry

Hilal Nur YOĞURTÇU[1]
Cem Cüneyt ERSANLI[2]

Introduction

X-rays are the basis of modern imaging techniques and ushered in a new era in medical science. Discovered in 1895 by the German physicist Wilhelm Conrad Röntgen, these rays are produced by the slowing down of high-energy electrons or electron transitions in the inner orbits of atoms. With wavelengths ranging from 0.1-100 Å, these electromagnetic waves have a wide range of industrial applications. X-rays are in the high-energy part of the electromagnetic spectrum and carry much higher energy than visible

[1] Sinop University, Graduate School of Education, Department of Physics, Sinop/Turkey, Orcid: 0009-0009-9762-5595, hilal.gundd@gmail.com
[2] Prof. Dr., Sinop University, Faculty of Arts and Sciences, Department of Physics, Sinop/Turkey, Orcid: 0000-0002-8113-5091, ccersanli@sinop.edu.tr, ccersanli@gmail.com
This study was produced under the supervision of the second author from the first author's master seminar.

light or radio waves. This high energy can be used to analyze the motion of subatomic particles or irregular structures. X-rays are often used to study the internal structure of objects, medical diagnostics, industrial applications and archaeological excavations. Located between radio waves and gamma rays in the electromagnetic spectrum, X-rays cannot be seen by the human eye and are categorized as invisible rays. However, thanks to their ability to penetrate into matter, they can visualize internal structures. Thanks to their high energy, X-rays can interact with matter to produce ionizing radiation. These properties should be used with caution as they can have harmful effects, especially on biological tissues. While X-rays are capable of penetrating many solids, they can be absorbed by dense and thick materials.

1. Importance of X-rays in Industry

X-rays have many important industrial uses. In this wide range, it stands out as a reliable and effective tool in critical processes such as materials testing, quality control and product safety.

Materials Testing and Quality Control: X-rays are used to detect defects in materials. It is possible to detect cracks, holes and similar defects in metal and composite materials. It is especially used to evaluate the quality of welded points. In addition, examining the internal structure of parts plays an important role in precision manufacturing processes.

Casting and Metallurgy: While X-rays are used to identify defects in casting processes, they are also very effective for alloy analysis. Thanks to these analyzes, the proportions and compositions

of the elements in the internal structure of materials can be clearly seen.

Food Industry: The presence of foreign bodies in food products can be detected with X-rays. Also, defects in packaging materials can be checked with this method.

Textile Industry: X-rays are used to identify weaving defects and quality problems in fabrics.

Electronics Industry: Solder joints in electronic components are examined with X-rays for quality control. In addition, production defects in the internal structure of integrated circuits can also be detected by this method.

Transportation Industry: X-rays are used to assess the quality of welding points on automobile and aircraft parts. It is also used to detect wear and defects in engine parts.

Industry and Building Materials: Internal cracks and defects in concrete structures can be revealed with X-rays. Also, fatigue-related damage to metal structures can be analyzed with this method.

2. Comparison of X-rays with Other Industrial Technologies

Each technology comes with its own advantages and limitations. Compared to other methods, X-rays generally have the advantage of penetrating deep into materials and examining the internal structure in detail. However, the most appropriate technology should be chosen depending on the area to be used and the specific needs.

Ultrasonic Inspection: This method uses the reflection of sound waves within the material to detect defects.

Comparison: X-rays can penetrate deeper than ultrasonic inspection and can be used on thick materials. However, ultrasonic inspection can be more sensitive in detecting small defects on the surface.

Magnetic Particle Inspection: Surface defects are detected with the help of a magnetic field and magnetic particles.

Comparison: X-rays can penetrate deep into the material, while magnetic particle inspection can only detect defects on the surface. Magnetic particle inspection can be more cost-effective, but is limited in depth.

Gamma Irradiation: Gamma rays are used to kill microorganisms in materials or sterilize products.

Comparison: Gamma rays are often used in sterilization and disinfection processes, while X-rays are preferred for examining the internal structure of materials and for quality control.

3. Industrial X-ray Imaging

Industrial X-ray equipment works through a complex process and it is necessary to study the basic steps to understand the functioning of these devices:

X-ray Tube: At the center of these devices is an X-ray tube. The tube contains a cathode (negative electrode) and an anode (positive electrode). High-energy electrons are emitted from the cathode.

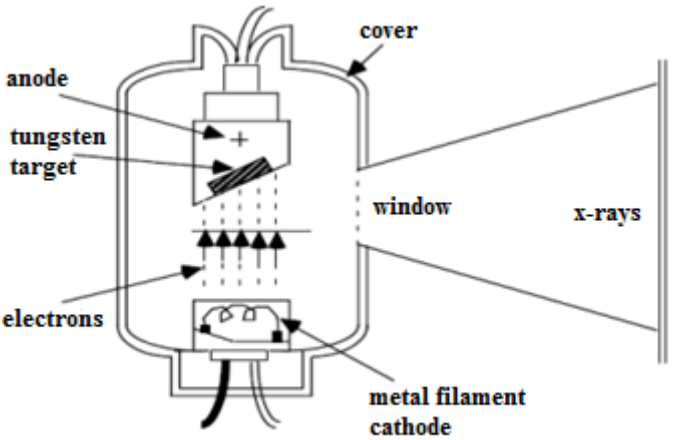

Figure 1: X-ray Tube

Acceleration of Electrons: High voltage accelerates the electrons leaving the cathode. These electrons quickly hit the anode and lose energy.

Generation of X-rays: When electrons hit the anode, they lose their energy and this process results in the production of X-rays. The anode is usually made of a metal with a high atomic number, such as tungsten, because such metals produce more X-rays (URL 1).

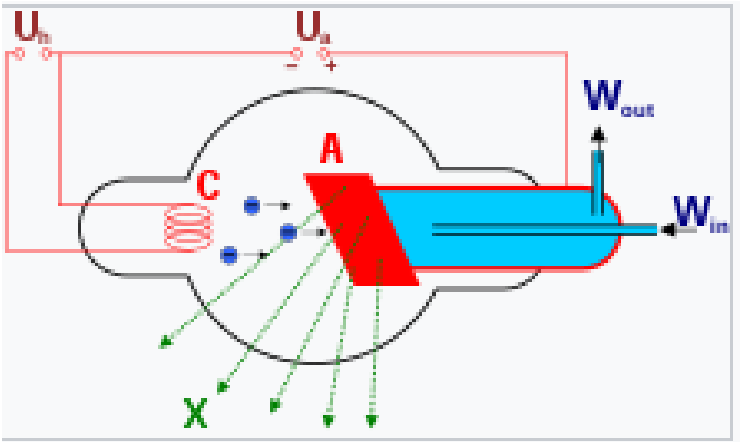

Figure 2: Working Principle of the X-ray Tube

Emission of X-rays: The resulting X-rays are emitted out of the tube and directed at the object to be examined.

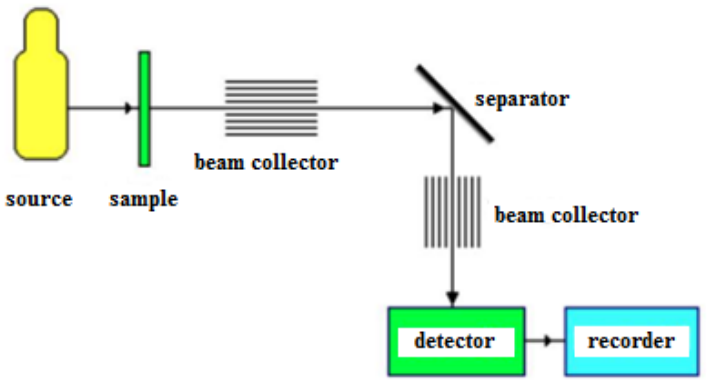

Figure 3: X-ray Absorption Spectrometer

Passage and Absorption: As X-rays pass through objects, some are absorbed by the material and the rest pass through. Denser and thicker materials absorb more X-rays, enabling the detection of density differences in the internal structure of the material.

Detection and Imaging: X-rays passing through the object reach a sensor. This sensor measures the intensity of the X-rays and the data is processed by computers to create an image of the internal structure of the object. This image allows possible defects to be detected.

Collimator (Optional): The collimator allows detailed examination of a specific area by adjusting the direction and focus of the X-rays.

Industrial X-ray instruments are critical for examining the internal structure of materials, flaw detection and quality control. These instruments are widely used in industries such as automotive, aerospace, construction and industrial production.

4. Uses of X-ray Imaging Techniques

X-ray imaging techniques are widely used in many industrial fields. Here are the main uses of these techniques in different industrial fields:

Material Testing:

- Flaw Detection: X-rays are used to detect defects such as cracks, holes or air bubbles in industrial materials such as metals, composite materials and weld joints.
- Material Composition Analysis: X-ray spectrometry allows the elements and components within materials to be analyzed.

Weld Inspection:

- Weld Defects: Defects in the weld joints, lack of penetration or homogeneity of the filler metal are evaluated by X-ray imaging.
- Weld Quality: X-rays provide quality control by examining the internal structure of welds and detect potential weld defects.

Quality Control and Verification:

- Product Quality: X-ray imaging is used to assess the internal structure of industrial products and helps determine whether products meet quality standards.
- Product Dimensioning: X-ray technology is used to dimension the internal structure of products and check whether components are compatible.

In-Part Inspection:

- Structural Analysis: X-ray imaging is used to examine the internal structure of complex parts in detail and to identify internal components.
- Precision Parts: X-ray technology is used to examine the internal structure of fragile parts such as electronic devices and precision mechanisms without damaging them.

These methods play an important role in critical processes such as quality control, analysis and defect detection in different industries.

Archaeology and Cultural Heritage Conservation

Examination of Ancient Objects: X-ray imaging techniques are used to analyze the internal structure of historical artifacts while preserving the materials used.

Restoration Studies: During the repair and maintenance of historical artifacts, detailed examination of the internal structure can be done with X-ray technology, which guides the restoration process.

Oil and Gas Industry

Pipelines and Weldments: X-ray imaging techniques are used in the oil and gas industry for the detection of defects and quality control of pipelines and weld joints.

X-ray Imaging Techniques: X-ray technology is used in many industrial fields thanks to its ability to examine the internal structure of objects in detail and without damaging them. These techniques are widely preferred to increase the reliability of manufacturing processes, improve product quality and ensure the accuracy of critical components.

5. Industrial X-ray Tomography

Basic Principles of X-ray Tomography: X-ray tomography is a method for visualizing the internal structure of objects in three dimensions.

X-ray Absorption and Attenuation: As X-rays pass through an object, they are absorbed at different rates by the materials within it. Dense materials (e.g. metal) absorb more X-rays, while less dense

materials (e.g. air) absorb less. The attenuation rate of X-rays varies depending on the density and thickness of the material.

Project Plan: The object is scanned with X-rays from different angles and the projections from these angles form cross-sectional images of the object.

Back-Projection Transformation: Projections taken from different angles are combined with the back-propagation method. This method reconstructs the internal structure of the object by placing the projections in the correct position and angle.

Reconstruction: The data obtained by backpropagation is processed through a computer program and cross-sectional images of the object are created. These cross-sections provide a detailed view of the object's internal structure.

Imaging and Analysis: The resulting cross-sectional images can be viewed and analyzed in 2D or 3D format. X-ray tomography is used in many fields from engineering to medicine, providing detailed information about internal structures without the need for surgical intervention. It is widely used in industry for materials testing, defect detection, quality control and product development, and in medicine for organ and tissue examination.

6. Use of X-ray Tomography in Industrial Applications

X-ray tomography is used in many industrial fields, from engineering to automotive, aerospace to energy, to examine the internal structure of parts in detail. This technique is a powerful tool for improving product quality, detecting defects, optimizing manufacturing processes and design verification. X-ray tomography is a critical imaging technique for detailed part inspection and

analysis in the industrial field. Some of the key application areas enabled by this technique:

Defect Analysis and Detailed Inspection

- **Structural Defects:** X-ray tomography detects structural defects such as cracks, holes, air bubbles or embedded foreign bodies in metal, plastic or composite materials.
- **Weld Inspection:** Used to examine weld joints in detail for defects, lack of penetration and problems such as porosity.

Analysis of Material Components

- **Material Distribution:** Evaluates material distribution and homogeneity within parts. Identify the boundaries and components of different materials.
- **Porosity Analysis:** The porosity and porosity levels and distributions in materials can be analyzed by X-ray tomography.

Production Quality and Tolerance Control

- Tolerances of Internal Structure: Detects internal structural tolerance violations that occur during the manufacturing process, which evaluates the quality and conformity of products.
- Machine Parts: The internal structure and assembly quality of industrial machine parts can be examined in detail.

Structural Analysis and Engineering Applications

- Material Durability: Material durability and potential harmful effects (e.g. metal fatigue) within structural components can be analyzed.
- Design Verification: The internal structure of structural designs and component performance are examined to assess how they will behave in real-world conditions.

Repair and Maintenance

- **Damage Detection:** Defects, cracks and degradations inside the damaged parts are evaluated by X-ray tomography.
- **Reparation Planning:** Detailed analysis of the internal structure of damaged parts is important for creating an effective repair or maintenance strategy.

7. Industrial X-ray Analysis

X-ray spectrometry is a method of analysis used to determine the types and amounts of elements in a substance. Here is basic information about this technique:

What is X-ray Spectrometry?

X-ray spectrometry determines the chemical composition of a sample by examining the interaction of X-rays sent into a sample with the elements in the sample. This method is widely used in many fields such as materials science, metallurgy, geology, biochemistry, archaeology, biology, physics and industry. X-ray spectrometry is a versatile technique that can be adapted to various analysis requirements and is considered an important tool in analytical

chemistry. This method has a wide range of applications with the ability to directly determine the amount and types of elements in samples.

How X-ray Spectrometry Works

1. X-ray Irradiation: An X-ray beam is sent into the sample and the X-rays penetrate into the sample.

2. Interaction of Elements: The atoms in the sample interact with the incoming X-rays. During this interaction, internal electrons absorb energy to fill the gaps in the outer shells and re-emit X-rays, producing fluorescence (scattering).

3. Spectrum Analysis: The X-ray spectrometry instrument analyzes the energy levels of the emitted X-rays. Each element produces X-rays at specific energy levels and these energy levels can be observed in the spectrum recorded by the instrument.

4. Element Analysis: The recorded spectrum contains the characteristic X-ray energies of each element. Using these characteristic energies, it is possible to determine the types and concentrations of elements in the sample.

Usage Areas and Examples

- Material Analysis: Compositional analysis of metallurgy, ceramics, plastics and other industrial materials.
- Mineralogy and Geology: Elemental compositional analysis of rocks and minerals.
- Chemical Analysis: Analysis of biological samples, organic compounds and biochemical processes.

- Archaeology and Cultural Heritage: Analysis of paints, inks and other materials from historical artifacts.
- Environmental Science: Pollution analysis of soil, water and air samples.

Use of X-ray Techniques for Composition Analysis of Materials

X-ray techniques are powerful tools used to analyze the internal structure and composition of materials in detail. Details on how these techniques work and in which fields they are used:

X-ray Fluorescence Spectrometry

- How it works: High-energy X-rays are sent into the sample. These X-rays interact with elements in the sample and produce characteristic X-rays. The energy levels of these emitted X-rays are analyzed to determine the chemical composition of the elements in the sample (URL 2).

- Areas of Use: It is widely used in the analysis of elements in many fields such as metallurgy, ore analysis, cement industry, archaeology and environmental analysis.

Energy Distribution X-ray Spectrometry

- How it works: A focused beam of electrons is sent at the sample. The electrons interact with electrons in the sample and produce characteristic X-rays. The energies of these X-rays are analyzed to determine the type and amount of elements.

- Areas of Use: Integrated with instruments such as scanning electron microscopes and transmission electron microscopes. It is used in areas such as surface analysis of materials, nanotechnology, biology and materials science.

X-ray Scattering Spectrometry

- How it works: The X-ray beam is sent to the sample and the sample scatters the X-rays according to its crystal structure. This scattering pattern allows the crystal structure of the sample to be analyzed.

- Areas of Use: Crystallography, mineralogy, materials science, metallurgy and structural analysis.

X-ray Spectrometry and X-ray Tomography

- How it works: Based on the principle of X-ray tomography. The sample is exposed to X-rays and a 3D structure of the sample is created using projections taken from different angles. Analysis of this structure helps to identify the elements and components in the sample.

- Areas of Use: It is used in industrial applications for analyzing the internal structure of materials, quality control, defect detection and material testing.

These X-ray techniques are reliable and effective tools for composition analysis of materials. They are widely used in industrial processes in many areas such as quality control, materials testing, product development and research.

Industrial X-ray Safety and Regulations

Safety Precautions in X-ray Use

X-ray use must be carried out with certain safety precautions to minimize health risks. The precautions to be taken ensure that X-ray use is carried out safely and effectively. When adequate safety

precautions are taken, X-ray techniques can be practiced both safely and efficiently.

Training and License: Persons operating X-ray equipment must be properly trained and licensed. Operators must be thoroughly trained in the safe use of the equipment.

- **Radiation Exposure:** X-ray exposure should be limited in accordance with national and international standards. Radiation exposure levels of operators and other personnel should be monitored regularly.
- **Personal Protective Equipment:** Appropriate personal protective equipment, e.g. lead apron and gloves, should be worn when using X-rays. This equipment should be regularly checked and maintained.
- **Area Safety:** Areas where X-rays are used must be clearly marked and access controlled. The area should be organized and secured to minimize the risk of radiation exposure.
- **Radiation Leakage Control:** X-ray equipment should be checked regularly and monitored for any radiation leaks. Devices and rooms should be regularly maintained to prevent leaks.
- **Pregnant Women and Children:** Pregnant women and children should avoid exposure to X-rays. In particular, direct X-ray exposure of pregnant women should be avoided.

- **Risk Assessment:** A comprehensive risk assessment should be carried out for each X-ray application. This assessment helps to determine the radiation risks to workers and others.
- **Legal and Ethical Rules:** All legal regulations and ethical rules regarding the use of X-rays must be followed. These codes include specific requirements for working with radiation.

Regulations and Standards Applicable to Industrial X-ray Applications

In industrial X-ray applications, there are various regulations and standards that set standards for worker health, environmental safety and public safety.

- **United States of America:**
  - **OSHA (Occupational Safety and Health Administration):** Regulates occupational health and safety standards.
  - **NRC (Nuclear Regulatory Commission):** Oversees radiation safety and nuclear energy practices.
- **European Union:**
  - EURATOM Directive: Sets nuclear energy and radiation safety standards in the European Union.
  - CE Marking: Industrial X-ray equipment must comply with CE marking requirements in the European Union.
- **International Standards:**
  - IEC (International Electrotechnical Commission) 60601: Sets standards for the safety of electrical medical devices.
  - ISO (International Organization for Standardization) 14001: Sets international standards for environmental management systems.

- **International Atomic Energy Agency (IAEA):** Provides guidance on nuclear safety and radiation safety.
- **Country Specific Standards:** Many countries establish national standards and regulations for their industrial X-ray applications. For example, Germany has the "Strahlenschutzverordnung" (Radiation Protection Ordinance).

These regulations and standards play an important role in industrial X-ray applications in terms of occupational health and safety, environmental impacts and public safety. Compliance with these standards ensures the safe and effective use of X-ray techniques. Therefore, it is of utmost importance to keep up to date with these standards.

Challenges in Industrial X-ray Applications

Challenges in Achieving High Quality Images

Achieving high quality images in industrial X-ray applications can face several challenges. These challenges can affect the accuracy and clarity of imaging results.

Density and Shape of the Object:

o **Dense Materials:** Dense objects absorb X-rays at a high rate, making it difficult for X-rays to penetrate deeply. Especially in dense materials, such as thick metal parts, it can be difficult to see the internal structure clearly.

o **Shape and Size of the Object:** Objects with complex shapes or thin structures can complicate the imaging process. In such objects, clear visualization of the internal structure may be difficult.

Surface Defects and Contrast Issues:

o **Surface Imperfections:** Imperfections or irregularities on the surface of objects can reduce contrast in X-ray images. This can make it difficult to detect internal defects or details.

o **Loss of Contrast:** Transition zones between different materials may experience loss of contrast, which can prevent accurate visualization of the internal structure.

Radiation Attenuation and Scattering:

o Attenuation and Scattering: X-rays attenuate and scatter as they pass through objects. In thick or dense materials, these phenomena can make it difficult to accurately image the internal structure.

Equipment Performance:

o **Equipment Quality:** The resolution, sensitivity and detector characteristics of X-ray equipment directly affect image quality. Old or low-quality equipment can make it difficult to obtain high-quality images.

Correct Settings and Technical Knowledge:

o **Technical Knowledge:** The correct settings of the X-ray machine must be made. Correct setting of parameters such as voltage, current and exposure time is essential for obtaining quality images.

Moving Objects:

o **Motion Problems:** Movement of the object during the examination may cause blurring and loss of detail in the image.

X-ray Penetration in Different Materials:

The passage of X-rays through different materials varies depending on the type and properties of the material:

1. Dense Materials: Dense materials, such as metal alloys, absorb X-rays to a high degree. This can make it difficult for X-rays to penetrate deeply and prevent accurate viewing of the internal structure of thick metal parts.
2. Low-Density Materials: Low-density materials, such as plastic or wood, absorb X-rays less. Examining the internal structure of these materials can be difficult because X-rays can pass through them quickly.
3. Mixed Materials: The presence of materials with different densities in an object can cause the X-ray to lose contrast in these transition regions. This can make it difficult to accurately view the internal structure.
4. Thick Materials: In very thick materials, it is difficult for X-rays to penetrate deeply. Sufficient penetrating power may be required to see the internal structure or defects at deep points.
5. Surface Coatings and Contaminants: Coatings, paints or contaminants on the surface of the material can adversely affect X-ray penetration. This can prevent accurate visualization of the internal structure of the object.

To meet these challenges, it is important to select the appropriate equipment and work under the supervision of operators with the right technical knowledge and experience. In addition, continuous quality control and calibration processes can help to obtain high-quality X-ray images.

Future Developments

Recent Developments in Industrial X-ray Technologies

Industrial X-ray technologies are constantly being improved and are expected to offer many more innovative features and applications in the future. Recent developments in this field include:

Digital Imaging Technologies:

o Digital Detectors: The transition from traditional film-based systems to digital detectors allows faster and more sensitive images to be obtained. Digital detectors provide clearer and more accurate images.

o High Resolution: New generation digital detectors offer higher resolution and can better detect smaller defects and details.

Artificial Intelligence and Data Analysis:

o Machine Learning and Data Analysis: Artificial intelligence-supported systems can automatically identify and analyze defects in X-ray images. This reduces human errors and shortens inspection times.

o Automated Decision-Making Systems: These systems quickly evaluate inspection results and provide rapid feedback to optimize production processes.

3D Imaging and Tomography:

o High-Speed 3D Tomography: Faster and more sensitive 3D tomography techniques will make it possible to examine the internal structure of objects in detail.

o Portable 3D Tomography Systems: Portable 3D tomography systems offer flexible solutions for field work and mobile production lines.

Advanced Material Identification:

o Spectral Imaging: Ability to analyze the composition and properties of materials in more detail using X-rays at different energy levels.

o Spectral Differentiation: Using spectral differentiation techniques to distinguish similar-looking materials provides more accurate results.

Environmentally Friendly Technologies:

o Lower Radiation Doses: New X-ray devices operate at lower radiation doses, improving safety for both operators and the environment.

o Energy Efficiency: Industrial X-ray devices are becoming more energy efficient, reducing operating costs and environmental impacts.

These developments will enable industrial X-ray technologies to become more accurate, faster, and more reliable. This will improve quality control processes, increase production efficiency, and raise safety standards.

New Methods and Applications

Some exciting new methods and applications are expected in the future of industrial X-ray technologies. Technological advances and research may bring about innovations in X-ray inspection methods, such as the following. These developments will enable industrial X-ray technologies to offer a wider range of applications and perform more precise inspections. This will help optimize manufacturing processes, improve quality control, and support the design of new materials.

1. Nanotechnology and Microscopic Level Investigations: X-ray microscopes can provide the opportunity to perform atomic and molecular level investigations in the field of nanotechnology. This can play a critical role in the development and production of new materials.
2. Fast and Real-Time Imaging: Advanced X-ray devices provide real-time quality control on the production line thanks to fast scanning and imaging techniques. This offers the opportunity for immediate intervention in production processes.
3. Spectrometric Analysis and Chemical Characterization: Advanced spectrometric analysis methods can determine the chemical composition and properties of materials in more detail using X-rays. This can be useful in improving the quality and performance of industrial materials.

4. High-Resolution 3D Imaging and Tomography: Higher-resolution 3D imaging and tomography techniques offer the opportunity to examine complex structures in more detail.
5. Flexible Electronics and Soft Materials Examination: Industrial X-ray techniques can improve the ability to examine the internal structure of soft materials, such as flexible electronic devices and biomedical applications.
6. Analysis of Environmentally Friendly Materials: X-ray analysis can support sustainable material development processes by more precisely determining the components and properties of environmentally friendly materials.
7. AI-Based Analysis: AI and machine learning can develop more sophisticated methods for analyzing X-ray images. This can be used to automatically identify and classify objects and defects.

Conclusion

X-rays are a critical tool in many fields such as materials science, quality control, security, archaeology and environmental sciences due to their wide range of applications and precise analysis capabilities in industrial applications. With technological developments, the capabilities of X-ray technologies are constantly expanding and new application areas are emerging. These developments make industrial processes more efficient and reliable, and also support environmental and cultural protection efforts. In

this study; information is given about the properties of X-rays, their importance in industry, industrial X-ray imaging, areas of use of X-ray imaging techniques, use of X-ray tomography in industrial applications, industrial X-ray analysis, use of X-ray techniques for composition analysis of materials, industrial X-ray safety and regulations, challenges encountered in industrial X-ray applications and future developments.

References

URL 1 (2024). X-Rays and Their Areas of Use. (Retrieved on 01/03/2024 from https://docs.neu.edu.tr/staff/jamal.fathi/BMT%20211 %20ders %20notu%20(X-Isinlari)_5.pdf).

URL 2 (2024). (Retrieved on 03/03/2024 from https://arum.ogu.edu.tr/Sayfa/Index/113/xisinifloresansspektrometresixrf#:~:text=X%2D%C4%B1%C5%9F%C4%B1n%C4%B1%20floresans%20spektrometresi%2C%20general,ZETIUM%20brand%20XRF%20cihar%C4%B1%20bulununmaktad%C4%B1r).

CHAPTER III

Dynamic correlation analysis of proteins with correlationplus program: past and future perspectives

Mustafa TEKPINAR[1]

Introduction

Proteins are macromolecules that play a vital role in the functioning of living things. Recently developed algorithms such as Alphafold (Jumper et al., 2021) and Rosettafold (Baek et al., 2021) have revolutionized the fields of biophysics, biochemistry and molecular biology in determining the protein structure just from the amino acid sequences. Thanks to these methods, three-dimensional structure of a protein can be determined within minutes with a high accuracy. In addition, databases like the Alphafold Database (Varadi et al., 2022) and ESM Metagenomic Atlas (Lin et al., 2023) are

[1] Doç. Dr., Van Yüzüncü Yıl Üniversitesi, Fen Fakültesi, Fizik Bölümü, Van/Türkiye, Orcid: 0000-0002-0207-0446, tekpinar@buffalo.edu

crucial because they provide already computed static structures of almost all proteome of many organisms.

As a result of deep learning algorithms and the databases generated from them, it is evident that finding relevant protein structures has become much easier. However, it is a known fact that proteins are not just static structures and they are dynamic. Dynamic nature of proteins can be explored with experimental method like nuclear magnetic resonance spectroscopy (Sekhar & Kay, 2019), and more recently with cryo-electron microscopy (Tsai, Wu, & Ho, 2022). In addition to the experimental methods, computational approaches such as normal mode analysis (NMA) based on elastic network models (ENMs) (Cui & Bahar, 2006) and molecular dynamics (MD) simulations (Karplus & McCammon, 2002) have also been developed to understand protein dynamics. Using these computational methods, the movements of proteins and the relationships between these movements and protein function can be investigated.

ENMs are powerful computational tools used in the study of protein dynamics, offering significant insights into the structural and functional behavior of proteins (Tirion, 1996). These models simplify the complex interactions within proteins by representing them as networks of nodes (typically corresponding to the C-alpha atoms of amino acids) interconnected by springs that simulate elastic forces. This coarse-grained approach allows researchers to efficiently analyze global motions and collective dynamics without the computational burden associated with detailed all-atom molecular dynamics simulations (Atilgan et al., 2001; Bahar, Atilgan, & Erman, 1997).

One of the key advantages of ENMs is their ability to predict large-scale conformational changes and allosteric effects based solely on structural information. By employing NMA, ENMs can identify low-frequency vibrational modes that correspond to significant collective motions within the protein structure. This capability has been particularly useful in understanding mechanisms of allosteric regulation, where changes in one part of a protein affect its activity at a distant site. For example, studies have demonstrated how variations in model parameters, such as distance cutoffs and stiffness, can influence predictions about protein dynamics and allostery, highlighting the importance of optimizing these parameters for accurate modeling (Dubanevics & McLeish, 2022).

Recent applications of ENMs extend beyond traditional protein dynamics studies to include investigations into protein unfolding pathways and mechanical properties. Research utilizing Gaussian Network Models (GNMs), a specific type of ENM (Bahar et al., 1997), has revealed insights into how proteins unfold under various conditions, such as thermal stress or external forces. These studies indicate that unfolding typically initiates in regions of high shear within the protein structure and propagates to areas of lower shear, providing a clearer picture of the unfolding mechanism (Kumar & Dutta, 2024). Furthermore, ENMs have proven valuable in analyzing diverse biological systems, including membranes, (Lezon, Shrivastava, Yang, & Bahar, 2009), ribosomal complexes (Wang, Rader, Bahar, & Jernigan, 2004) and viral capsids (Tama & Brooks, 2005) demonstrating their versatility across different protein families and functions.

In short, ENMs serve as an essential framework for exploring the dynamics of proteins, bridging the gap between structure and function. Their ability to provide rapid predictions about protein behavior at a low computational cost makes them an invaluable tool in structural biology and biophysics research. Despite their coarse-grained resolution, they provide valuable information about residue correlations within a protein as well.

Molecular dynamics (MD) simulations are one of the cornerstones in the study of protein dynamics. These simulations allow researchers to model time-dependent behavior of proteins at an atomic level by solving Newton's equations of motion interatively. Since their inception in the early 1980s, MD simulations have evolved significantly, enabling detailed investigations into protein folding, conformational changes, and interactions with ligands and other biomolecules (Salsbury, 2010; Sinha, Tam, & Wang, 2022). The ability to simulate molecular systems over time scales from nanoseconds to microseconds has provided insights into the dynamic nature of proteins that are often inaccessible through experimental methods alone.

One of the primary applications of MD simulations in protein dynamics research is the exploration of conformational changes associated with protein function. For instance, studies have shown how ligand binding can induce significant structural changes in proteins, affecting their activity and stability (Sinha et al., 2022). By analyzing the trajectories generated from MD simulations, researchers can identify key residues involved in these conformational transitions and elucidate the mechanisms behind allostery—where a change in one part of a protein influences another

part, often critical for enzymatic activity. This understanding is crucial for drug design, as it allows for the identification of potential binding sites and the prediction of how drugs might alter protein dynamics.

Moreover, advancements in computational power and algorithms have facilitated the simulation of larger and more complex systems, including multi-protein complexes and membrane proteins and even whole cells (Perilla et al., 2015; Stevens et al., 2023). Modern MD simulations can handle systems upto billions of atoms, providing a comprehensive view of molecular interactions within biological environments (Dommer et al., 2023). The use of various force fields, such as CHARMM (MacKerell et al., 1998), OPLS (Kaminski, Friesner, Tirado-Rives, & Jorgensen, 2001) and AMBER (Lindorff-Larsen et al., 2010), allows researchers to tailor simulations to specific types of proteins or conditions, enhancing the accuracy and relevance of the results. Additionally, combining MD simulations with experimental data has proven effective in validating findings and refining models, further bridging the gap between computational predictions and biological reality (Chan, Trabuco, Schreiner, & Schulten, 2012).

In summary, molecular dynamics simulations are an invaluable tool for investigating protein dynamics. They enable researchers to visualize and analyze the intricate motions that underlie protein function and interactions. As computational techniques continue to advance, MD simulations will likely play an even more significant role in understanding complex biological processes at a molecular level.

In addition to various utilization of MD simulations, they can be used to investigate dynamical correlations of proteins a well. Understanding coupled/correlated motions within proteins or protein complexes from MD trajectories is essential to find key residues that play various functions in allostery, ligation and conformational transitions. There are two types dynamical correlations that can be calculated from MD trajectories: Dynamical cross-correlations (Ichiye & Karplus, 1991) and linear mutual information (Lange & Grubmuller, 2006). Both of them are widely employed to investigate impact of ligand binding, mutational effects and allosteric effects. These quantities are also used to build graphs/networks to identify key residues in a single protein or a protein complex.

There are several packages that calculate dynamical cross-correlations and related network-based quantities from MD simulation trajectories. A recent review summarizes the state-of-the-art in this field (Yehorova, Di Geronimo, Robinson, Kasson, & Kamerlin, 2024). In this work, we will only focus on correlationplus and provide details on its past usage and future potential for analyzing molecular dynamics trajectories (Tekpinar, Neron, & Delarue, 2021).

How to employ correlationplus program using molecular dynamics trajectories

Correlationplus program is a versatile program with four main modules and an auxillary module, all written in Python programming language. Below, name, function and usage of each module will be explained. I'll assume that the enduser has a reference pdb file and a trajectory file for the rest of the text. In addition, periodic boundary wrapping of the trajectory must have already been performed.

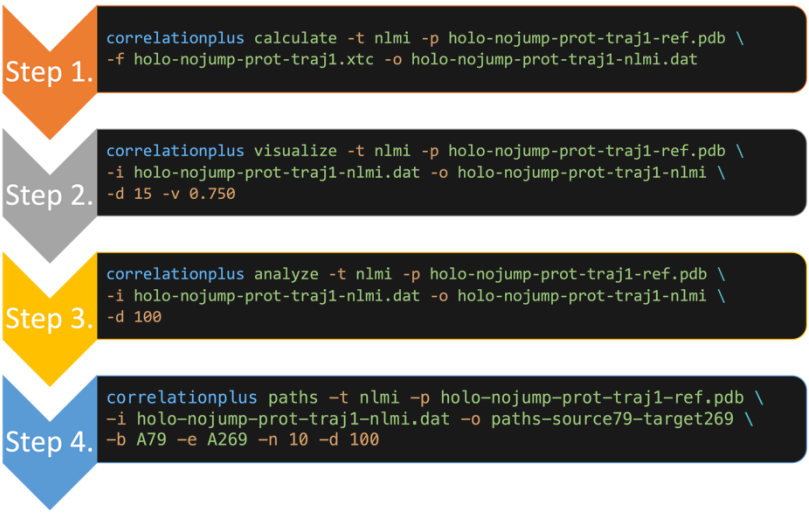

Figure 1: Workflow of correlation calculations with correlationplus is a four-step process. Only normalized linear mutual information is used in this example but the workflow can be repeated by replacing nlmi with ndcc as well.

1. calculate: This module calculates two dynamical correlation metrics: linear mutual information (lmi) and dynamical cross-correlation (dcc). Type of the target correlation can be selected with '-t nlmi' or '-t ndcc'. The lowercase n before lmi or dcc indicate that the output should be normalized. Normalized lmi (nlmi) is in the range of [0, 1], while ndcc is between [-1, 1]. The most important output of this module is a symmetric matrix in plain text format (See Step 1 in Figure 1).

2. visualize: After a correlation matrix is calculated, it is necessary to visualize it. The visualization in 2D as a

heatmap and projection of the correlations onto the protein structure can be obtained with visualize module. When projecting the correlations onto protein structure, distance and correlation values can be restrained. For example, if you want to visualize the correlations higher than 0.750 between amino acids that have a pairwise distance of 15.0 Å or more, you should add '-d 15 -v 0.750' parameters while running this module. This module generates protein projection output scripts for Pymol (Schrodinger, 2010) and VMD (Humphrey, Dalke, & Schulten, 1996) protein visualization programs (See Step 2 in Figure 1).

3. analyze: This module aims to build a graph by assuming that Calpha atoms constitute the nodes and the dynamical correlations are weights of the edges between the nodes. NetworkX Python module was used to build and analyze the graph in correlationplus (Hagberg, Schult, & Swart, 2008). The edges between low correlation nodes can be eliminated by adding a minimum cutoff value. For example, using '-v 0.3' will assume that the nodes with correlation values lower than 0.3 are not interacting with each other, and therefore, there will not be any edges between them. Furthermore, a distance cutoff beyond which residues are assumed to be not interacting can be implemented with "'-d 100" argument (Please note that the distance unit is Angstrom here). After the graph is created, several centrality metrics such as betweenness,

closeness, current_flow_betweenness, current_flow_closeness (underscores between the words cannot be omitted) and eigenvector centralities can be calculated. Even though it has not been tested on large datasets, a simple community detection algorithm was also implemented and it can be called with the additional "-c community" option. Some previous algorithms used some intermediate steps between graph construction and centrality calculations. For instance, the nodes that are not within a certain distance during 75% of the trajectory were assumed not to be interacting and the edges between them were removed (Sethi, Eargle, Black, & Luthey-Schulten, 2009). The author of this work believes that this kind of restrictions prevent to investigate large scale conformational transitions with dynamical network approaches and therefore, they have not been implemented in correlationplus by default. Another important point is consistency of the centralities across replicas of molecular dynamics trajectories. The author's experience shows that current flow betweenness, current flow closeness and eigenvector centralities are typically more consistent across different MD replicas compared to plain betweenness and closeness (See Step 3 in Figure 1 as an example command).

4. paths: correlationplus can calculate shortest paths between two sites of a protein with this module. A

source residue (such as A79: 79th residue in chain A) and a target residue (such as A269: 269th residue in chain A) have to be specified for path calculation. Paths between active, allosteric, mutant or ligated sites can be investigated depending on the biological problem at hand. Number of paths to be generated can be specified with "-n" option. The user can denote maximal length beyond which pairwise interactions will be considered as zero with "-d" parameter. If the interactions beyond 100 Å are considered to be zero, it can be specified as "-d 100" as exemplified in Step 4 of Figure 1.

5. diffMap: Sometimes, it is necessary to subtract two correlation matrices to see impact of a mutation, ligand binding, pH or temperature changes. diffMap is an auxillary module that help to perform this operation and generate difference heatmaps.

Use Cases of Correlationplus Program

Correlationplus have been downloaded over 9000 times according to conda data as of November 2024. It has been cited about 30 times as of writing of this text according to Scopus. The usage of it covered a wide range of research from mutational effect investigation to enzyme optimization. Here, I provide a group of papers utilizing correlationplus in various contexts:

1. Understanding Protein Dynamics:

Several studies analyze the dynamical correlations between residues in proteins to understand their functional mechanisms. For

example, a paper by Gao et al. employs dynamic cross-correlation network analysis to engineer a halide methyltransferase, highlighting how residue interactions impact protein function and stability (Gao et al., 2024). As a result of dynamic cross-correlation network analysis, the authors claim an 82-fold increase of enzyme efficiency as compared to the wild-type (WT).

2. Allosteric Regulation:

Dynamical correlations are crucial for studying allosteric inhibition and regulation in proteins. In a research by Roy et al., the authors investigated distinct binding pockets and protomer preferences in the AcrB efflux pump, emphasizing how dynamical correlations inform allosteric mechanisms (Roy, Bera, & Patra, 2024).

3. Structural and Functional Insights:

Some studies use dynamical correlations to derive structural and functional insights into protein interactions and mutations. The study by Banerjee et al. examines mutations affecting the dynamics of specific loops in proteins, revealing how these changes correlate with functional outcomes (Banerjee, Rath, Darji, & Mandal, 2023).

4. Engineering and Design:

Dynamical correlations are applied in engineering new proteins or modifying existing ones for enhanced functionality. A research by Yang et al. discusses how engineering key loops can modulate catalytic activity and thermostability through an understanding of dynamic residue interactions (Yang et al., 2023).

The work of Gao et al. can also be classified under this category as well (Gao et al., 2024).

5. Disease Mechanisms:

Some studies focus on disease-related mechanisms by analyzing dynamical correlations in mutated proteins or during pathogen interactions. For example, Mandal and Rath evaluate spike protein interactions with ACE2 variants, providing insights into how temperature changes affects the dynamical correlations and eventually how they influence viral infectivity of various mutants (Mandal & Rath, 2023). Another paper by Chong et al. analyze free energy and dynamic cross-correlations of residues in the context of antibody-receptor binding affinities for SARS-CoV-2 (Chong, Saparpakorn, Sangma, Lee, & Hannongbua, 2023). The authors use elastic network model, and therefore a single pdb file, to build dynamical cross-correlation maps with correlationplus. This approach uses cross-correlations and residue energy to explain the weakening of binding upon mutations in the RBD.

In conclusion, the utilization of correlationplus in these studies highlights it as a powerful tool for elucidating protein function, understanding allosteric mechanisms, guiding engineering efforts, and investigating disease-related dynamics through comprehensive molecular analyses.

Future Perspectives and Conclusions

Correlationplus program was designed to employ both elastic network models and molecular dynamics trajectories. Therefore, only Calpha representation of amino acids are used due to this design principle. However, this can be a limitation for molecular dynamics

simulation data, which contain mostly all atoms of a system. For example, side-chain correlations obtained from MD simulations can also be important (Taddese, Garnier, Abdi, Henrion, & Chabbert, 2020). Giving the user to select representative atoms is a possible avenue for further development of correlationplus.

An important problem in protein science when calculating position dependent quantities is impact of structural alignment on the derived quantity (Karplus & Ichiye, 1996; Zhou, Cook, & Karplus, 2000). Dynamical cross-correlations are also position dependent quantities. Therefore, observed correlations between amino acids pairs will be sensitive to the aligned regions. In correlationplus, the first frame is selected as the reference structure and entire protein structure is aligned to Calpha representation of the protein before all correlations are calculated. However, using distance correlations instead of position-dependent correlations may overcome the alignment problem completely. Therefore, implementation of distance correlations can be useful for the protein dynamics community.

Another exciting development avenue is to include other biomolecules such as lipids (Westerlund, Fleetwood, Perez-Conesa, & Delemotte, 2020), DNA and RNA in the correlation analysis (Kasahara, Fukuda, & Nakamura, 2014). This can be quite beneficial to undestand role of lipids and DNA/RNA in allosteric signal transfer.

Correlationplus can be installed with two popular installation systems: pip and conda. In addition, it is possible to run it without installation using docker. Despite these efforts to make

correlationplus easy-to-install and easy-to-use, it is still a command driven program. Installation of the program, in particular in Windows operating system, can still be a challenge due to numerous reasons. Moreover, commandline programs may not be the first choise of experimental biology, biochemistry and biophysics communities, which could benefit significantly from such tools. As a result, removing the installation barrier with approaches like Google Colab or web servers can enhance its usability. Providing interactive plots and protein projections instead of static png images can help the users to quickly build hypothesis on impact of dynamics. As a result, building an iteractive web interface constitutes a major improvement target for correlationplus. Another option to enhance correlationplus visualizations is to integrate it with common protein visualization software like VMD, Pymol or ChimeraX (Goddard et al., 2018).

To summarize, correlationplus has been used for various purposes from enzyme design to allosteric interaction investigations. Considering abundant availability of protein structures due to deep learning algorithms, protein dynamics investigations will also increase. Therefore, programs like correlationplus will be needed more and more. Implementation of methodical and graphical improvements in correlationplus will serve a better understanding of protein dynamics.

References

Atilgan, A. R., Durell, S. R., Jernigan, R. L., Demirel, M. C., Keskin, O., & Bahar, I. (2001). Anisotropy of fluctuation dynamics of proteins with an elastic network model. *Biophys J, 80*(1), 505-515. doi:S0006-3495(01)76033-X [pii]]]>
<![CDATA[10.1016/S0006-3495(01)76033-X

Baek, M., DiMaio, F., Anishchenko, I., Dauparas, J., Ovchinnikov, S., Lee, G. R., . . . Baker, D. (2021). Accurate prediction of protein structures and interactions using a three-track neural network. *Science, 373*(6557), 871-876. doi:10.1126/science.abj8754

Bahar, I., Atilgan, A. R., & Erman, B. (1997). Direct evaluation of thermal fluctuations in proteins using a single-parameter harmonic potential. *Fold Des, 2*(3), 173-181. Retrieved from http://www.ncbi.nlm.nih.gov/pubmed/9218955

Banerjee, D., Rath, S. L., Darji, S. A., & Mandal, N. (2023). Mutations in V84I & A184V of blaTEM cluster plays a pivotal role in the dynamics of Ω-loop leading to genesis of IR-TEM. *Journal of Biomolecular Structure and Dynamics*. doi:10.1080/07391102.2023.2291168

Chan, K. Y., Trabuco, L. G., Schreiner, E., & Schulten, K. (2012). Cryo-electron microscopy modeling by the molecular dynamics flexible fitting method. *Biopolymers, 97*(9), 678-686. doi:10.1002/bip.22042

Chong, W. L., Saparpakorn, P., Sangma, C., Lee, V. S., & Hannongbua, S. (2023). Insight into free energy and dynamic cross-

correlations of residue for binding affinity of antibody and receptor binding domain SARS-CoV-2. *Heliyon, 9*(1). doi:10.1016/j.heliyon.2022.e12667

Cui, Q., & Bahar, I. (2006). *Normal mode analysis : theory and applications to biological and chemical systems*. Boca Raton: Chapman & Hall/CRC.

Dommer, A., Casalino, L., Kearns, F., Rosenfeld, M., Wauer, N., Ahn, S. H., . . . Amaro, R. E. (2023). #COVIDisAirborne: AI-enabled multiscale computational microscopy of delta SARS-CoV-2 in a respiratory aerosol. *Int J High Perform Comput Appl, 37*(1), 28-44. doi:10.1177/10943420221128233

Dubanevics, I., & McLeish, T. C. B. (2022). Optimising Elastic Network Models for Protein Dynamics and Allostery: Spatial and Modal Cut-offs and Backbone Stiffness. *J Mol Biol, 434*(17), 167696. doi:10.1016/j.jmb.2022.167696

Gao, C.-Y., Yang, G.-Y., Ding, X.-W., Xu, J.-H., Cheng, X., Zheng, G.-W., & Chen, Q. (2024). Engineering of Halide Methyltransferase BxHMT through Dynamic Cross-Correlation Network Analysis. *Angewandte Chemie - International Edition, 63*(25). doi:10.1002/anie.202401235

Goddard, T. D., Huang, C. C., Meng, E. C., Pettersen, E. F., Couch, G. S., Morris, J. H., & Ferrin, T. E. (2018). UCSF ChimeraX: Meeting modern challenges in visualization and analysis. *Protein Sci, 27*(1), 14-25. doi:10.1002/pro.3235

Hagberg, A. A., Schult, D. A., & Swart, P. J. (2008). Exploring Network Structure, Dynamics, and Function using NetworkX. *Proceedings of the 7th Python in Science Conference*, 11-16.

Humphrey, W., Dalke, A., & Schulten, K. (1996). VMD: visual molecular dynamics. *Journal of Molecular Graphics, 14*(1), 33-38, 27-38. Retrieved from http://www.ncbi.nlm.nih.gov/pubmed/8744570

Ichiye, T., & Karplus, M. (1991). Collective motions in proteins: a covariance analysis of atomic fluctuations in molecular dynamics and normal mode simulations. *Proteins, 11*(3), 205-217. doi:10.1002/prot.340110305

Jumper, J., Evans, R., Pritzel, A., Green, T., Figurnov, M., Ronneberger, O., . . . Hassabis, D. (2021). Highly accurate protein structure prediction with AlphaFold. *Nature*. doi:10.1038/s41586-021-03819-2

Kaminski, G. A., Friesner, R. A., Tirado-Rives, J., & Jorgensen, W. L. (2001). Evaluation and reparametrization of the OPLS-AA force field for proteins via comparison with accurate quantum chemical calculations on peptides. *Journal of Physical Chemistry B, 105*(28), 6474-6487. doi:Doi 10.1021/Jp003919d

Karplus, M., & Ichiye, T. (1996). Comment on a "fluctuation and cross correlation analysis of protein motions observed in nanosecond molecular dynamics simulations". *J Mol Biol, 263*(2), 120-122. doi:10.1006/jmbi.1996.0562

Karplus, M., & McCammon, J. A. (2002). Molecular dynamics simulations of biomolecules. *Nature Structural Biology, 9*(9), 646-652. Retrieved from <Go to ISI>://000177656200007

Kasahara, K., Fukuda, I., & Nakamura, H. (2014). A novel approach of dynamic cross correlation analysis on molecular dynamics simulations and its application to Ets1 dimer-DNA complex. *PLoS One, 9*(11), e112419. doi:10.1371/journal.pone.0112419

Kumar, R., & Dutta, S. (2024). Exploring the unfolding pathways of protein families using Elastic Network Model. *Sci Rep, 14*(1), 23905. doi:10.1038/s41598-024-75436-8

Lange, O. F., & Grubmuller, H. (2006). Generalized correlation for biomolecular dynamics. *Proteins, 62*(4), 1053-1061. doi:10.1002/prot.20784

Lezon, T. R., Shrivastava, I. H., Yang, Z., & Bahar, I. (2009). Elastic network models for biomolecular dynamics: theory and application to membrane proteins and viruses. *Handbook on biological networks*, 129-158.

Lin, Z., Akin, H., Rao, R., Hie, B., Zhu, Z., Lu, W., . . . Rives, A. (2023). Evolutionary-scale prediction of atomic-level protein structure with a language model. *Science, 379*(6637), 1123-1130. doi:10.1126/science.ade2574

Lindorff-Larsen, K., Piana, S., Palmo, K., Maragakis, P., Klepeis, J. L., Dror, R. O., & Shaw, D. E. (2010). Improved side-chain torsion potentials for the Amber ff99SB protein force field.

Proteins-Structure Function and Bioinformatics, 78(8), 1950-1958. doi:Doi 10.1002/Prot.22711

MacKerell, A. D., Brooks, C. L., Nilsson, L., Roux, B., Won, Y., & Karplus, M. (1998). {CHARMM}: The Energy Function and Its Parameterization with an Overview of the Program. In Schleyer (Ed.), (Vol. 1, pp. 271-277): John Wiley & Sons: Chichester.

Mandal, N., & Rath, S. L. (2023). Evaluating the Spike–hACE2 interactions in the wild type and variants of concern of SARS -CoV-2 at different temperatures. *Frontiers in Physics, 11*. doi:10.3389/fphy.2023.1320437

Perilla, J. R., Goh, B. C., Cassidy, C. K., Liu, B., Bernardi, R. C., Rudack, T., . . . Schulten, K. (2015). Molecular dynamics simulations of large macromolecular complexes. *Curr Opin Struct Biol, 31*, 64-74. doi:10.1016/j.sbi.2015.03.007

Roy, R. K., Bera, A., & Patra, N. (2024). Insights into Allosteric Inhibition of the AcrB Efflux Pump: Role of Distinct Binding Pockets, Protomer Preferences, and Crosstalk Disruption. *Journal of Chemical Information and Modeling, 64*(15), 5964-5976. doi:10.1021/acs.jcim.4c00306

Salsbury, F. R., Jr. (2010). Molecular dynamics simulations of protein dynamics and their relevance to drug discovery. *Current Opinion in Pharmacology, 10*(6), 738-744. doi:10.1016/j.coph.2010.09.016

Schrodinger, LLC. (2010). *The PyMOL Molecular Graphics System, Version 1.3r1*.

Sekhar, A., & Kay, L. E. (2019). An NMR View of Protein Dynamics in Health and Disease. *Annual Review of Biophysics, Vol 42, 48*, 297-319. doi:10.1146/annurev-biophys-052118-115647

Sethi, A., Eargle, J., Black, A. A., & Luthey-Schulten, Z. (2009). Dynamical networks in tRNA:protein complexes. *Proc Natl Acad Sci U S A, 106*(16), 6620-6625. doi:10.1073/pnas.0810961106

Sinha, S., Tam, B., & Wang, S. M. (2022). Applications of Molecular Dynamics Simulation in Protein Study. *Membranes (Basel), 12*(9). doi:10.3390/membranes12090844

Stevens, J. A., Grunewald, F., van Tilburg, P. A. M., Konig, M., Gilbert, B. R., Brier, T. A., . . . Marrink, S. J. (2023). Molecular dynamics simulation of an entire cell. *Front Chem, 11*, 1106495. doi:10.3389/fchem.2023.1106495

Taddese, B., Garnier, A., Abdi, H., Henrion, D., & Chabbert, M. (2020). Deciphering collaborative sidechain motions in proteins during molecular dynamics simulations. *Sci Rep, 10*(1), 15901. doi:10.1038/s41598-020-72766-1

Tama, F., & Brooks, C. L. (2005). Diversity and identity of the mechanical properties of icosahedral viral capsids studied with elastic network normal mode analysis. *Biophysical Journal, 88*(1), 231a-232a. Retrieved from <Go to ISI>://WOS:000226378501128

Tekpinar, M., Neron, B., & Delarue, M. (2021). Extracting Dynamical Correlations and Identifying Key Residues for Allosteric Communication in Proteins by correlationplus. *J Chem Inf Model, 61*(10), 4832-4838. doi:10.1021/acs.jcim.1c00742

Tirion, M. M. (1996). Large Amplitude Elastic Motions in Proteins from a Single-Parameter, Atomic Analysis. *Phys Rev Lett, 77*(9), 1905-1908. Retrieved from http://www.ncbi.nlm.nih.gov/entrez/query.fcgi?cmd=Retrieve&db=PubMed&dopt=Citation&list_uids=10063201

Tsai, M. D., Wu, W. J., & Ho, M. C. (2022). Enzymology and Dynamics by Cryogenic Electron Microscopy. *Annual Review of Biophysics, Vol 42, 51*, 19-38. doi:10.1146/annurev-biophys-100121-075228

Varadi, M., Anyango, S., Deshpande, M., Nair, S., Natassia, C., Yordanova, G., . . . Velankar, S. (2022). AlphaFold Protein Structure Database: massively expanding the structural coverage of protein-sequence space with high-accuracy models. *Nucleic Acids Res, 50*(D1), D439-D444. doi:10.1093/nar/gkab1061

Wang, Y. M., Rader, A. J., Bahar, I., & Jernigan, R. L. (2004). Global ribosome motions revealed with elastic network model. *Journal of Structural Biology, 147*(3), 302-314. doi:10.1016/j.jsb.2004.01.005

Westerlund, A. M., Fleetwood, O., Perez-Conesa, S., & Delemotte, L. (2020). Network analysis reveals how lipids and other cofactors influence membrane protein allostery. *J Chem Phys, 153*(14), 141103. doi:10.1063/5.0020974

Yang, J., Zhang, X., Sun, Q., Li, R., Wang, X., Zhao, G., . . . Zheng, F. (2023). Modulation of the catalytic activity and thermostability of a thermostable GH7 endoglucanase by engineering the key loop B3. *International Journal of Biological Macromolecules, 248*. doi:10.1016/j.ijbiomac.2023.125945

Yehorova, D., Di Geronimo, B., Robinson, M., Kasson, P. M., & Kamerlin, S. C. L. (2024). Using residue interaction networks to understand protein function and evolution and to engineer new proteins. *Current Opinion in Structural Biology, 89*. doi:10.1016/j.sbi.2024.102922

Zhou, Y., Cook, M., & Karplus, M. (2000). Protein motions at zero-total angular momentum: the importance of long-range correlations. *Biophys J, 79*(6), 2902-2908. doi:10.1016/S0006-3495(00)76527-1

CHAPTER IV

Investigation of the Physical Properties of HfC Material Using DFT-Based Simulation Method

Cengiz SOYKAN[1]

Introduction

Scientific and engineering studies focus on solving problems that require understanding the structural and mechanical properties of materials. Materials science has made significant progress in industrial applications through the accurate prediction and optimization of these properties. Traditional experimental methods may fall short due to high costs, long durations, and, in some cases, limited accuracy. Therefore, theoretical and computational methods, especially Density Functional Theory (DFT) and first-principles methods, are increasingly being preferred.

DFT and first-principles methods allow the calculation of atomic and electronic structures based on fundamental physical principles. These approaches reduce dependence on experimental

[1] Assoc. Prof. Dr., Kırşehir Ahi Evran University, Health Services Vocational School, Department of Medical Services and Techniques, Kırşehir/Turkey, Orcid: 0000-0003-0897-2384, cengiz.soykan@ahievran.edu.tr

data while offering high accuracy and predictive capability. DFT-based simulations on crystal structures not only perform structural optimization derived from the material's symmetry but also examine energy stability and electronic states in detail. Furthermore, the calculation of mechanical properties (such as elastic moduli, bulk modulus, and shear modulus) provides critical information for assessing the suitability of materials for engineering applications (Sholl & Steckel, 2009).

In this section, the structural and mechanical properties of the HfC crystal structure will be calculated using DFT and first-principles methods. First, the lattice constants (a, b, c Å) and volume ($Å^3$) of the crystal material will be obtained. Then, based on the calculated structural properties, the elastic constants (Cij), bulk modulus (B), shear modulus (G), Young's modulus (E), and Poisson's ratio (v) of the crystal phase will be determined. In the results section, all calculated data will be compared with other theoretical and experimental studies for evaluation. The role of these methods in material design, providing atomic-level accuracy, and their contributions to engineering solutions will be discussed.

Transition metal carbides stand out as an important class of materials in applications requiring high temperature, hardness, and chemical stability. Among these materials, HfC (Hafnium Carbide) is at the center of both academic and industrial research due to its extraordinary physical properties. HfC is known for its high melting point (~3890 °C), hardness, and oxidation resistance at high temperatures. These properties make it especially suitable for use in the aerospace industry, in heat shields for hypersonic vehicles, and in high-temperature applications.

The physical properties of the HfC crystal structure, while exhibiting the typical characteristics of transition metal carbides,

offer unique advantages due to the large atomic weight of the hafnium atom combined with its carbide structure. The high elastic modulus enhances mechanical stability, while its low density allows for lightweight materials. Furthermore, its superior electrical and thermal conductivity makes it attractive for electronic and energy applications. In addition to these properties, advancements in the methods used to produce HfC ensure that the material can be applied in a broader range of fields. However, simulation-based studies conducted before transitioning to experimental processes or production provide a low-cost tool for better understanding or improving the material's physical properties compared to experimental methods.

Numerous theoretical and experimental studies have been conducted on the structural and mechanical properties of HfC crystals. Recent studies published in the literature are listed in Tables 1, 2, and 3 to be compared with our results (Zaoui et al., 2005; Rogl et al., 1977; Feng et al., 2011; Singh et al., 2008; Krasnenko et al., 2014; Nartowski et al., 1999; Wu et al., 2005; Krajewski et al., 1998; Isaev et al., 2007; Yang et al., 2012).

HfC has a halite (rock salt) structure and crystallizes in the cubic Fm-3m space group. Hf^{+4} is bonded to six equivalent C^{-4} atoms, forming a mixture of edge- and corner-sharing HfC_6 octahedra. The corner-sharing octahedra are not tilted. C^{-4}, in turn, is bonded to six equivalent Hf^{+4} atoms, forming a mixture of edge- and corner-sharing CHf_6 octahedra.

In this section, the structural and mechanical properties of the HfC crystal will be discussed in detail. The crystal structure, bonding characteristics, and mechanical durability will be examined. Our results will be compared with previous theoretical and experimental studies to analyze consistencies and discrepancies. Additionally, the

potential of this material in advanced technology applications will be evaluated.

2. Method

In this study, first-principles calculations were performed to calculate the structural and mechanical properties of HfC. The calculations were carried out using the CASTEP software with Density Functional Theory (DFT) (Clark et al., 2005; Kresse et al., 1996; Kresse et al., 1996; Kresse et al., 1994). The exchange-correlation functional was considered using the generalized gradient approximation (GGA-PBE) functional approach (Perdew et al., 1996). This approach is commonly used for accurately modeling the electronic structure of transition metal borides.

The structural properties of HfC were optimized according to the criteria of energy tolerance of 10^{-5} eV/atom, maximum force of 0.03 eV/Å, and maximum displacement of 0.001 Å (Fischer et al., 1992). To ensure the accuracy of the calculations, an energy cutoff value of 650 eV was chosen. This energy value enhances the accuracy of the crystal structure parameters, ensuring the reliability of the calculations.

The k-point distribution in the Brillouin zone was set to 12x12x12 (Monkhorst et al., 1976). This k-point density balanced the speed and accuracy of the calculations, ensuring the correct determination of the structural parameters of HfC. As a result of the structural optimizations, the lattice constants (a, b, c, Å) and volume (V, $Å^3$) of HfC were obtained. Additionally, the energy minimization of ZrB_2 was performed, and the lowest energy configuration was determined.

The mechanical properties, including the elastic constants (C_{ij}), bulk modulus (B), shear modulus (G), Young's modulus (E),

and Poisson's ratio (v) of HfC, have been calculated. The elastic constants were determined by applying homogeneous deformations and using the resulting stress-strain relationships. Specifically, the strain-stress method used for calculating the elastic constants is an ideal technique for accurately reflecting the material's mechanical strength and elastic properties.

The bulk modulus and shear modulus calculations were performed using the Voigt-Reuss-Hill (VRH) approximation. This approach increased the accuracy of the elastic constants and mechanical moduli, allowing for a comprehensive study of the mechanical strength of HfC. As a result of these calculations, information was obtained about the material's compressibility and resistance to deformation.

3. Results

The structural and mechanical properties of cubic HfC were investigated using Density Functional Theory (DFT) calculations with the Generalized Gradient Approximation (GGA) and the Perdew-Burke-Ernzerhof (PBE) functional. Additionally, the significance of these properties for high-stress applications was evaluated, and the consistency with previous experimental and theoretical studies was discussed. The results are presented below.

The crystal structure of cubic HfC, as shown in Figure 1, exhibits a well-ordered arrangement where hafnium (Hf) atoms are located at the corners and face centers, while carbon (C) atoms are positioned at the edge centers and the center of the structure. This configuration is characterized by the Fm-3m space group symmetry.

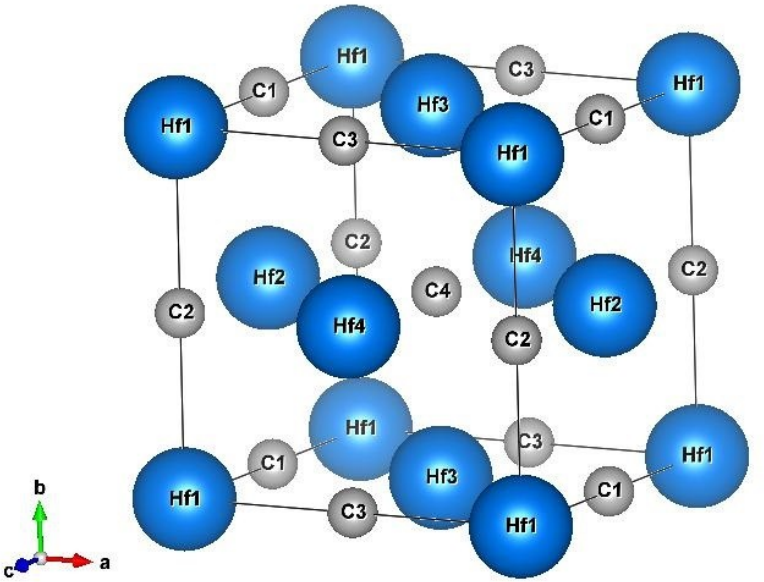

Figure 1: Crystal structure of cubic HfC.

Table 1: Lattice parameters of cubic HfC.

Cry.		Lattice constants (A^0), a, b, c			Volume (A^3)	Ref.
HfC	Teo.	4.656	4.656	4.656	100.934	This work
	Teo.	4.715	4.715	4.715	104.943	Krasnenko
	Teo.	4.657	4.657	4.657	100.999	Zaoui
	Teo.	4.708	4.708	4.708	104.354	Feng
	Teo.	4.708	4.708	4.708	104.354	Yang
	Teo.	4.651	4.651	4.651	100.610	Isaev
	Exp.	4.640	4.640	4.640	99.897	Rogl
	Exp.	4.639	4.639	4.639	99.833	Nartowski
	Exp.	4.640	4.640	4.640	99.897	Wu

The calculated lattice parameters and unit cell volume for HfC are presented in Table 1 and compared with previous theoretical and experimental studies. In this study, the obtained lattice constants (a = b = c = 4.656 Å) and volume (V = 100.934 Å³) are largely consistent with other theoretical studies lattice constants; 4.651–4.715 Å, volume; 100.610–104.943 Å³ and are closer to experimental results (4.639–4.640 Å; 99.833–99.897 Å³) compared to other theoretical calculations, which supports the reliability of our calculations. However, each calculation may show slight variations depending on the methodology and initial conditions used. This highlights how the accuracy of calculations is influenced by the chosen theory and parameters.

Discrepancies between theoretical and experimental results may arise from factors such as computational methods, experimental conditions, temperature and thermal expansion, crystal defects, and material preparation techniques. While theoretical studies assume ideal crystal structures, impurities and defects in experimental samples can lead to these differences. However, despite these imperfections, the fact that the results fall within acceptable limits is evidence of the reliability of the theoretical and computational techniques.

Table 2: Elastic constants C_{ij} of cubic HfC.

Cry.		C_{11}	C_{12}	C_{44}	**Ref.**
HfC	Teo.	469.856	95.799	180.936	This work
	Teo.	507.100	103.000	164.800	Krasnenko
	Teo.			152.000	Zaoui
	Exp.	500.000		180.000	Feng
	Exp.		105.000		Singh

Elastic constants are an effective tool for understanding the mechanical behavior of materials. In particular, whether a crystal structure is mechanically stable can be evaluated by calculating its elastic constants. The necessary and sufficient mathematical conditions for a crystal system to be mechanically stable are as follows (Mouhat et al., 2014):

- The C_{ij} matrix must be positive definite.
- All eigenvalues of the C_{ij} matrix must be positive.
- The Sylvester criterion must be satisfied.
- All the principal minors of the C_{ij} matrix must be positive.

These criteria ensure the mechanical stability of the material under mechanical stress. For cubic crystal systems, only three independent elastic constants, C_{11}, C_{12}, and C_{44}, are available. The mechanical stability criteria for cubic systems at 0 GPa are given below (Mouhat et al., 2014; Soykan, 2020).

$$(C_{11} - C_{12}) > 0 \quad (1)$$

$$C_{11} > 0, C_{12} > 0, C_{44} > 0 \quad (2)$$

$$C_{11} + 2C_{12} > 0 \quad (3)$$

$$C_{12} < B < C_{11} \quad (4)$$

Crystal systems that satisfy the following conditions for elastic constants are mechanically stable. When discussing the stability of a crystal system, it is not sufficient to merely have a minimum energy level. In some cases, there may be lower minimum energy levels as well. Therefore, when evaluating stability, it is essential to ensure that, in addition to structural stability, the

conditions for mechanical stability are also met. All of the calculated elastic constants satisfy the conditions $C_{11} > 0$, $C_{12} > 0$, and $C_{44} > 0$. Additionally, the value of $(C_{11} - C_{12})$ was calculated to be 374 GPa, satisfying the mechanical stability condition. Finally, the Bulk modulus, which we calculated as 220.485 GPa, is smaller than C_{11} (469.856 GPa) and larger than C_{12} (95.799 GPa). As seen, all mechanical stability conditions are satisfied.

In this study, the calculated elastic constants and other theoretical-experimental studies are listed in Table 2. The results obtained from our calculations are in agreement with both experimental and theoretical works, although there are some small differences. The C_{11} elastic constant, calculated as 409.856 GPa, is approximately 6.03% smaller than the experimental value from Feng et al. (Feng et al., 2011). Additionally, it is about 7.33% smaller than the value from Krasnenko's theoretical study (Krasnenko et al., 2014). The calculated value of C_{12} (95.799 GPa) is approximately 8.76% smaller than the experimental value from Singh et al. (Singh et al., 2008) and about 6.99% smaller than the theoretical value from Krasnenko et al. (Krasnenko et al., 2014). The calculated value of C_{44} (180.936 GPa) is identical to the experimental value from Feng et al. (Feng et al., 2011). Additionally, the results are approximately 8.92% and 15.44% larger than the theoretical works of Krasnenko and Zaoui, respectively. Our results are in excellent agreement with the studies of Feng, Krasnenko, and Singh (the differences between the values calculated using different methods for the elastic constants are acceptable, with differences up to about 20%). The largest discrepancy is with the result from Zaoui et al. (Zaoui et al., 2005). The reason for this is that Zaoui performed their calculations using the LDA approach, while we used the GGA approach. The GGA approach takes into account the variation of electron density,

whereas the LDA approach calculates based on a constant electron density. Therefore, the results obtained with the GGA approach are closer to the natural state. The validity of this is evidenced by the fact that our results match exactly with the experimental study by Feng. Focusing on Table 2, there is approximately a 15.55% difference between the results of Feng and Zaoui (Feng et al., 2011; Zaoui et al., 2005). This result demonstrates that the GGA approach is more successful than the LDA approach in calculating elastic constants.

Table 3: Calculated Bulk Modulus (B), Shear Modulus (G), Young's Modulus (E), and Poisson's ratio (v) for Cubic HfC.

Mate. P (GPa)		***B***	***G***	***E***	***υ***	**Ref.**
HfC	Teo.	220.485	183.349	430.669	0.174	This work
	Teo.	237.700				Krasnenko
	Teo.	233.000				Feng
	Teo.	247.000	181.00	437.00	0.205	Yang
	Teo.	238.000				Isaev
	Exp.	263.000				Nartowski
	Exp.			430.000	0.180	Krajewski

Based on the DFT theory and simulations performed using the CASTEP code, the elastic constants and the bulk modulus (B), shear modulus (G), and Young's modulus (E) calculated using the Voigt-Reuss-Hill (VRH) approach provide further insights into the material's mechanical behavior. As shown in Table 3 above, the mechanical properties of cubic HfC emphasize the material's high hardness and rigidity.

In this study, the calculated elastic moduli are: Bulk modulus B = 220.485 GPa, Shear modulus G = 183.349 GPa, Young's

modulus E = 430.669 GPa, and Poisson's ratio ν = 0.174. The calculated Bulk modulus (B) value of 220.485 GPa is in excellent agreement with other theoretical studies (Krasnenko et al., 2014; Feng et al., 2011; Yang et al., 2012; Isaev et al., 2007).

However, the Bulk modulus (B) calculated in this study is approximately 16.2% smaller than the value reported in Nartowski's experimental work (Nartowski et al., 1999). The Shear modulus (G), calculated as 183.349 GPa, is in excellent agreement with Yang's theoretical work (Yang et al., 2012). The Young's modulus (E), calculated as 430.669 GPa, is identical to the value reported in Krajewski's experimental work (Krajewski et al., 1998) and only about 1.44% smaller than the value from Yang's theoretical work (Yang et al., 2012).

Finally, the Poisson ratio, calculated as 0.174, is only 3.33% smaller than the value reported in Krajewski's experimental work (Krajewski et al., 1998). Additionally, there is approximately a 15.12% difference with Yang's theoretical work (Yang et al., 2012). In Yang's theoretical study, the Vanderbilt ultrasoft pseudopotential was used, whereas in our work, the OTFG norm-conserving pseudopotential was preferred. The reason for this choice is that while the OTFG norm-conserving pseudopotentials require higher computational clusters in terms of computational load, they provide higher accuracy and precision. The norm-conservation principle is strictly applied, ensuring that the electron density norm is always kept constant, which enhances the accuracy. When more accurate results are required or in light atom systems, the norm-conserving pseudopotential is preferred. In contrast, Yang's calculations using the ultrasoft pseudopotential (USPP) relax the norm-conservation condition, allowing for smaller plane-wave-based calculations. This approach achieves a level of accuracy proportional to the reduced

computational load. While it yields reasonably accurate results, the absence of norm conservation introduces limitations in cases that demand very high precision. In this regard, the approximately 38.89% difference between Yang's calculated Poisson ratio of 0.205 and Krajewski's measured experimental value of 0.180 highlights the importance of potential selection. The difference in the Poisson ratio obtained through the norm-conserving pseudopotential is only about 3.33%. Therefore, the agreement of our results with experimental studies is quite satisfactory.

Poisson's ratio (ν) represents the ratio of deformation in one direction to the deformation in the perpendicular direction under stress. When the Poisson ratio is low, the material can be more brittle, whereas a higher Poisson ratio indicates that the material is more flexible and resilient. Materials with covalent bonding typically exhibit a small Poisson ratio (around $\nu = 0.1$), while ionic materials have a Poisson ratio of 0.25 or higher. The Poisson ratio calculated for HfC in this study is 0.174, indicating that, although HfC is hard, it has a brittle structure. This suggests that under high pressure, instead of undergoing plastic deformation, HfC is more prone to cracking.

The HfC material possesses high Bulk, Young, and Shear moduli, which indicates its strong mechanical strength. These properties make HfC suitable for industrial applications that require high hardness and abrasion resistance, especially in environments with high temperatures and abrasive conditions, such as cutting tools, fusion reactors, and rocket engines. However, its low Poisson’s ratio (0.174) increases the brittleness of HfC, indicating that the material is more likely to crack rather than undergo plastic deformation under high pressure. Therefore, the use of HfC must be carefully designed, taking into account the risk of cracking under

high stress, and material properties should be optimized for specific applications.

References

Clark, S. J., Segall, M. D., Pickard, C. J., Hasnip, P. J., Probert, M. I. J., Refson, K., & Payne, M. C. (2005). First principles methods using CASTEP. *Zeitschrift für Kristallographie - Crystalline Materials, 220*(5–6), 567–570. https://doi.org/10.1524/zkri.220.5.567.65075

Feng, W.-X., Cui, S.-X., Hu, H.-Q., Zhang, G.-Q., & Lv, Z.-T. (2011). Electronic structure and elastic constants of TiC_xN_{1-x}, $Zr_xNb_{1-x}C$ and HfC_xN_{1-x} alloys: A first-principles study. *Physica B: Physics of Condensed Matter, 406(18), 3631*-3635. https://doi.org/10.1016/j.physb.2011.06.058

Fischer, T. H., & Almlof, J. (1992). General methods for geometry and wave function optimization. *The Journal of Physical Chemistry, 96*(24), 9768–9774. https://doi.org/10.1021/j100202a074

Isaev, E. I., Simak, S. I., Abrikosov, I. A., Ahuja, R., Vekilov, Y. K., Katsnelson, M. I., Lichtenstein, A. I., & Johansson, B. (2007). Phonon related properties of transition metals, their carbides, and nitrides: A first-principles study. *Journal of Applied Physics, 10, 123519.* https://doi.org/10.1063/1.2747230

Krajewski, A., D'Alessio, L., & De Maria, G. (1998). Physiso-Chemical and Thermophysical Properties of Cubic Binary Carbides. *Crystal Research and Technology, 33, 341.* https://doi.org/10.1002/(SICI)1521-4079(1998)33:3<341::AID-CRAT341>3.0.CO;2-I

Krasnenko, V., & Brik, M.G. (2014). First-principles calculations of the structural, elastic and electronic properties of

MN_xC_{1-x} (M = Ti, Zr, Hf; $0 \leq x \leq 1$) carbonitrides at ambient and elevated hydrostatic pressure. *Solid State Sciences*, 28, 1-8. https://doi.org/10.1016/j.solidstatesciences.2013.11.012

Kresse, G., & Hafner, J. (1994). Norm-conserving and ultrasoft pseudopotentials for first-row and transition elements. *Journal of Physics: Condensed Matter, 6*(40), 8245. https://doi.org/10.1088/0953-8984/6/40/010

Kresse, G., & Furthmüller, J. (1996). Efficiency of ab-initio total energy calculations for metals and semiconductors using a plane-wave basis set. *Computational Materials Science, 6*(1), 15–50. https://doi.org/10.1016/0927-0256(96)00008-0

Kresse, G., & Furthmüller, J. (1996). Efficient iterative schemes for ab initio total-energy calculations using a plane-wave basis set. *Physical Review B, 54*(16), 11169. https://doi.org/10.1103/PhysRevB.54.11169

Monkhorst, H. J., & Pack, J. D. (1976). Special points for Brillouin-zone integrations. *Physical Review B, 13*(12), 5188–5192. https://doi.org/10.1103/PhysRevB.13.5188

Mouhat, F., & Coudert, F. X. (2014). Necessary and sufficient elastic stability conditions in various crystal systems. *Physical Review B, 90, 224104*. https://doi.org/10.1103/PhysRevB.90.224104

Nartowski, A. M., Parkin, I. P., MacKenzie, M., Craven, A. J., & MacLeod, I. (1999). Solid state metathesis routes to transition metal carbides. *Journal of Materials Chemistry, 9, 1275-1281.* https://doi.org/10.1039/A808642G

Perdew, J. P., Burke, K., & Ernzerhof, M. (1996). Generalized gradient approximation made simple. *Physical Review Letters, 77*(18), 3865–3868. https://doi.org/10.1103/PhysRevLett.77.3865

Rogl, P., Naik, S. K., & Rudy, E. (1977). A Constitutional Diagram of the System TiC-HfC-WC. *Monatsh. Chem., 108, 1189–1211*. https://doi.org/10.1007/BF00897701

Singh, R. K., Singh, R. P., Singh, M. P., & Srivastava, P. C. (2008). Ultrasonic attenuation due to phonon–phonon interaction, thermoelastic loss and dislocation damping in transition metal carbides. *Journal of Physics: Condensed Matter, 20, 345227*. https://doi.org/0.1088/0953-8984/20/34/345227

Soykan, C. (2020). A theoretical approach to the structural, elastic and electronic properties of $Ti_{8-x}V_{4-\gamma}Mo_{x+\gamma+z}Al_{4-z}$ lightweight shape memory alloys for biomaterial implant applications. Physica B: Physics of Condensed Matter, 598, 412416. https://doi.org/10.1016/j.physb.2020.412416

Wu, Z. G., Chen, X.-J., Struzhkin, V. V., & Cohen, R. E. (2005). Trends in elasticity and electronic structure of transition-metal nitrides and carbides from first principles. *Physical Review B, 71, 214103*. https://doi.org/10.1103/PhysRevB.71.214103

Yang, J., & Gao, F. (2012). First principles calculations of mechanical properties of cubic 5d transition metal monocarbides. *Physica B: Physics of Condensed Matter, 407, 3527-3534*. https://doi.org/10.1016/j.physb.2012.05.016

Zaoui, A., Bouhafs, B., & Ruterana, P. (2005). First-principles calculations on the electronic structure of TiCxN1−x, ZrxNb1−xC

and HfCxN1−x alloys. *Materials Chemistry and Physics, 91, 108-115*. https://doi.org/10.1016/j.matchemphys.2004.10.056

CHAPTER V

An Ab-*initio* Study on the Crystal Structure and Mechanical Properties of Hexagonal Zirconium Diboride

Cengiz SOYKAN[1]

Introduction

Zirconium diboride (ZrB_2), a key member of the ultra-high temperature ceramics (UHTCs) family, exhibits exceptional physical properties such as a high melting point, significant hardness, excellent thermal and electrical conductivity, low work function, and strong oxidation resistance (Opeka et al., 1999; Fahrenholtz et al., 2007; Wang et al., 2009). These unique characteristics make ZrB_2 an ideal choice for thermal protection in extreme chemical and thermal conditions, including hypersonic flight and atmospheric reentry (Levine et al., 2002; Savino et al., 2005; Opeka et al., 2004).

[1] Assoc. Prof. Dr., Kırşehir Ahi Evran University, Health Services Vocational School, Department of Medical Services and Techniques, Kırşehir/Turkey, Orcid: 0000-0003-0897-2384, cengiz.soykan@ahievran.edu.tr

UHTCs generally comprise compounds that maintain chemical and physical stability at high temperatures and in oxidizing environments. Typically, UHTCs with melting temperatures exceeding 3000 K are made up of refractory borides, carbides, nitrides, and oxides of early transition metals (Opeka et al., 1999; Fahrenholtz et al., 2007; Wang et al., 2009; Levine et al., 2002; Savino et al., 2005; Opeka et al., 2004; Cai et al., 2006; Wang et al., 2009).

In the field of solid-state theory, predicting the hypothetical structures of inorganic crystal solids based solely on chemical composition information, without referring to experimental structural data, is a significant and challenging undertaking in materials design (DiSalvo, 1990; Pannetier et al., 1990; Oganov & Glass, 2008; Catlow & Price, 1990; Schön et al., 1996). Experimental and theoretical studies on the fundamental physical properties of ZrB_2 are available (Fahrenholtz et al., 2007; Vajeeston et al., 2001; Wang et al., 1994; Zhang et al., 2008; Li et al., 2010; Card Number, 34-0423; Okamoto et al., 2003).

ZrB_2 crystallizes in the P6/mmm space group and has an omega-type hexagonal structure. The B^{2-} atoms form a 9-coordinated geometric structure by bonding with six equivalent Zr^{4+} atoms and three equivalent B^{2-} atoms. The Zr^{4+} atoms, in turn, bond with twelve equivalent B^{2-} atoms, forming a mixture of edge- and face-sharing ZrB_{12} cuboctahedra.

This chapter will discuss the crystal structure, bonding characteristics, and mechanical durability of ZrB_2, while also evaluating its potential for advanced technology applications. A detailed analysis of its structural and mechanical properties will be provided.

2. Method

In this study, first-principles calculations were performed to determine the structural and mechanical properties of ZrB_2. The calculations were carried out using the CASTEP software, based on density functional theory (DFT) (Clark et al., 2005; Kresse et al., 1996; Kresse et al., 1996; Kresse et al., 1994). The exchange-correlation function was considered using the generalized gradient approximation (GGA-PBE) functional approach (Perdew et al., 1996). This approach is commonly used for accurately modeling the electronic structure of transition metal borides.

The structural properties of ZrB_2 were optimized according to criteria with an energy tolerance of 10^{-5} eV/atom, a maximum force of 0.03 eV/Å, and a maximum displacement of 0.001 Å (Fischer et al., 1992). To ensure the accuracy of the calculations, an energy cutoff value of 650 eV was chosen. This energy value improves the accuracy of the crystal structure parameters, thereby ensuring the reliability of the calculations.

The k-point distribution in the Brillouin zone was set to 12x12x12 (Monkhorst et al., 1976). This k-point density balances the speed and accuracy of the calculations, ensuring the correct determination of the structural parameters of ZrB_2. As a result of the structural optimizations, the lattice constants (a, b, c, Å) and volume (V, $Å^3$) of ZrB_2 were obtained. Additionally, the optimization process led to the energy minimization of ZrB_2, identifying the lowest energy configuration.

The mechanical properties of ZrB_2, including the elastic constants (C_{ij}), bulk modulus (B), shear modulus (G), Young's modulus (E), and Poisson's ratio (v), were calculated. The elastic constants were determined by applying homogeneous deformations

and using the resulting stress-strain relationships. In particular, the strain-stress method used to calculate the elastic constants is an ideal technique for accurately reflecting the material's mechanical durability and elastic properties.

The bulk modulus and shear modulus calculations were performed using the Voigt-Reuss-Hill (VRH) approach. This method improves the accuracy of the elastic constants and mechanical moduli, allowing for a comprehensive examination of ZrB_2's mechanical strength. As a result of these calculations, insights were gained into the material's compressibility and resistance to deformation.

To evaluate the accuracy of the calculations, the structural parameters of ZrB_2 were compared with other experimental data from the literature, and it was observed that the obtained results are in good agreement (Card Number 34-0423; Okamoto et al., 2003; Vajeeston et al., 2001; Fahrenholtz et al., 2007). Additionally, the calculated mechanical properties were compared with previous theoretical studies in the literature, and similar results were obtained (Vajeeston et al., 2001; Zhang et al., 2008; Wang et al., 1994). These findings confirm the reliability and accuracy of the computational method.

3. Results

The structural and mechanical properties of hexagonal ZrB_2 were investigated using Density Functional Theory (DFT) calculations with the Generalized Gradient Approximation (GGA) and Perdew-Burke-Ernzerhof (PBE) functional, as presented below. Additionally, the agreement with prior experimental and theoretical studies is analyzed, and the importance of these properties for applications under high stress is evaluated.

The crystal structure of hexagonal ZrB_2, shown in Figure 1, exhibits a layered structure where zirconium (Zr) atoms are arranged in a single plane, and boron (B) atoms are arranged in a honeycomb-like structure. This structure is characterized by the P6/mmm space group symmetry.

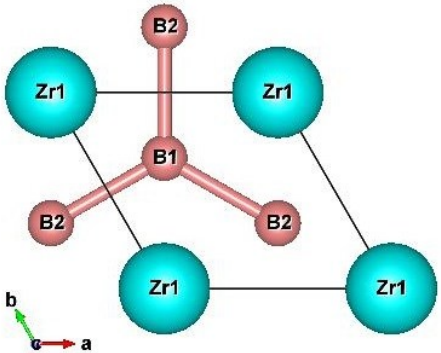

Figure 1: The crystal structure of hexagonal ZrB_2.

Table 1: The lattice parameters of ZrB_2.

Cry.		Lattice Constans (A^0), a, b, c			Volume (A^3)	Ref.
	Teo.	3.172	3.172	3.534	30.793	This work
	Teo.	3.170	3.170	3.548	30.880	Li
	Teo.	3.197	3.197	3.561	31.520	Vajeeston
ZrB_2	Teo.	3.168	3.168	3.536		Zhang
	Teo.	3.165	3.165	3.547	30.771	Wang
	Exp.	3.169	3.169	3.530	30.701	Card Number
	Exp.	3.170	3.170	3.533	30.746	Vajeeston

Table 1 presents the our calculated structural properties for ZrB_2, along with a comparison to previous studies. The lattice parameters of the hexagonal ZrB_2 crystal structure are calculated as a = b = 3.172 Å, c = 3.534 Å, and the unit cell volume V = 30.793 $Å^3$.

The theoretical calculations of ZrB_2 have been conducted in various studies, generally yielding similar results. While most of these studies show small differences in lattice parameters, the calculated values are quite close to each other. For instance, the values found in Li's work show good agreement with those obtained in this study, which reports parameters of 3.170 Å, 3.170 Å, and 3.548 Å (unit cell volume of 30.880 $Å^3$) (Li et al., 2010). In Vajeeston's study, the lattice parameters are given as 3.197 Å, 3.197 Å, and 3.561 Å, showing slightly larger differences along with a unit cell volume of 31.520 $Å^3$ (Vajeeston et al., 2001). Zhang and Wang's studies also present similar values. Zhang's results for a, b, and c are 3.168 Å, 3.168 Å, and 3.536 Å, while Wang's are 3.165 Å, 3.165 Å, and 3.547 Å. These results also align well with the values obtained in this study, showing only small differences (Zhang et al., 2008; Wang et al., 1994).

Experimental studies provide data obtained through measurements to determine the structural properties of ZrB_2 (Vajeeston et al., 2001; Card Number 34-0423). When compared with our calculations, the experimental results show excellent agreement. While the experimental data are generally very close to our results and theoretical values, some small deviations are observed due to differences in measurement methods and conditions. However, each calculation may show small differences depending on the methodology and initial conditions used. This highlights how the accuracy of the calculations is dependent on the theory and parameters employed.

Table 2: The calculated elastic constants C_{ij} of hexagonal ZrB_2.

P (GPa)	C_{11}	C_{12}	C_{13}	C_{33}	C_{44}	C_{66}	Ref.
Teo.	553.60	59.72	112.70	431.40	249.67	246.94	This work
Teo.	504.40	90.50	112.00	427.40	240.90		Li
Teo.	578.00	65.00	121.00	436.00	252.00		Zhang
	586.00	71.00	138.00	472.00	271.00		
Exp.	581.00	55.00	121.00	445.00	240.00		Okamoto

Table 2 presents the elastic constants (C_{ij}) calculated for ZrB_2. All six independent elastic constants ($C_{11} > 0$, $C_{12} > 0$, $C_{13} > 0$, $C_{33} > 0$, $C_{44} > 0$, and $C_{66} > 0$) are positive for hexagonal crystal systems. Additionally, the conditions $C_{11} > |2C_{12}|$ and $(C_{11} + 2C_{12})C_{33} > 2C_{13}^2$ are also satisfied. All the calculated Cij elastic constant values meet the mechanical stability criteria established for hexagonal crystal systems (Yan et al., 2011). These results indicate that the bonds within the crystal exhibit a distinct anisotropic structure.

In this study, the elastic constants are calculated as follows: C_{11} = 553.60 GPa, C_{12} = 59.72 GPa, C_{13} = 112.70 GPa, C_{33} = 431.40 GPa, C_{44} = 249.67 GPa, and C_{66} = 246.94 GPa. In Li's study, the values were C_{11} = 504.40 GPa, C_{12} = 90.50 GPa, and C_{13} = 112.00 GPa (Li et al., 2010). While the C_{11} and C_{12} elastic constants are slightly higher in this study, Li's study shows a higher value for C_{12}. In Zhang's study, the elastic constants are reported over a wider range: C_{11} = 578.00 GPa, C_{12} = 65.00 GPa, C_{13} = 121.00 GPa, C_{33} = 436.00 GPa, C_{44} = 252.00 GPa, and C_{66} = 271.00 GPa (Zhang et al., 2008). The theoretical results provided are similar to those obtained in this study, but differences, especially in the C_{11} and C_{13} values, are observed. These differences may arise due to the influence of the theoretical model and computational methods used.

In Okamoto's experimental study, the values obtained for the elastic constants are C_{11} = 581.00 GPa, C_{12} = 55.00 GPa, C_{13} = 121.00 GPa, C_{33} = 445.00 GPa, and C_{66} = 240.00 GPa (Okamoto et al., 2003). In this study, the calculated C_{11} value shows strong agreement with the findings of Okamoto. However, the results for C_{12} and C_{13} show some differences. Specifically, the C_{12} value is lower in this study compared to Okamoto's work. These differences may arise due to experimental conditions, sample purity, or measurement techniques. While Okamoto's results are largely consistent with the theoretical calculations in this study, some small differences are also observed.

The mechanical properties of hexagonal ZrB_2, as presented in Table 3, highlight its exceptional hardness and rigidity. These properties, derived from the elastic constants obtained through DFT-based simulations using the CASTEP code, include the bulk modulus (B), shear modulus (G), and Young's modulus (E), offering deeper insights into the material's mechanical behavior.

Table 3: The calculated bulk modulus B, shear modulus G, Young's modulus E, and Poisson's ratio v for ZrB_2.

Material P (GPa)		B	G	E	υ	**Ref.**
ZrB_2	Teo.	233.80	230.11	519.80	0.132	This work
	Teo.	228.80	208.50	483.50	0.148	Li
	Teo.	238.00	226.00	520.00	0.137	Zhang
	Teo.	195.00				Vajeeston
	Exp.	215.00		489.00		Fahrenholtz
	Exp.	215.00				Vajeeston

In this study, the calculated elastic moduli are as follows: Bulk modulus B = 233.80 GPa, Shear modulus G = 230.11 GPa, Young's modulus E = 519.80 GPa, and Poisson's ratio ν = 0.132.

In Li's study, the Bulk modulus was calculated as 228.80 GPa, the Shear modulus as 208.50 GPa, and the Young's modulus as 483.50 GPa, with a Poisson's ratio of 0.148 (Li et al., 2010). In our study, the Bulk modulus and Shear modulus were calculated to be slightly higher than those in Li's results, while a difference in the Young's modulus was also observed. These discrepancies can be attributed to differences in the computational methods and theoretical models used.

In Zhang's study, the Bulk modulus was determined to be 238.00 GPa, the Shear modulus as 226.00 GPa, and the Young's modulus as 520.00 GPa. These results are in good agreement with the values calculated in our study (Zhang et al., 2008). In Vajeeston's study, the Bulk modulus was calculated to be 195.00 GPa, but other moduli were not provided. This may suggest the use of a different theoretical approach or model in their calculations (Vajeeston et al., 2001).

In Fahrenholtz's experimental study, the Bulk modulus was measured at 215.00 GPa, and the Young's modulus was found to be 489.00 GPa, with the Poisson ratio not provided. These results are generally in agreement with the theoretical calculations in this study. The similarity in the Young's modulus values is particularly noteworthy. The small differences in the Bulk modulus could be attributed to experimental conditions or factors such as sample purity. In Vajeeston's experimental work, only the Bulk modulus was reported as 215.00 GPa, which is in close agreement with the theoretical calculations presented in this study.

The Poisson ratio has not been reported experimentally; however, it was found to be 0.148 and 0.137 in the theoretical studies by Li and Zhang, respectively. In this study, the calculated Poisson ratio is 0.132. This value is highly consistent with Zhang's result and relatively close to Li's findings. The Poisson ratio (ν) represents the ratio of deformation in one direction to deformation in the perpendicular direction of a material. A lower Poisson ratio indicates that the material is more brittle, while a higher Poisson ratio suggests greater flexibility and toughness. If the bonding structure of materials is covalent, the Poisson ratio is small (around $v = 0.1$); on the other hand, if it is ionic, the Poisson ratio is 0.25 or higher. The Poisson ratio we calculated is 0.132. This low Poisson ratio indicates that ZrB_2, while hard, has a brittle nature, meaning it tends to fracture easily under high pressure rather than undergoing plastic deformation.

The calculated structural and mechanical properties of ZrB_2 make it an ideal material for a wide range of industrial applications. Its high hardness and low Poisson ratio contribute to its durability under high temperatures and proportional mechanical stress. These characteristics enhance its suitability for industries such as defense, aerospace technologies, and high-temperature applications. Additionally, its high resistance to wear and mechanical durability make it applicable in industrial fields like armored vehicles and cutting tools. Consequently, ZrB_2 holds potential as a material for various industrial sectors where high temperature, mechanical durability, and thermal conductivity are critical requirements.

This study has shown that the structural integrity and mechanical durability of ZrB_2 stem from its anisotropic bonding structure and hexagonal symmetry. These findings suggest that ZrB_2 is a promising candidate for advanced engineering applications.

References

Cai, Y. Q., Zhang, L. T., Zeng, Q. F., Cheng, L. F., & Xu, Y. D. (2006). First-principles study of vibrational and dielectric properties of β−Si_3N_4 Physical Review B, 74(17), 174301. https://doi.org/10.1103/PhysRevB.74.174301

Catlow, C. R. A., & Price, G. D. (1990). Computer modelling of solid-state inorganic materials. Nature, 347 (6290), 243–248.

Clark, S. J., Segall, M. D., Pickard, C. J., Hasnip, P. J., Probert, M. I. J., Refson, K., & Payne, M. C. (2005). First principles methods using CASTEP. *Zeitschrift für Kristallographie - Crystalline Materials, 220*(5–6), 567–570. https://doi.org/10.1524/zkri.220.5.567.65075

DiSalvo, F. J. (1990). Thermoelectric cooling and power generation. Science, 247(4946), 649–655. https://doi.org/10.1126/science.285.5428.703

Fahrenholtz, W. G., Hilmas, G. E., Talmy, I. G., & Zaykoski, J. A. (2007). Refractory diborides of zirconium and hafnium. Journal of the American Ceramic Society, 90(5), 1347–1364. https://doi.org/10.1111/j.1551-2916.2007.01583.x

Fischer, T. H., & Almlof, J. (1992). General methods for geometry and wave function optimization. *The Journal of Physical Chemistry, 96*(24), 9768–9774. https://doi.org/10.1021/j100202a074

International Centre for Diffraction Data. (n.d.). Powder diffraction file, Card Number 34-0423.

Kresse, G., & Hafner, J. (1994). Norm-conserving and ultrasoft pseudopotentials for first-row and transition elements. *Journal of Physics: Condensed Matter, 6*(40), 8245. https://doi.org/10.1088/0953-8984/6/40/010

Kresse, G., & Furthmüller, J. (1996). Efficiency of ab-initio total energy calculations for metals and semiconductors using a plane-wave basis set. *Computational Materials Science, 6*(1), 15–50. https://doi.org/10.1016/0927-0256(96)00008-0

Kresse, G., & Furthmüller, J. (1996). Efficient iterative schemes for ab initio total-energy calculations using a plane-wave basis set. *Physical Review B, 54*(16), 11169. https://doi.org/10.1103/PhysRevB.54.11169

Levine, S. R., Opila, E. J., Halbig, M. C., Kiser, J. D., Singh, M., & Salem, J. A. (2002). Evaluation of ultra-high-temperature ceramics for aeropropulsion use. Journal of the European Ceramic Society, 22(14–15), 2757–2767. https://doi.org/10.1016/S0955-2219(02)00140-1

Li, H., Zhang, L., Zeng, Q., Wang, J., Cheng, L., Ren, H., & Guan, K. (2010). Crystal structure and elastic properties of ZrB compared with ZrB2: A first-principles study. Computational Materials Science, 49, 814-819. https://doi.org/10.1016/j.commatsci.2010.06.027

Monkhorst, H. J., & Pack, J. D. (1976). Special points for Brillouin-zone integrations. *Physical Review B, 13*(12), 5188–5192. https://doi.org/10.1103/PhysRevB.13.5188

Oganov, A. R., & Glass, C. W. (2008). Crystal structure prediction using ab initio evolutionary techniques: Principles and applications. Journal of Physics: Condensed Matter, 20(6), 064210. https://doi.org/ 10.1088/0953-8984/20/6/064210

Okamoto, N. L., Kusakari, M., Tanaka, K., Inui, H., Yamaguchi, M., & Otani, S. (2003). Thermal conductivity of single-crystal ZrB_2 and TiB_2. Journal of Applied Physics, 93(1), 88–93. https://doi.org/10.1063/1.1525404

Opeka, M. M., Talmy, I. G., & Zaykoski, J. A. (2004). Oxidation-based materials selection for 2000◦C+hypersonic aerosurfaces: Theoretical considerations and historical experience. Journal of Materials Science, 39(19), 5887–5904.

Opeka, M. M., Talmy, I. G., Wuchina, E. J., Zaykoski, J. A., & Causey, S. J. (1999). Mechanical, Thermal, and Oxidation Properties of Refractory Hafnium and zirconium Compounds. Journal of the European Ceramic Society, 19(13–14), 2405–2414. https://doi.org/10.1016/S0955-2219(99)00129-6

Pannetier, J., Bassas-Alsina, J., Rodriguez-Carvajal, J., & Caignaert, V. (1990). Prediction of crystal structures from crystal chemistry rules by simulated annealing. Nature, 346 (6282), 343–345.

Perdew, J. P., Burke, K., & Ernzerhof, M. (1996). Generalized gradient approximation made simple. *Physical Review Letters, 77*(18), 3865–3868. https://doi.org/10.1103/PhysRevLett.77.3865

Savino, R., Fumo, M. D. S., Paterna, D., & Serpico, M. (2005). Aerothermodynamic study of UHTC-based thermal protection

systemsStudio aerotermodinamico di sistemi di protezione termica basati su UHTC. Aerospace Science and Technology, 9(2), 151–160. https://doi.org/10.1016/j.ast.2004.12.003

Schön, J. C., & Jansen, M. (1996). First Step Towards Planning of Syntheses in Solid-State Chemistry: Determination of Promising Structure Candidates by Global Optimization. Angewandte Chemie International Edition, 35(12), 1286–1306. https://doi.org/10.1002/anie.199612861

Vajeeston, P., Ravindran, P., Ravi, C., & Asokamani, R. (2001). Electronic structure, bonding, and ground-state properties of AlB2-type transition-metal diborides. Physical Review B, 63(4), 045115. https://doi.org/10.1103/PhysRevB.63.045115

Wang, J. J., Zhang, L. T., Zeng, Q. F., Vignoles, G. L., Cheng, L. F., & Guette, A. (2009). Adsorption of atomic and molecular oxygen on 3C-SiC(111) and (111) surfaces: A first-principles study. Physical Review B, 79(12), 125304. https://doi.org/10.1103/PhysRevB.79.125304

Wang, X. B., Tian, D. C., & Wang, L. L. (1994). Structural and electronic properties of ZrB_2. Journal of Physics: Condensed Matter, 6, 185.

Wang, Y. G., Liu, W., Cheng, L. F., & Zhang, L. T. (2009). Preparation and properties of 2D C/ZrB2-SiC ultra high temperature ceramic composites. Materials Science and Engineering: A, 524(1–2), 129–133. https://doi.org/10.1016/j.msea.2009.07.005

Yan, H., Wei, Q., Chang, S., & Guo, P. (2011). A first-principle calculation of structural, mechanical and electronic

properties of titanium borides. *Transactions of Nonferrous Metals Society of China, 21*, 1627–1633. https://doi.org/10.1016/S1003-6326(11)60906-0

Zhang, X. H., Luo, X. G., Han, J. C., Li, J. P., & Han, W. B. (2008). Electronic structure, elasticity and hardness of diborides of zirconium and hafnium: First principles calculations. Computational Materials Science, 44(2), 411–421. https://doi.org/10.1016/j.commatsci.2008.04.002

CHAPTER VI

Health-Related Applications of Ionizing Radiation

Firdevs Banu ÖZDEMİR[1]
Tuba ÖZDEMİR ÖGE[2]
Mecit ÖGE[3]

1. Introduction

The term 'radiation' is used to describe penetrating rays, meaning rays capable of passing through matter. Radiation refers to the form of energy in waves or particles, or energy emitted in this manner. Electromagnetic radiations, arranged in increasing order of frequency, include radio waves, microwaves, infrared radiation, visible light, ultraviolet radiation, X-rays, and gamma rays.

[1] Kütahya Health Sciences University, Simav Health Services Vocational School, Simav-Kütahya, Türkiye (ORCID: 0000-0002-7935-2062) email: firdevsbanu.ozdemir@ksbu.edu.tr
[2] Bartın University, Faculty of Forestry, Department of Forestry Industry Engineering, Bartin, Turkey (ORCID ID, 0000-0001-6690-7199) e-mail: tozdemir@bartin.edu.tr
[3] Bartın University, Faculty of Engineering, Architecture and Design, Department of Mechanical Engineering, Bartın, Türkiye (ORCID: 0000-0001-5243-0828) email: mecitoge@bartin.edu.tr

Electromagnetic radiation can be listed in ascending order of frequency as follows. In this sequence, as frequency increases, the wavelength decreases, and the energy of the radiation rises.

The common characteristic of rays with different types and sources is their ability to penetrate matter and the human body. The penetration capabilities of various radiations differ. Low-energy rays, such as visible light, are not penetrative. However, X-rays and gamma rays, which share the same fundamental characteristics as visible light, differ in their penetration ability due to their higher energy and shorter wavelengths. Lower-frequency radiation predominantly exhibits wave-like behavior, while ultraviolet radiation or those with higher frequencies are better explained through their particle nature. The most common forms of particle radiation are alpha and beta radiation, typically produced during radioactive decay. Ionizing radiation, specifically from radon (Rn-222) and its decay products, emits highly ionizing alpha particles, which are a major source of natural radiation exposure. It also discusses the health risks associated with prolonged exposure to ionizing radiation from radon in water, linking it to potential cancer risks due to its ability to damage biological tissues (Özdemir, 2006). Ionizing radiation can be quantified using highly sensitive radiation detectors (Özdemir, 2016). Ionizing radiation plays a vital role in the healthcare sector. Radiology, radiotherapy, diagnostic radionuclide use, and other medical imaging applications almost all utilize ionizing radiation. Therefore, it is very important to have detailed information about the basic principles of ionizing radiation, its areas of use, potential risks, safe applications and future developments.

2. What is Ionizing Radiation?

Radiation is the transfer of energy in the form of electromagnetic waves or particles. Ionizing radiation is a type of high-energy radiation that separates electrons from atoms and causes the formation of ions. Alpha and beta particles, X and γ-rays are among the types of ionizing radiation. High-energy radiation causes serious effects on biological systems. Ionizing electromagnetic radiation, such as X-rays and γ-rays, has the ability to break chemical bonds in the substance it comes into contact with. Despite its harmful effects on living things, X and γ-rays, which are types of ionizing radiation, have a wide range of use in the diagnosis and treatment of diseases (Cho et al., 2015).

3. The Importance of Ionizing Radiation in the Health Sector

Ionizing radiation is frequently preferred in the medical field for both diagnosis and treatment purposes. Types of ionizing radiation, such as X-rays and γ-rays, have a wide range of uses from medical imaging to cancer treatment. However, the safe and effective application of these technologies necessitates the existence of certain regulations and control mechanisms for patients and healthcare professionals. For ensuring radiation safety, it is essential to comply with international standards and protocols introduced by international institutions such as International Commission on Radiological Protection (ICRP), which provide guidelines on protection from radiation exposure.

3.1. Ionizing Radiation in Imaging Techniques

In the field of medical imaging, ionizing radiation is used as an important element of advanced technology devices such as X-ray devices, computerized tomography (CT) and positron emission

tomography (PET). These methods are of critical importance in the early diagnosis of diseases and the planning of the treatment process. However, radiation exposure must be meticulously controlled when using these devices (Brenner & Hall, 2007).

X-ray devices provide detailed images of the internal structures of the body using X-rays for medical imaging purposes. X-rays are high-energy electromagnetic waves and are absorbed at varying rates according to the different properties of the tissues. These absorption differences make it possible to distinguish between bones, soft tissues and air-filled spaces by enhancing the contrast. X-ray devices consist of basic components such as an X-ray tube, collimator, detector and imaging system. The X-ray tube produces X-rays by the sudden deceleration of electrons accelerated between the cathode and anode; during this process, the kinetic energy of the electrons is converted into photon energy. The X-rays formed are directed and focused to the target area with the help of a collimator. Detectors detect the X-rays passing through the tissues and convert them into electrical signals, and then these signals are processed by the imaging system to create an image. The design of X-ray devices is constantly being improved to improve image quality and reduce the amount of radiation patients are exposed to (Hobbie et al. 2015).

Photoelectric effect occurs when photons interact with and eject electrons from an atom, leading to ionization, which is effective at higher photon energies that exceed electron binding energy. In Compton scattering, a photon collides with a loosely bound electron, loses energy, and changes direction, thus influencing interactions at moderate photon energies (Özdemir, 2011).

In radioscopy and radiography applications, short-wavelength hard beams obtained from X-ray tubes operating at

accelerating voltages of 500-200 kV are generally preferred. These beams are absorbed at various rates depending on the differences in the atomic weight, thickness and density of tissues in the human body, and thus provide images in different gray tones on X-ray films (Dhawan, 2011). X-ray imaging is based on the principle that tissues absorb X-rays at different rates; bones absorb more X-rays, and soft tissues absorb less X-rays. X-rays passing through the patient are directed to the detector, where they are converted to light and then to voltage and digitized. A grid is placed in front of the detector to increase image contrast. For example, in a chest X-ray, the ribs appear light gray, while the soft tissues of the lungs appear dark gray (Smith & Webb, 2010). The widespread use of digital detectors has made dose optimization possible while accelerating the imaging process. In addition, portable X-ray devices offer the opportunity to make rapid diagnoses in emergency situations and intensive care units. In order for X-ray devices to be used safely and effectively, operators must have sufficient knowledge about the operating principles of the devices and radiation safety. Therefore, regular training and quality control processes are of great importance for the safety of both patients and healthcare professionals.

Computed Tomography (CT) devices are advanced medical imaging devices that create cross-sectional images of the body using X-rays. CT scans are created by combining X-ray data taken from different angles by a computer, allowing organs, bones and soft tissues to be examined in detail (Seeram, 2023). CT devices work on the principle that high-energy X-rays are absorbed at different rates as they pass through body tissues. Differences in the absorption rates of tissues vary depending on their properties such as density and composition, allowing different tissues to be distinguished from each other. For example, bone tissues absorb more X-rays due to their

high density and appear in lighter tones (white) in the images, while soft tissues and air-filled areas are represented in darker tones due to less absorption (Kalender, 2011). Since X-rays used in Computed Tomography (CT) scans contain ionizing radiation, it is of great importance to minimize the radiation dose to which patients are exposed. In this regard, low-dose protocols and advanced imaging techniques are applied in modern CT devices, thus reducing radiation exposure without compromising image quality. In conclusion, CT devices are advanced imaging systems that create detailed cross-sectional images of the body using X-rays and are of vital importance in medical diagnostic processes. Thanks to technological advances, the imaging quality of CT devices is constantly improving, while at the same time, the radiation doses to which patients are exposed are minimized (Boone et al., 2019).

Mammography devices are medical imaging systems that provide high-resolution images using low-energy X-rays for detailed imaging of breast tissue. These devices produce low-energy X-rays with X-ray tubes that generally operate between 20-30 kilovolts (kV). Such X-rays allow the detection of cancerous lesions by better emphasizing density differences in breast tissue and play a critical role in early diagnosis processes (Hogg, et al., 2015). The energy level of X-rays used in mammography devices is carefully determined to provide the best contrast between different components of breast tissue. Low-energy X-rays offer a significant advantage in the early diagnosis process by making the differences between fat tissue, glandular tissue and potential tumors more apparent. The dosage of X-rays used in mammography devices is carefully optimized to minimize the amount of radiation that patients are exposed to. This approach is of great importance both in terms of ensuring patient safety and maintaining high image quality. As a

result, the low-energy X-rays used in mammography devices are designed to provide detailed, high-contrast images of breast tissue. This feature is critical for early diagnosis of breast cancer and effective treatment planning (Dance et al., 2011). The risk of breast cancer from radiation in mammography screening in women over the age of 40 is reported to be low compared to the mortality reduction provided by screening and should not be a deterrent (Yaffe, M. J., & Mainprize, J. G., 2011). Mammography is a widely used method for early diagnosis of breast cancer, but more advanced tomographic methods such as breast tomosynthesis have been developed with digital technologies. Breast tomosynthesis, which has the potential to replace mammography, has been investigated through research in areas such as system design, geometry, technical improvement, X-ray scattering, and radiation dose (Sechopoulos, 2013).

During fluoroscopy, which is another methodology, a contrast agent that can be tracked with X-rays is given to the patient and its movement inside the body is monitored (Wang et al., 2006).

3.2 Radiotherapy and Ionizing Radiation

Radiation therapy is a treatment method that aims to destroy cancer cells using ionizing radiation. With this method, radiation is applied to the target area and the growth and spread of cancerous tissues are prevented. Modern radiotherapy techniques aim to increase the effectiveness of the treatment while minimizing side effects. While ionizing radiation is used in the treatment of both cancer and non-cancer diseases, the increasing importance of this exposure, even at low doses, with cancer and other diseases requires that medical, occupational and environmental effects be taken into account (Hamada, 2024).

Radiation therapy is basically divided into two groups as external and internal radiotherapy. In external radiotherapy, radiation is directed from outside the body to the target area, while internal radiotherapy (brachytherapy) is performed by placing radioactive substances directly into the area to be treated. These methods are widely used in the treatment of many diseases, especially cancer treatment (Joiner & van der Kogel, 2016). In cancer treatment, ionizing radiation can be applied alone or in combination with other treatment methods. Radiotherapy has been shown to increase treatment success, especially when applied with chemotherapy. This method aims to focus only on the targeted area and cause minimum damage to healthy tissues.

Radiation therapy usage rates vary between countries. In the study conducted by Delaney and colleagues, based on evidence-based guidelines, radiotherapy use trees were created and analyzed with epidemiological data in order to estimate the ideal rate at which cancer patients should receive radiotherapy at least once in their lifetime. (Delaney et al., 2005).

3.2.1 High Energy Photon in Radiotherapy

High energy photons of 6 MV and above are frequently preferred in the treatment of deep tumors. These energies minimize skin damage and allow higher doses to be delivered effectively to the tumor area. However, neutron contamination may occur as a result of interaction with heavy metals in the structure of linear accelerators during the use of high-energy photons. This unwanted radiation exposure requires careful measurement and control of neutron dose.

Şahin et al. (2016) examined the dosimetric properties of physical and virtual wedge filters used in radiotherapy and evaluated

their advantages and disadvantages. Measurements were made with 6 MV and 15 MV X-rays at different field sizes and depths. It was observed that the environmental dose of virtual wedge filters was higher than physical wedges, but the wedge angle had no effect in small areas, and this effect increased in large areas. While the environmental dose increased as the depth and field size increased in physical wedges, the environmental dose decreased as the wedge angle increased. Virtual wedge filters provide advantages due to ease of set-up, short treatment time and angle alternatives in planning (Şahin, et al., 2016).

In radiotherapy applications where high-energy photons are used, the effects of equipment such as treatment tables on the dose distribution should also be considered. For example, research on the effect of carbon fiber tables on dose distribution suggests that such equipment should be taken into consideration in treatment planning (Gürsoy, 2013).

3.2.2 Gamma Ray in Radiotherapy

The Co-60 device consists of a source emitting 1.25 MeV γ-rays, a gantry that can rotate 360 degrees, a collimator that directs the beam, and a control console. The source inside the lead shield aligns with the collimator during irradiation and the field size can be adjusted. The device is effective in the treatment of tumors with a depth of 10 cm, skin doses are high and the dose distribution at the field edge is limited. In patients with a thickness greater than 20 cm, linear accelerators should be preferred, especially for the abdomen and hip regions (MEGEP, 2012).

Gamma Knife radiosurgery is an effective method in the treatment of brain and skull base lesions, but multidisciplinary evaluation and planning are required for patient suitability. Gamma Knife radiosurgery is a method that treats lesions safely and precisely by

targeting γ-rays emitted from a 201 cobalt-60 source with millimeter accuracy. This method, which is applied using stereotactic frame and imaging technologies, provides effective results in the treatment of cerebral vascular malformations, tumors, trigeminal neuralgia and some movement and psychiatric disorders. It shows superior success especially for arteriovenous malformations, acoustic neuromas and cerebral metastases (Lindquist, 1995).

3.2.3 Accelerated Electron

High energy electron beams (up to 20 MeV) show a sharp dose decrease with depth and this feature can be improved by adding photon fraction. This technique allows use up to 17 cm depth near sensitive organs. In addition, dose increase is possible with sharp penumbra and contrast beams at 4-5 cm depth. The skin can be protected by transmitting photons from the same portal as electrons. These physical features have been used in the optimization of clinical treatments (Karlsson & Zackrisson, 1997).

3.3 Nuclear Medicine

Ionizing radiation is used for both diagnostic and therapeutic purposes in nuclear medicine. Since 1936, different radioactive isotopes have been used in the field of nuclear medicine (Samei & Peck, 2019). In 1938, the first article on the diagnostic use of Iodine (131I) in thyroid diseases was published, leading to the rapid development of nuclear medicine. Nuclear scintigraphy is a functional imaging method that reflects metabolic activities; X-ray, CT and MRI provide anatomical imaging. Nuclear medicine imaging includes SPECT and PET techniques. Despite their low spatial resolution, these methods have high molar sensitivity, which allows the study of small changes in physiology (Lecomte, 2009).

Positron Emission Tomography/Computed Tomography (PET/CT), an advanced treatment imaging method, provides the retention of metabolic and anatomical information together and provides detailed imaging of target tissues with ionizing radiation obtained from radioactive isotopes. It is one of the fastest developing technologies in medical imaging and is available in more than 5000 centers worldwide (Beyer et al., 2011). Positron Emission Tomography (PET) is based on the detection of 511 keV annihilation photons formed by the interaction of positrons and electrons. Radionuclides such as Carbon-11, Fluorine-18 and Gallium-68 are used. CT images provide scintigraphic separation and attenuation correction. PET image quality has increased with TOF (Time of Flight) technology. The radiation dose in PET/CT examinations is 15-25 mSv and is below annual limits (Demir, 2015). SPECT imaging is based on the detection of gamma photons emitted from radioactive materials by detectors and the conversion of these into cross-sectional images by a computer (Cherry, 2004). The collimator determines the spatial map of the radiation by passing only parallel photons and is made of highly interactive materials such as lead or tungsten (Smith & Webb, 2010).

In nuclear medicine, radiopharmaceuticals are molecules containing radionuclides, utilized in nuclear medicine for diagnostic and therapeutic purposes. Diagnostic applications involve gamma-emitting substances, while therapeutic uses involve beta-emitting materials. These agents allow for the examination of physiological changes, facilitating the early diagnosis of diseases and enhancing treatment efficacy. They are used safely and extensively worldwide (Gündoğdu et al., 2018).

4. Conclusion

The side effects of ionizing radiation vary depending on the

amount and duration of exposure. While fatigue, weakness and moderate effects on the central nervous system may be observed in the short term, there may be an increased risk of cancer in the long term. Therefore, effective use of dosimeters and correct application of protective equipment are of great importance (ICRP, 2007). Radiation therapy is used not only in the treatment of cancer, but also in the treatment of thyroid diseases, cardiovascular disorders, etc. Radioactive iodine applications, in particular, are a highly effective method in the treatment of hyperthyroidism and thyroid disorders (Cooper et al., 2009). It is anticipated that the areas of use of ionizing radiation will expand further thanks to developing technologies. High-sensitivity radiotherapy methods such as proton therapy and carbon ion therapy may provide revolutionary advances in cancer treatment. In addition, studies on the potential use of radiation in the fields of nanotechnology and gene therapy are rapidly continuing. Charged particle therapy provides high local control with selective energy deposition of tumors, while causing less damage to healthy tissues, reducing the risk of complications and offering rapid healing. It is advantageous for tumors close to radiosensitive tissues or in areas with difficult surgical access. However, few randomized trials have compared this method with X-rays, and the cost-benefit ratio is still controversial. Research is focused on reducing the cost and increasing the effectiveness of this treatment (Loeffler & Durante, 2013).

Ionizing radiation has an important place in the medical field. However, more research and development studies are needed to be carried out in order to use it effectively and safely. In addition, it is of great importance to strengthen legal regulations and expand training programs to minimize radiation exposure of healthcare professionals.

References

Brenner, D. J., & Hall, E. J. (2007). Computed tomography—an increasing source of radiation exposure. *New England Journal of Medicine*, 357(22), 2277-2284. https://doi.org/10.1056/NEJMra072149

Beyer T., Czernin J., Freudenberg L. S. (2011). Variations in clinical PET/CT operations: results of an international survey of active PET/CT users. Journal of Nuclear Medicine, 52, 303–310.

Boone, J. M., & Hendee, W. R. (2019). Radiation dose and image quality in CT: How to balance risk and benefit. *Radiology, 293*(3), 632-640. https://doi.org/10.1148/radiol.2020192036

Cherry, S. R. (2004). In vivo molecular and genomic imaging: new challenges for imaging physics. *Physics in Medicine & Biology*, *49*(3), R13.

Cho, Y. H., Kim, S. Y., Woo, H. D., Kim, Y. J., Ha, S. W., & Chung, H. W. (2015). Delayed numerical chromosome aberrations in human fibroblasts by low dose of radiation. *International journal of environmental research and public health*, *12*(12), 15162-15172.

Cooper, D. S., Doherty, G. M., Haugen, B. R., Kloos, R. T., Lee, S. L., Mandel, S. J., ... & Sherman, S. I. (2009). Revised American Thyroid Association management guidelines for patients with thyroid nodules and differentiated thyroid cancer. *Thyroid*, 19(11), 1167-1214. https://doi.org/10.1089/thy.2009.0110

Dance, D. R., Young, K. C., & van Engen, R. E. (2011). Estimation of mean glandular dose for breast tomosynthesis: factors for use with the UK, European and IAEA breast dosimetry protocols.

Physics in Medicine & Biology, 56(2), 453-471. https://doi.org/10.1088/0031-9155/56/2/012

Delaney, G., Jacob, S., Featherstone, C., & Barton, M. (2005). The role of radiotherapy in cancer treatment: Estimating optimal utilization from a review of evidence-based clinical guidelines. *Cancer*, 104(6), 1129-1137. https://doi.org/10.1002/cncr.21324

Delbeke D. (1999). Oncological application of FDG PET imaging. Journal of Nuclear Medicine, 1706-15.

Demir, M. (2015). POSITRON EMISSION TOMOGRAPHY (PET) PHYSICS. Bulletin of Thoracic Surgery/Toraks Cerrahisi Bülteni, 6(2).

Dhawan, A. P. (2011). Medical image analysis. John Wiley & Sons.

Gündoğdu, E.A, Özgenç, E., Ekinci, M., İlem Özdemir, D., Aşıkoğlu, M. Radiopharmaceuticals Used in Imaging and Treatment in Nuclear Medicine. *Journal of Literature Pharmacy Sciences 2018, 7(1).*

Gürsoy, G. (2013). Determination of the effect of carbon fiber table on dose distribution for high energy photon beams used in radiotherapy (Master's thesis, Institute of Science).

Hall, E. J., & Giaccia, A. J. (2012). *Radiobiology for the radiologist*. Lippincott Williams & Wilkins.

Hamada, N. (2024). *Cancer and Non-Cancer Effects Following Ionizing Irradiation. Cancers 2024, 16, 1141*.

Hobbie, R. K., & Roth, B. J. (2015). Medical uses of X-rays. In *Intermediate Physics for Medicine and Biology* (pp. 461–502). Springer. https://doi.org/10.1007/978-3-319-12682-1_16

Hogg, P., Kelly, J., & Mercer, C. (2015). Digital Mammography. Springer.

ICRP (2007). The 2007 Recommendations of the International Commission on Radiological Protection. *Annals of the ICRP*, 37(2-4), 1-332. https://doi.org/10.1016/j.icrp.2007.10.001

Joiner, M. C., & van der Kogel, A. (2016). *Basic clinical radiobiology*. CRC press.

Kalender, W. A. (2011). *Computed tomography: fundamentals, system technology, image quality, applications*. John Wiley & Sons.

Karlsson, M., & Zackrisson, B. (1997). Exploration of new treatment modalities offered by high energy (up to 50 MeV) electrons and photons. *Radiotherapy and oncology*, *43*(3), 303-309.

Lecomte, R. (2009). Novel detector technology for clinical PET. *European Journal of Nuclear Medicine and Molecular Imaging*, 36(Suppl 1), S69–S85. https://doi.org/10.1007/s00259-008-1054-0.

Lindquist, C. (1995, July). Gamma knife radiosurgery. In *Seminars in radiation oncology* (Vol. 5, No. 3, pp. 197-202). WB Saunders.

Loeffler, J. S., & Durante, M. (2013). Charged particle therapy—optimization, challenges and future directions. *Nature*

Reviews Clinical Oncology, 10(7), 411-424. https://doi.org/10.1038/nrclinonc.2013.79

Ministry of National Education. (2012). Radiotherapy application plan. Vocational and Technical Education Programs (MEGEP). Retrieved from https://megep.meb.gov.tr

Özdemir, F. B. (2006). Afyon ve çevresindeki kuyu sularında Radon (RN-222) aktivitesi tayini [Master's thesis, Afyon Kocatepe Üniversitesi].

Özdemir, T. (2011). *Simulation, modelling and analysis processes in silicon detectors* [Doctoral dissertation, Süleyman Demirel University].

Özdemir, F. B. (2016). *The Being Carrying Out of Data Collection, Analysis and Simulation Studies in the Construction Steps of Multi-Channel Silicon Radiation Detector* [Doctoral dissertation, Süleyman Demirel University].

Samei, E., & Peck, D. J. (2019). *Hendee's Physics of Medical Imaging*. John Wiley & Sons.

Sechopoulos, I. (2013). A review of breast tomosynthesis. Part I. The image acquisition process. *Medical Physics, 40*(1), 014301. https://doi.org/10.1118/1.4770279

Seeram, E. (2023). Computed Tomography: Basic Physics and Technology. In *X-Ray Imaging Systems for Biomedical Engineering Technology: An Essential Guide* (pp. 77-105). Cham: Springer International Publishing.

Smith, N. B., & Webb, A. (2010). Introduction to medical imaging: physics, engineering and clinical applications. Cambridge university press.

Şahin, A., Tunç, S., Kaynak, Z. G., & Özkan, L. (2016). Comparison of Dosimetric Properties of Physical and Virtual Wedge Filters in High Energy Photons. Uludağ University Faculty of Medicine Journal, 42(1), 1-7.

Wang, L. H., McKenzie-Brown, A. M., & Hord, A. (2006). The Handbook of C-Arm Fluoroscopy-Guided Spinal Injections. CRC Press.

Yaffe, M. J., & Mainprize, J. G. (2011). Risk of radiation-induced breast cancer from mammographic screening. *Radiology, 258*(1), 98-105. https://doi.org/10.1148/radiol.10100655

CHAPTER VII

Chemically Produced SnS and Metal Doped SnS Thin Films; Synthesis, Characterization and Photocatalytic Applications

Sultan GÖKTAŞ[1]
Gülsen ŞAHİN
Abdullah GÖKTAŞ

1. Introduction

There are rapid technological changes to meet the needs that arise with the increasing population around the world. It is essential that any material developed with these technological changes be affordable, practical and easily obtainable. Especially recent developments in the field of energy requirements, space travel and environmental pollution clearly show us that new multifunctional materials need to be produced. In this context, the only field that can solve the above-mentioned problems is nanotechnology products

[1] Dr. Sultan GÖKTAŞ, Harran University, Faculty of Science and Arts, Department of Chemistry, Şanlıurfa/TURKEY, Orcid: 0009-0000-7084-9710, sultangoktas@harran.edu.tr

like thin films, nanopowder, nanowires, etc. In this section, we will focus especially on the production techniques of thin films. Thin films, which date back centuries, were unknowingly used as ornaments and decorations on different glass and ceramics. However, scientific investigations have started since the 1940s and interest in their construction technology continues until today [Sönmezoğlu, Koç, and Akın, 2012; Green, 2014].

Thin films can be defined as coating materials that are formed as a thin layer by arranging the atoms or molecules of the material to be coated on a base that helps the formation of the film on the surface, and their thickness is generally ranging from 1μm to 10 nm. Thin films, which form the basis of the micro- and nano-structured various material industry and have an important scenario in technological and scientific investigations [Göktaş, 2013]. The basic characteristics of thin film nanocrystalline materials, such as optical, mechanical, magnetic, and electrical are extraordinary compared to those of bulk materials. In these materials, more efficient properties and different behaviors can occur due to the higher surface-to-volume ratio [Pejova & Grozdanov, 2006]. In addition, in nanostructured thin films, when the crystal size or grain size of them being small enough (i.e., being at the quantum limit or being comparable to the Bohr radius) it results into the interference of the optical absorption/transmission spectra and causing the band structures to be divided into discrete energy levels [El-dosky et al., 2018; Goktas, Tumbul, & Aslan, 2019]. Currently, thin film technology is actively pioneering many innovative and modern space, aviation, computer, healthcare, military and robotic developments.

They are used in different applications, considering thin films with different characteristics used for different purposes. Thin films are frequently used in many applications such as conduction/insulation, magnetic memory, photo detectors, photocatalysts, gas detectors, optical circuits, corrosion-resistant coatings and device manufacturing due to their relatively superior and tunable structural, electrical, magnetic, photocatalytic, chemical stability and environmentally friendly properties [Ghosh, Paul & Mandal, 2024]. Recently, in parallel with the increasing needs of the growing human population around the world, rapid changes and developments in thin film materials and their usage, and also the development of new multi-functional materials as well technologies have become inevitable. Based on this, many physical and chemical methods have been developed to improve the performance, structure and physical properties of thin film materials in various applications and to observe new properties [Göktaş, 2007; Rao and Shekhawat, (2013)].

Thin film production can be cost-effective or expensive, depending on the used method. However, it is advantageous to choose some environmentally friendly and green synthesis methods. Moreover, in some methods, it is a great advantage that the film can be coated on substrates various dimensions and materials of the desired shape and that various parameters can be adjusted (e.g. thickness, composition adjustment, coating area, etc.). Therefore, films with the desired properties, functions and film quality are produced using different film production techniques and different parameters on different substrates to use different film morphologies for different purposes [Goktas, Aslan & Mutlu, 2014; Goktas, Tumbul, & Aslan, 2019]. So, this study aims to examine in detail the methods that can produce metal doped SnS thin films using chemical methods, and the effects

of the critical parameters of these methods on the structural, morphological, optical and photocatalytic properties of these films.

2. Thin Film preparation techniques for the metal doped SnS thin films

2.1. Sol-gel Technique

It is known that this technique is one of the well-known wet chemical processes, used broadly for the production of the many oxides and sulphide materials. This is mainly due to its advantages (superior homogeneity, controllable stoichiometry, great purity, phase-solid powders at a relatively lower temperature and flexibility of producing dense materials) over other techniques. In this technique, the term of "sol" denotes a colloidal suspension emergence and "gel" denotes the alteration of "sol" to dense gel or solid matter. It is possible to produce different ceramic and glass materials, which can be highly pure and spherical powders, thin film coatings ceramic fibers, microporous inorganic membranes, and monolithic by using this technique. It is also handable and practical to produce mentioned materials [Alain, 1998; Goktas, Mutlu & Kawashi, 2012; Jilani, Abdel-Wahab & Hammad, 2017].

In the sol-gel techniques, which are described below, three processes can be used (dipping, spraying and spinning) in fabricating thin films utilizing fluid sol or precursor solution gelation.

2.1.1 Dip coating process

This method is generally used to produce film layers on substrates, which have different shapes and sizes. The dip coating method is based on the following principle in which the substrate material is immersed at a certain speed and again at the same speed. The dip coating method consists of various stages as given in Fig.1. These

stages are respectively: (i) dipping, (ii) pulling up, (iii) coating, (iv) percolation and (v) evaporation. During immersion, the substrate is immersed into the sol at a constant speed perpendicular to the solution surface, after diving at the desired speed and waiting for 3-5 seconds is slowly pulled upwards. In the third stage, namely coating, a parabolic fluid layer is formed due to capillary pressure between the substrate and the sol as well gravitational force. At the end of pulling up, the excess is left while the droplets filter from the edges of the substrate and leave the surface. Sol droplets that cannot leave the surface through the filtration process evaporate and fly away. From these processes, a coated film is obtained.

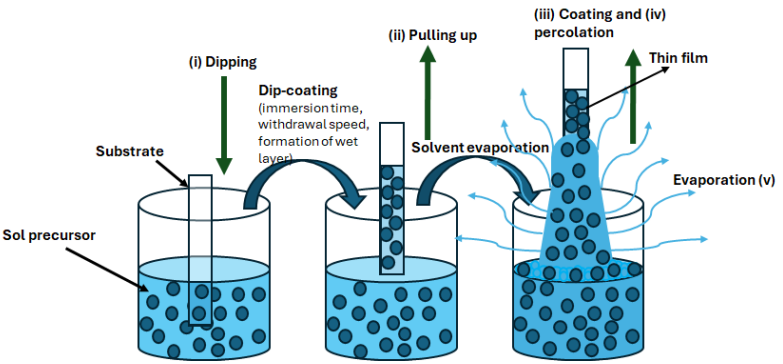

Figure 1: Schematic dip coating process

For two decades the sol-gel dip coating process has been used to prepare thin films. Several research groups have used it to prepare SnS and doped SnS thin films. For instance, Chaki et al. (2016) used sol-gel dip coating technique to produce SnS thin films. The produced thin films have orthorhombic structure with Sn_2S_3 secondary phase. The produced SnS thin films have relatively higher optical band gap (1.24 eV) due to presence of the Sn_2S_3 parasitic phase. Hall and I-V characterizations have shown that it has p-type conductivity and is convenient for the optoelectronic devices.

Recently Aslan et al. (2022) has prepared SnS thin films, derived from used different starting chemicals as given in Fig.2, by utilizing sol-gel dip coating technique. The results have shown that the produced films have orthorhombic pure SnS phase and secondary phases (SnO, SnS_2, and SnO_2) according to chemicals and Sn/S molar ratios. The presence of the secondary phases was observed in XRD and Raman analysis. The high-quality thin films were observed in thin films obtained from solution A and at molar ratio of SnS of 1/1 (see Fig.3).

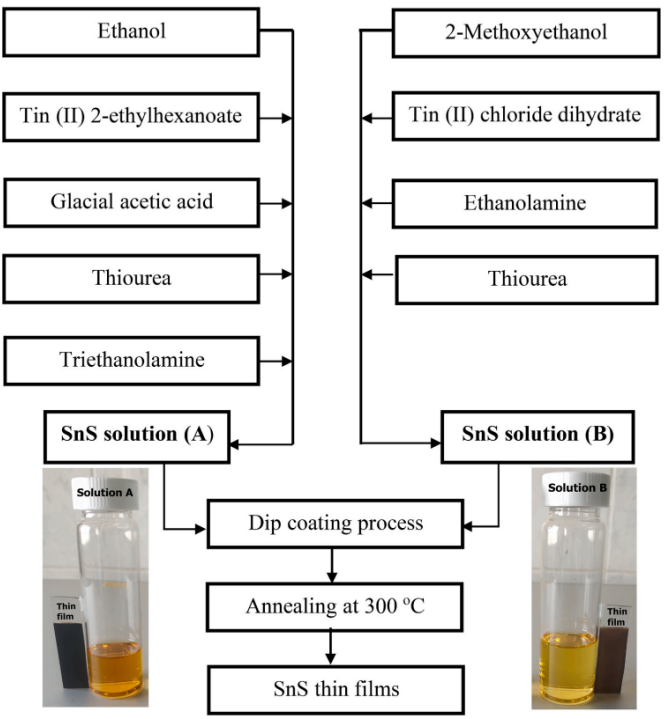

Figure 2: Follow chart of the sol-gel dip coated SnS thin films, reproduced with permission of Elsevier, Copyright (Aslan et al. 2022).

The outcomes obtained by the XRD and Raman analyses, it can be summarized that the synthesized thin films by sol-gel dip coating and using solutions from precursor B with a Sn/S molar ratio of 1/4 consists of only the SnS_2 phase.

According to UV-Vis analysis the results of the transmittance and calculated band gap (E_g) values of the SnS thin films upon on Sn/S ratios were presented in Figure 4a and b, indicating results from various solutions. As seen from these figures, the optical transmittance of thin films derived from solution A increases in the visible region as the sulfur content increases except for the Sn/S ratio of 1/(1/2). However, it decreases in the case of the films produced by solution B.

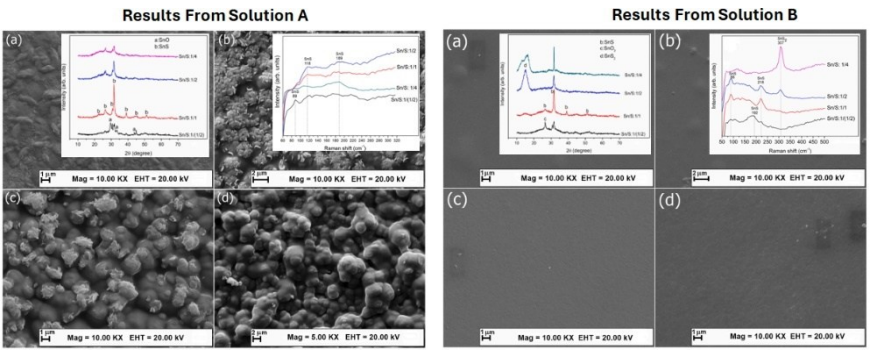

Figure 3: SEM analysis of SnS thin films prepared with precursor solution of A and B, dependent on Sn/S molar ratios of (a) 1/1/2), (b) 1/1, (c) 1/2 and (d) ¼ (inset shows XRD and Raman measurements). Reproduced with permission of Elsevier, Copyright (Aslan et al., 2022).

The optical transmittance of the two types of the films decreases significantly in the visible region representing these thin films absorb considerable light content that are important for the solar light driven optoelectronic and photocatalytic applications.

The calculated forbidden E_g of the sample with an Sn/S molar ratio of 1/(1/2) is approximately 1.95 eV. This value drops to 1.35 eV for samples with a molar ratio of 1/1 (for precursor solution A). On the other hand, the E_g of films obtained from solution B with an Sn/S molar ratio of 1/1 was obtained as 1.8 eV. When the amount of sulfur in the solution results in its maximum value, the E_g enhances by up to 2.4 eV. The samples with the higher band gaps, obtained from precursor B, are thought to belong to the SnS_2 phase. So, the content of S and secondary phases are key points for the obtained E_g values of the SnS thin films.

According to Hall effect measurement all film samples derived by precursor solution A have p-type properties and their electrical resistivity and carrier concentrations, respectively are around 10^6 Ω cm and 10^{11} cm^{-3} (see Figure 5).

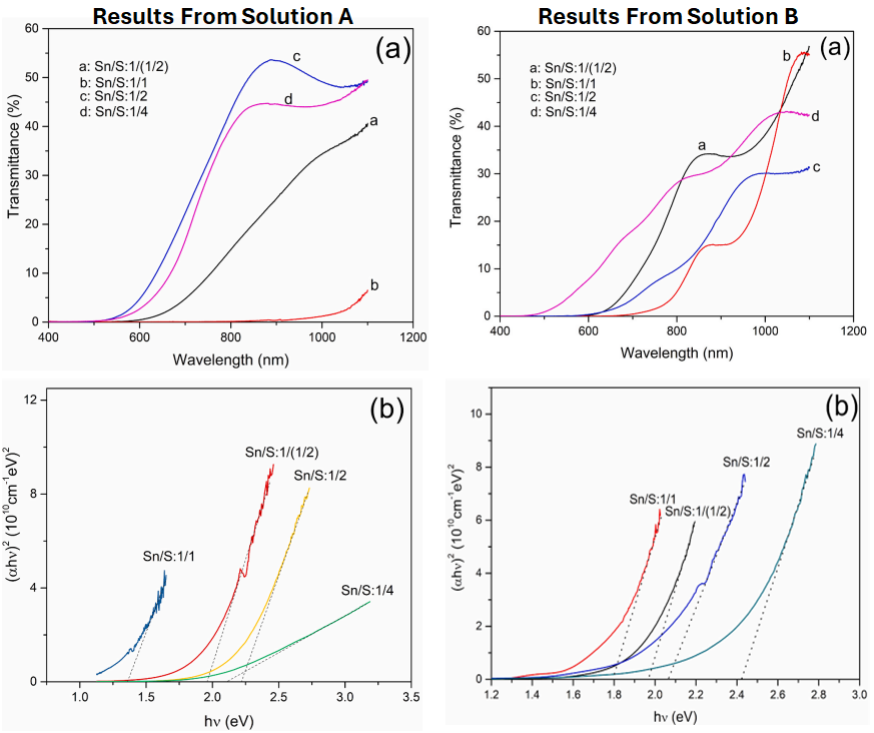

Figure 4: Optical transmittance spectrums (a) and optical band gaps (b) of the produced SnS thin films prepared with precursor solution of A and B, dependent on Sn/S molar ratios of (a) 1/1/2), (b) 1/1, (c) 1/2 and (d) ¼ (inset shows XRD and Raman measurements). Reproduced with permission of Elsevier, Copyright (Aslan et al., 2022).

On the other hand, the film samples fabricated via precursor solution B solutions with tin (II) chloride dihydrate, the p-type feature samples except for with a Sn/S ratio of 1/2 and 1/4, indicating n-type conductivity. The electrical resistivity reduces from 9.1×10^{5} Ωcm to 5.2×10^{1} Ωcm as the sulfur content in the solution increases. Nevertheless, while the sulfur amount in the solution is further

increased, resistivity enhances again. The I–V measurements of the bilayers obtained from the prepared thin films show ohmic and p-n junction behaviors. Amongst all, the best p-n junction behaviors were observed as shown in Figure 5.

Precursor	Sn/S molar ratio in solution	Resistivity (Ωcm)	Carrier concentration (cm^{-3})	Conductivity type
Precursor A	1/(1/2)	1.4×10^{6}	2.6×10^{11}	p
Precursor A	1/1	5.3×10^{6}	8.1×10^{10}	P
Precursor A	1/2	2.5×10^{6}	1.4×10^{12}	p
Precursor A	1/4	2.8×10^{6}	5.8×10^{11}	p
Precursor B	1/(1/2)	9.1×10^{5}	2.5×10^{11}	p
Precursor B	1/1	1.1×10^{5}	8.0×10^{11}	p
Precursor B	1/2	5.2×10^{1}	1.9×10^{14}	n
Precursor B	1/4	8.8×10^{1}	2.3×10^{12}	n

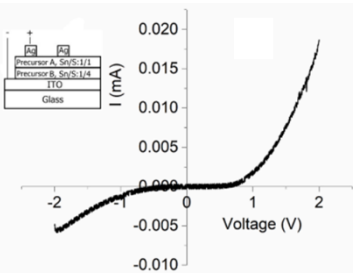

Figure 5: Hall measurement results and I–V characteristics of prepared bilayers prepared by Solution A (Sn/S: 1/1) and B (Sn/S: 1/4). Reproduced with permission of Elsevier, Copyright (Aslan et al., 2022).

The Zn-substituted SnS thin film derived by sol-gel dip coating as schematically presented in Figure 6 [Goktas et al., 2022] is another good example for aim of the presented study and especially about optoelectronic and photocatalytic applications. In mentioned study, Zn-substituted SnS thin films ($Sn_{1-x}Zn_xS$) were produced for different Zn substitution levels (x = 0.00–0.20). The structural analyses (XRD and Raman) showed that the produced films had orthorhombic of SnS crystalline, and the crystallization degree was highest for the 1 % Zn substitution level (see Figure 7a-c). The same trend was also observed in SEM analysis. The presence and the contents of the Zn^{2+}, Sn^{2+}, and S^{2-} were proved by EDX and XPS analyses (see Figure 7d-e).

According to the UV-Vis and photoluminescence (PL) measurements the transmittance, absorbance, reflectance and PL of

the $Sn_{1-x}Zn_xS$ were given in Figure 8a-d, respectively. It is obvious that among the 1 at. % Zn substituted SnS thin film has the highest transmittance and PL intensity whereas it shows lowest absorbance and reflectivity indicating best crystalline quality as confirmed in XRD and SEM analysis.

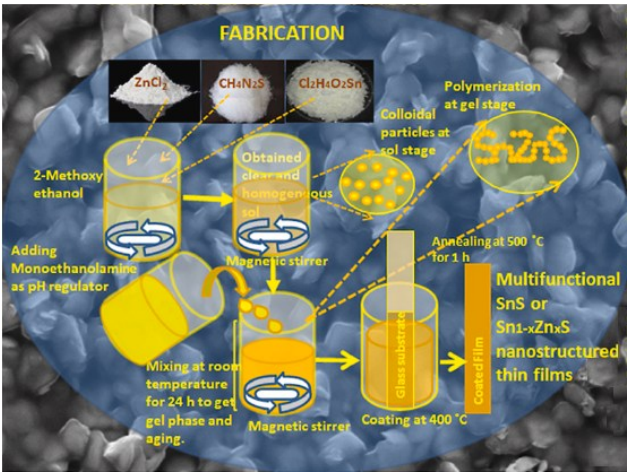

Figure 6: Scheme of the $Sn_{1-x}Zn_xS$ thin films procedure using sol-gel dip coating. Reproduced with permission of Elsevier, Copyright (Goktas et al., 2022).

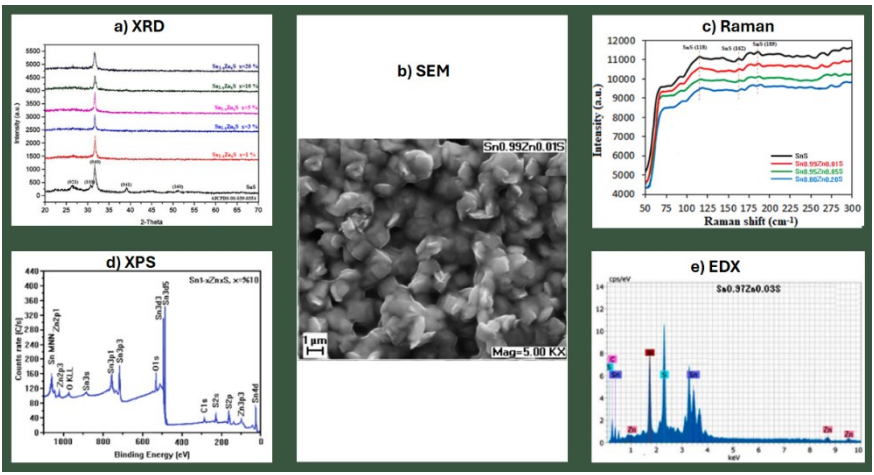

Figure 7:(a) XRD, (b) SEM, (c)Raman, (d) XPS, and (e) EDX analyses of the $Sn_{1-x}Zn_xS$ thin films. Reproduced with permission of Elsevier, Copyright (Goktas et al., 2022).

The hall measurements showed that the $Sn_{1-x}Zn_xS$ thin films had p-type conductivity. Amongst all Zn-substituted SnS thin films, the 1 at. % Zn substituted SnS thin showed the lowest resistivity, whereas highest mobility and carrier concentration.

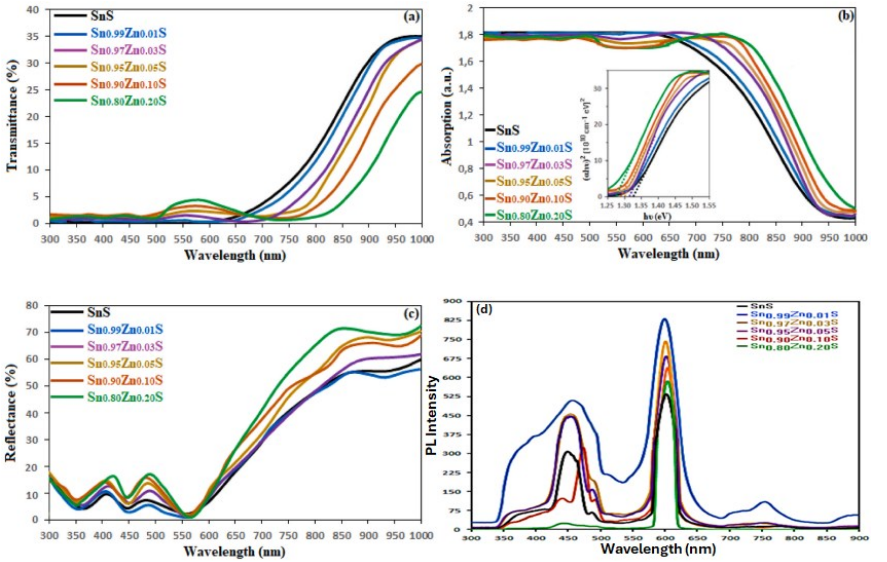

Figure 8:(a)Transmittance, (b)absorbance, (c)reflectance, and (d) PL spectra of the $Sn_{1-x}Zn_xS$ thin films. Reproduced with permission of Elsevier, Copyright (Goktas et al., 2022).

The same trend was observed in the photosensitivity applications; It had the highest photosensitivity (225 at. %).

In the same study the photocatalytic action of SnS and Zn substituted SnS nanostructured thin films were tested for the photo-degradation of MB under UV and solar lights. In addition, the role of pH on photocatalytic efficiency under UV radiation was also scrutinized. The results of the photocatalytic tests have indicated that the pH and used light type are key parameters to get highest photocatalytic efficacy (η) within a short time. The 1 at. % Zn substituted SnS thin exhibited the highest η values of 90 (at pH=11) in 210 min and 100 (at pH=11) for 25 min for the used radiation sources of UV light and sunlight, respectively (see Figure 9). The observed outcomes have been attributed to the followings; (i) the highest crystallinity, (ii)

synergistic effect of pH, (iii) active surface area, (iv) relatively low Sn vacancies (v) light absorption sites, and (vi) the reflectivity capacitance of samples.

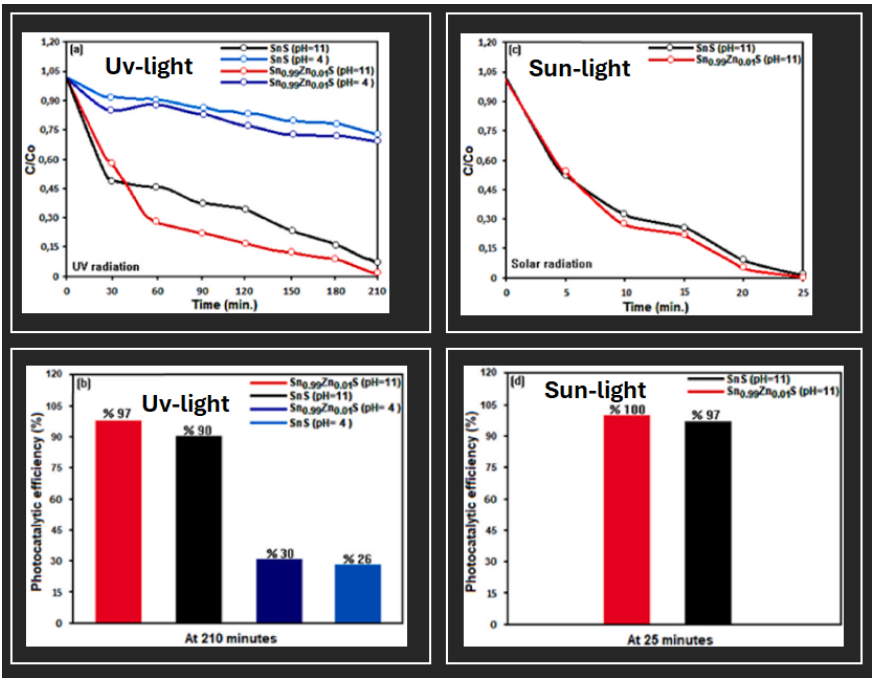

Figure 9: (a)Transmittance, (b)absorbance, (c)reflectance, and (d) PL spectra of the $Sn_{1-x}Zn_xS$ thin films. Reproduced with permission of Elsevier, Copyright (Goktas et al., 2022).

2.1.1 Successive Ionic Layer Adsorption and Reaction (SILAR) technique

SILAR deposition technique consists of main three reactions like the adsorption and reaction of ions that are anions and cations from solutions and the rinsing process, which use the deionized water to avoid precipitation in the solution [Soomin, 2022]. This technique involves four main paces such as adsorption, where the cation

adsorbs on the substrate facet, the first rinsing with water in which the excess adsorbed ions are rinsed off, the reaction process, which introduces the anionic ion into the system, and the second rinsing where the unreacted species and excess ions are pulled out (see Figure 10).

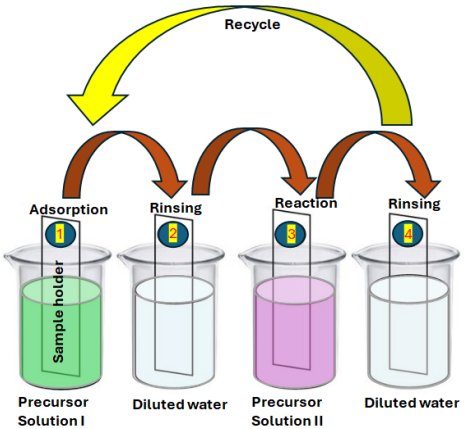

Figure 10:The film deposition process of SILAR method

The creation of thin films on the sample holder and regulating their thickness can be noticed via replicating above mentioned rounds. The several parameters can affect its event such as number of cycles during immersion, complexing agents, rinse times, concentrations of the precursor solutions, pH, viscosity, immersion times, and the nature of the used precursors. In addition, the SILAR is one of the simplest techniques in terms of better flexibility of substrate selection, large area fabrication capability, stable and adhesive film deposition, low processing temperature for film fabrication, and repeatability. This technique is very economic as it does not require any complicated equipment. The advantages of the SILAR method are as followed as; (i) including a large area deposition, (ii) could be performed by any substrate relatively lower at lower temperatures

utilizing simple process and inexpensive tools (iii), the molar ratio of the constituents, the film thickness, film morphology, and particle size can be simply regulated (iv), it is possible to save cost for the used materials and technique; (v) no need to vacuum conditions, (vi) there is perfect growth rate, and (vii) no precipitate in the container after reaction completed [Soonmin, 2022]. Moreover, the structural, optical and electrical properties of the produced SnS based thin films as well as the photocatalytic applications could be affected above mentioned parameters, which are active in SILAR technique as detailed above. This section will discuss the recent advances in synthesis, characterization and photocatalytic properties of SnS or metal-doped SnS thin films by SILAR. It will explain the important factors affecting photocatalytic efficiency of the mentioned films.

SILAR-deposited SnS thin films was successfully fabricated by Aparna et al. [Aparna, Reshma & Meril, 2024]. The deposition of the film samples was schematically sketched in Figure 11.

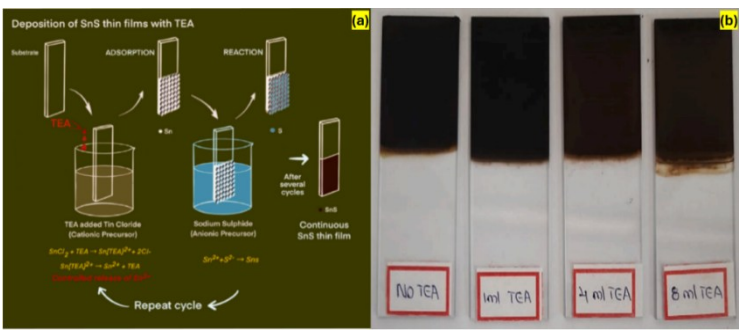

Figure 11: (a) Schematic representation of the deposition of SnS thin films by SILAR and (b) The Images of SILAR deposited SnS thin films having different amounts of complexing agent (TEA). Reproduced with permission of Elsevier, Copyright (Aparna et al., 2024-I).

The produced films were characterized by XRD, SEM, EDX, XPS, TGA, and Uv-Vis spectrophotometer. From the analysis it was observed that the SnS thin films are polycrystalline in nature with an orthorhombic crystal structure (Figure 12a). The surface morphology of the films was changed by amount of the triethylamine (TEA) and the grains had nanorod shapes (Figure 12b). The EDX (Figure 12b) and XPS (Figure 12b) analysis confirmed that the produced films really had Sn/Sn^{2+} and S/S^{2-} atoms or ions in their structures. TGA analysis showed that the films were thermally stable up to 280 ºC.

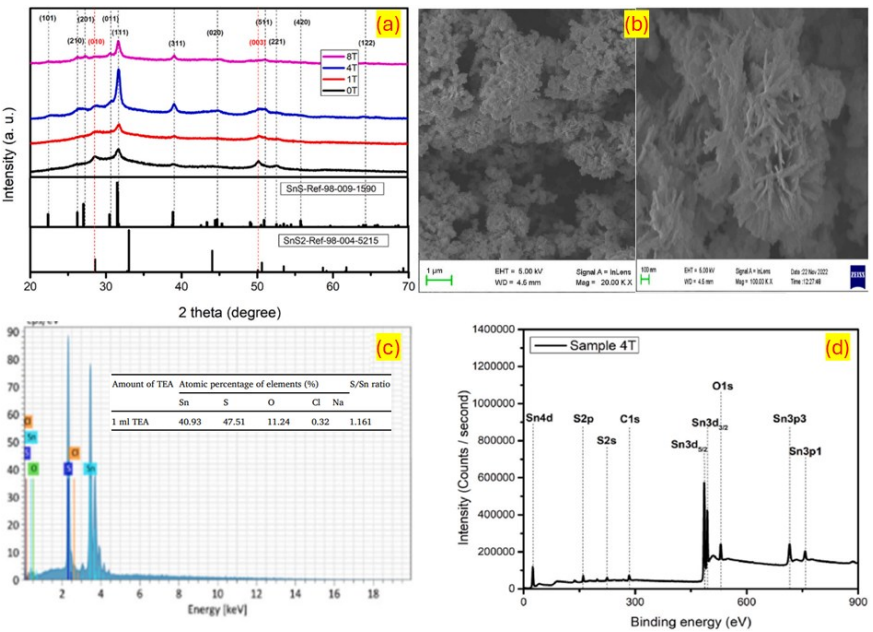

Figure 12: (a) XRD, (b) SEM , (c)EDX, and (d) XPS analysis of the deposition of SnS thin films with 1T by SILAR. Reproduced with permission of Elsevier, Copyright (Aparna et al., 2024-I).

In addition, the optical band gap values were decreased from 2.24 to 1.58 eV while the absorbance intensity was increased as the amount of the used TEA increased (Figure 13a and b). Moreover, the photodegradation of the MB dye with irradiation time under the action of SnS thin film photocatalyst was successfully performed. In 90 min nearly 95 at. % of the MB was degraded as seen in Figure 14a. According to the fluctuation of (C/C_0) with irradiation period for all samples in Figure 14b, the film sample having a higher concentration of TEA (T8) indicated better photocatalytic activity. Similarly, as seen in Figure 14c, the highest rate constant (0.038 min^{-1}) was obtained for the same sample.

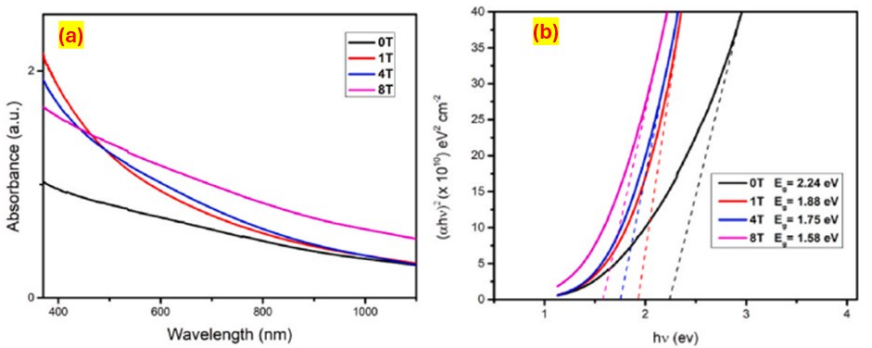

Figure 13: (a) Absorbance and (d) Tauc plot of SnS thin flms. Reproduced with permission of Elsevier, Copyright (Aparna et al., 2024-I).

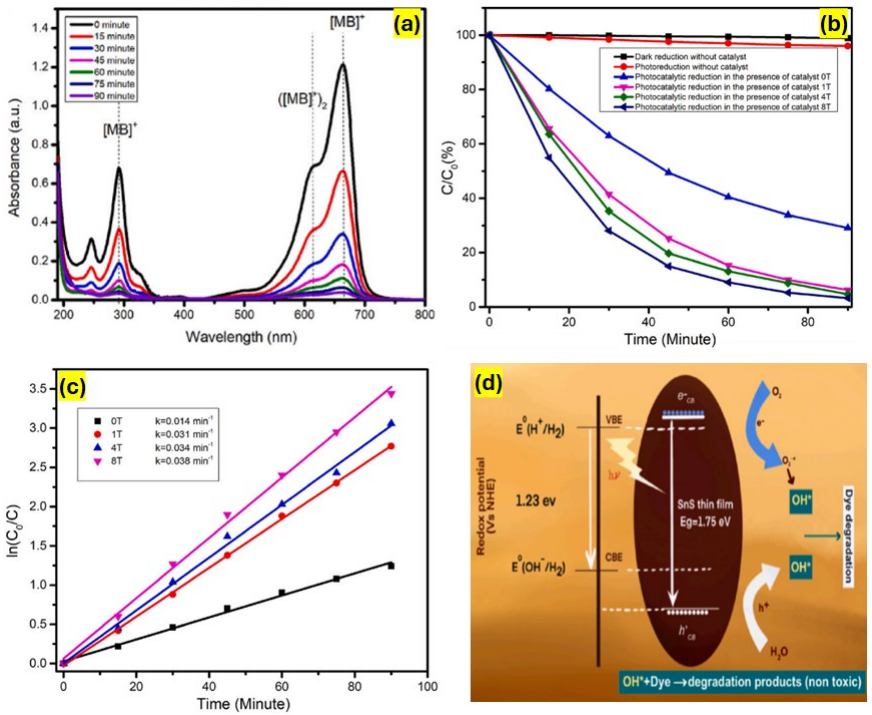

Figure 14: (a) Time-dependent absorption spectra of the aqueous solution of MB, utilizing SnS thin films (b) C/Co, (c) degradation kinetics of MB dye, and (d) a schematic illustration of the dye degradation mechanism of the SILAR deposited SnS thin films. Reproduced with permission of Elsevier, Copyright (Aparna et al., 2024-I).

The relatively highest photocatalytic activity of the T8 sample is attributed to the synergic effects of the decreased band gap, reduced EHP recombination, increased crystallinity, and higher separation between photo generated electrons and holes because of the enhanced TEA concentration. Figure 14d shows the schematic

illustration of the mechanism for the photocatalytic degradation of dye under visible light irradiation.

In another study of the on SnS thin films derived by modified SILAR method (see Figure 15 for preparation steps schematically), dark catalytic properties of the SnS thin films have been investigated [Aparna, Reshma & Meril, 2024]. In this study the using the different Sn molar ratios of 0.035, 0.04, 0.045, and 0.05 M were named C.035, C.04, C.045, and C.05, respectively.

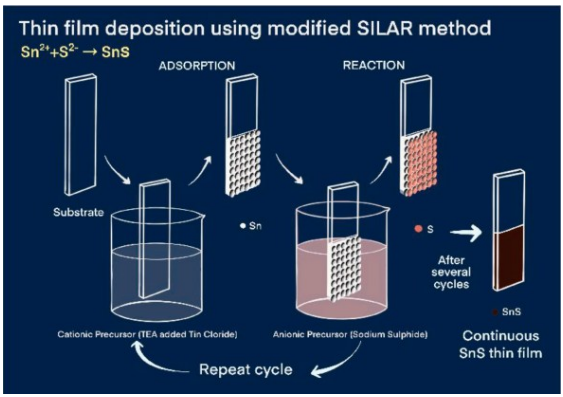

Figure 15: (a) Schematic representation of the deposition of SnS thin films by modified SILAR method. Reproduced with permission of Elsevier, Copyright (Aparna et al., 2024-II).

The fabricated films have herzenbergate-SnS with an orthorhombic crystal structure and preferred orientation along the (111) crystal plane according to XRD analysis (see Figure 16a). These film compositions are composed of the Sn, S, Cl and O atoms according to the EDX analysis as seen in Figure 16b. Similar results were also observed in XPS analysis as depicted in Figure 16c. In addition, these films facet morphology resemble to nano-flakes that provide

sufficient surface coverage, and they were extremely adherent without clear pinholes or breaks (Figure 16d).

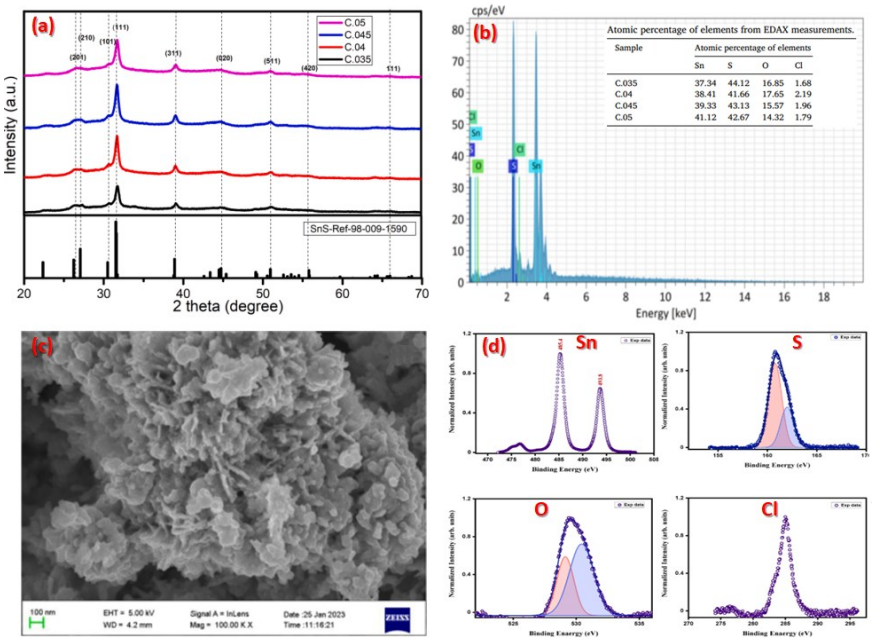

Figure 16: (a) XRD, (b) FESEM, (c)EDX, and (d) XPS analysis of the deposition of SnS thin films with by modified SILAR technique. Reproduced with permission of Elsevier, Copyright (Aparna et al., 2024-II).

The optical analysis including the absorption spectra of the thin film samples indicated good absorption in the visible region (see Figure 17a). Using this absorbance data, the optical bandgap of the thin film was tabulated utilizing the Tauc relation. The tabulated results showed that The deposited SnS thin films had a higher bandgap value than the bulk tin sulfide (1.43 eV) as seen in Figure 17b.

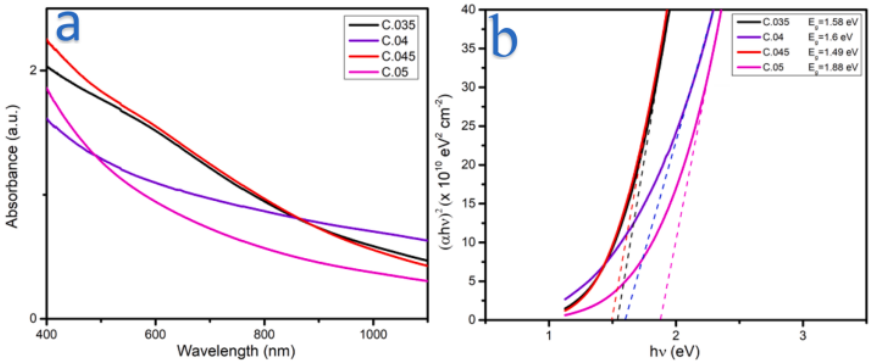

Figure 17: (a) Absorbance and (d) Tauc plot of SnS thin films. Reproduced with permission of Elsevier, Copyright (Aparna et al., 2024-II).

Moreover, the photodegradation of the MB dye with irradiation time under the action of SnS dark photocatalyst was prosperously carried out. Nearly 95 at. % of the MB was degraded in 90 min without using any light source as can be seen in Figure 18a. According to the fluctuation of the C/C_0 with irradiation period for all samples in Figure 18b, the film sample of C. 035 exhibited better photocatalytic activity and relatively higher C/C_0 variation. Similarly, as seen in inset of the Figure 18b, the highest rate constant (0.096 min^{-1}) was obtained for the same sample.

Figure 18c shows the deterioration plots of MB with and without a scavenger. Compared to MB solutions without scavengers, isopropanol-containing MB solutions had a reduced degradation profile due to reducing of hydroxyl radicals in the existence of scavengers. The stability and reusability of the presented dark photocatalyst were confirmed by five successive tests, the catalyst proved to be quite effective (Figure 18d). Even after five uses, the efficacy was only deteriorating by 3.5 %.

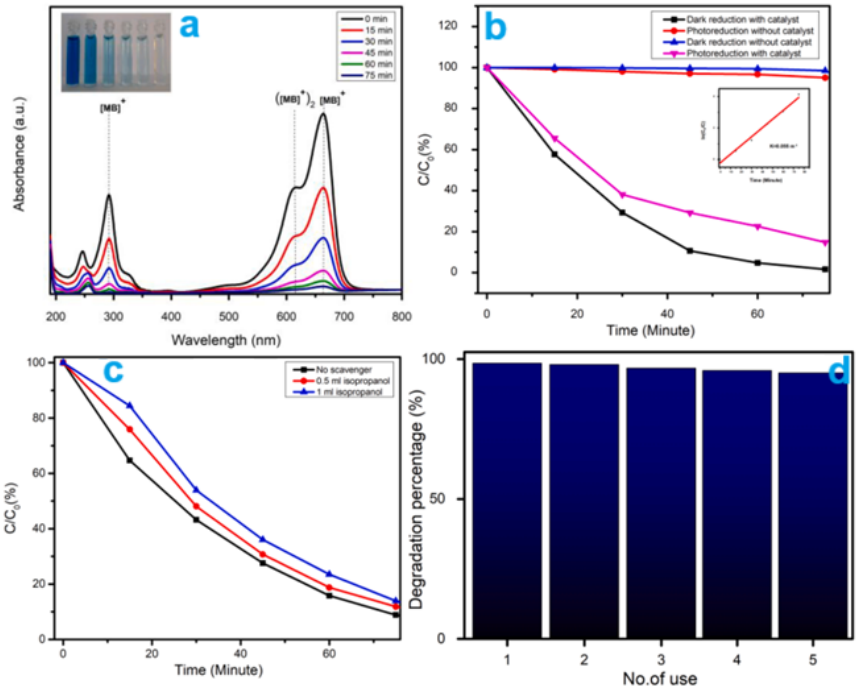

Figure 18: (a) Time-dependent adsorption spectra of MB dye solution under dark in the presence of catalyst C.035. The inset is the image demonstrating the decolorization of MB dye following each 15 min of catalytic activity, (b) Dark catalytic degradation of MB dye by SnS thin film catalyst. The inset shows kinetic plot of dye degradation, (c) Degradation of MB in the presence of hydroxyl radical scavenger, and (d) reusability of catalyst over five successive experimental runs. Reproduced with permission of Elsevier, Copyright (Aparna et al., 2024-II).

The catalytic efficiency of dark catalyst SnS thin films was also tested against for two more major commercial dyes: rhodamine B (RhB) and methyl orange (MO). Thirty percent of the RhB dye degrades in 30 min, and 90 % degrades in 120 min (Figure 19a),

whereas 87 % of the MO degraded (Figure 19b) under dark ambient conditions. Rather than these it was observed that there had been huge impact of the stirring on the degradation of the dyes as could be seen in Figure 19c.

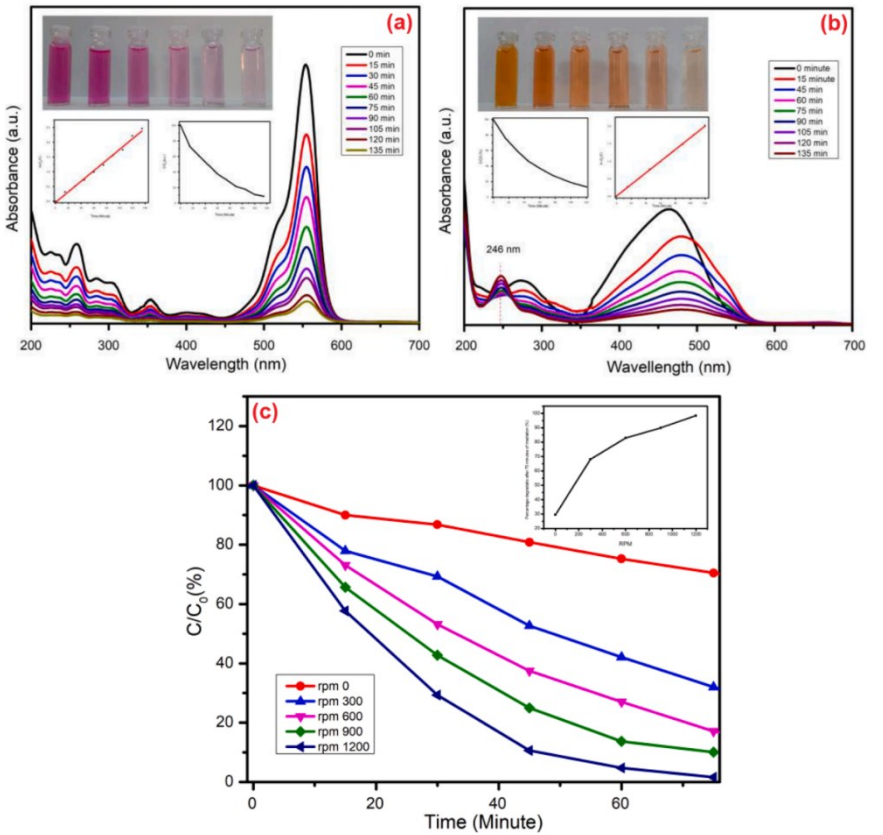

Figure 19: Time-dependent adsorption spectra of (a) RhB and (b) MO dyes solution under dark in the presence of catalyst C.035. The inset shows kinetic plot of dyes degradation, (c) Variation in the dark catalytic degradation efficiency with magnetic stirring. The inset shows the percentage degradation after 75 min of dark

catalytic reaction. Reproduced with permission of Elsevier, Copyright (Aparna et al., 2024-II).

It is well known that several factors and key parameters play huge rules in photocatalysis such as band gap, defects, active surface area, crystallinity, dosage of the photocatalysts and the pH, concentration heating, stirring rate of organic dyes as well as used light sources and powers [Goktas 2023; Goktas 2024]. The impact of these parameters and factors were clearly observed in doped and undoped SnS thin films as mentioned above. The chemical reactions for the photocatalysis of the SnS or doped SnS thin films can be followings;

$$\text{SnS/doped SnS} + \text{UV/Solar radiation} \rightarrow \text{SnS/doped SnS } (h^+) \quad (1)$$

$$\text{SnS/doped SnS } (e^-) + (O_2) \rightarrow (*O^{2-}) \quad (2)$$

$$(*O_2^-) + H_2O \rightarrow *HO_2 + OH \quad (3)$$

$$\text{SnS/doped SnS } (h^+) + (OH^-) \rightarrow *OH \quad (4)$$

$$*OH + \text{MB/RhB/MO} \rightarrow CO_2 + H_2O \quad (5)$$

$$h^+ + \text{MB/RhB/MO} \rightarrow CO_2 + H_2O \quad (6)$$

When the solution bath containing any organic dye (MB, RhB, and MO) and SnS or doped SnS photocatalysts are exposed to UV/Solar light the photoinduced electrons (e^-) derive from the conduction band (C_B) of SnS or doped SnS photocatalyst films are absorbed by circulated oxygen within the H_2O to create superoxide radicals ($*O_2^-$) as given in the reaction number of (1) and (2). The created ($*O_2^-$) further interact with H_2O molecules and brings about hydroxyl radicals ($*OH$). The correlative interactions through the case process are demonstrated in the equations (3) to (4). Conversely, the holes (h^+) created by valance band (V_B) of the SnS or doped SnS underneath UV/Solar emission are transferred to the V_B of SnS or doped SnS thin films, resulting in generation of the

(∗OH) also. The interaction held during this process was presented in equation (4). The resolved O_2 and negatively charged (∗OH) inside the water interacts as e^- and h^+ forager in under the action of e^--h^+ setting apart. Furthermore, at high value of pH=11, it is expected to have higher OH^- ions concentration than that of pH = 4, acting like hydroxyl radical [Goktas, Aslan, Arslan & Kilic, 2022]. The presence of the high content (∗OH) easily oxidize organic dyes exist inside the organic dye solution (equation (3) bath as well as the high oxidative potential of the h^+, coming from SnS/doped SnS catalysts results in direct combustion of organic dyes (see equation (4)). At the end of these reactions the organic dyes will be degraded, and H_2O and CO_2 will be created according to equations 5 and 6. According to the above-mentioned all photocatalysts as seen in Table I the highest degradation rate was observed for the sol-gel derived $Zn_{1-x}Sn_xS$ thin film photocatalyst in 25 min.

Table 1: The operational parameters and efficacy of the reviewed of doped SnS and SnS photocatalysts

Photocatalyst dosage	**Dye/ Concentration**	**Synthesis route**	**pH**	**η /Exposure time**	**Ref.**
SnS thin films/6 pieces	MB/10^{-5}M	Sol-gel	4	26 %/ 210 min	[Goktas et al., 2022]
1 % Zn substituted SnS thin films/6 pieces	MB/10^{-5}M	Sol-gel	4	30 %/210 min	[Goktas et al., 2022]
SnS thin films/6 pieces	MB/10^{-5}M	Sol-gel	11	97 %/25 min	[Goktas et al., 2022]
1 % Zn substituted SnS thin films/6 pieces	MB/10^{-5}M	Sol-gel	11	100 %/25 min	[Goktas et al., 2022]
SnS thin films/1 piece	MB/(10 mg/l)	SILAR	6.3	97 %/90 min	[Aparna et al., 2024-I]
SnS thin films/1 piece	MB/10 (mg/L)	SILAR	6.3	100%/90 min	[Aparna et al., 2024-II]
SnS thin films/1 piece	MO/10 (mg/L)	SILAR	6.3	87%/120 min	[Aparna et al., 2024-II]
SnS thin films/1 piece	RhB/10 (mg/L)	SILAR	6.3	90%/120 min	[Aparna et al., 2024-II)

As seen from Table 1, the efficacy of the various photocatalysts depends on the several parameters rather than crystallite size, defects, active surface area, and facet morphologies. These parameters known as operational parameters such pH, photocatalyst dosage, dye concentration, stirring rate of the dye solution, heating temperatures of the dye solution etc. It is obvious that the efficiency

of the Zn-substituted SnS thin films is relatively than those of others as given in Table 1. This is mainly because of the high pH value of the MB solution and used relatively higher photocatalyst dosage as compared with others.

References

Aparna N, Reshma S P, Mathew M. (2024). Tailoring the properties of SnS thin films deposited at room temperature by varying the amount of complexing agent for enhanced photocatalytic activity. *Materials Today Sustainability 27* 100941.

Aslan, F., Arslan, F., Tumbul, A. & Goktas, A. (2022). Synthesis and characterization of solution processed p-SnS and n-SnS_2 thin films: Effect of starting chemicals. *Optical Materials 127,* 112270.

Alain, P.C. (1998). Introduction to Sol--Gel Processing: The International Series in Sol-Gel Processing: Technology & Applications. (1998). New York: Kluwer Academic Publisher.

Chaki, S. H., Chaudhary, M. D. & Deshpande, M. P. (2016). SnS thin films deposited by chemical bath deposition, dip coating and SILAR techniques. *Journal of Semiconductors, 37 (5),* 053001.

El-Desoky, M. M., El-Barbary, G. A., El Refaey, D. E., & El-Tantawy, F. (2018). Optical constants and dispersion parameters of La-doped ZnS nanocrystalline films prepared by sol–gel technique. *Optik, 168*, 764-777.

Goktas, A., Aslan, F., & Mutlu, I. H. (2014). Effect of preparation technique on the selected characteristics of $Zn_{1-x}Co_xO$ nanocrystalline thin films deposited by sol–gel and magnetron sputtering. *Journal of alloys and compounds*, *615*, 765-778.

Goktas, A., Tumbul, A., & Aslan, F. (2019). A new approach to growth of chemically depositable different ZnS

nanostructures. *Journal of Sol-Gel Science and Technology*, *90*, 487-497.

Göktaş, A. (2007). Sol-Jel Metodu ile Manyetik Film Yapımı ve Karakterizasyonunun İncelenmesi. *Yüksek Lisans, Harran Ünv*.

Göktaş, A. (2013). II-IV tabanlı seyreltilmiş magnetik yarı iletken ince filmlerin yapısal, optiksel ve manyetik özelliklerinin incelenmesi/Investigation of structural, optical and magnetic properties of II-IV based diluted magnetic semiconductor thin films. *Fen Bilimleri Enstitüsü*, Şanlıurfa/Türkiye.

Goktas, A., Mutlu, I.H., Kawashi, A. (2012). Growth and characterization of $La_{1-x}A_xMnO_3$ (A=Ag and K, x=0.33) epitaxial and polycrystalline manganite thin films derived by sol–gel dip-coating technique, *Thin Solid Films, 520(19),* 6138-6144.

Göktaş, S. (2023). Metilen mavisi organik boyasının güneş ışığında katalizörsüz yıkımı. *International Conference on Engineering, Natural and Social Sciences (ICENSOS-2023)*, 4-6 April 2023, Konya, TURKEY (pp. 364–367).

Göktaş, S. (2024). Synergic effects of pH, reaction temperature, and various light sources on the photodegradation of methylene blue without photocatalyst: a relatively high degradation efficiency. *Chemistry Africa 7*, 4425–4437.

Göktaş, S., & Sahin, G. (2023). Methylene blue concentration and pH-induced photocatalytic degradation of methylene blue without photocatalyst under visible light. *International Journal of Advanced Natural Sciences and Engineering Researches*, *7*(6), 176-181.

Sahin, G., Goktas, A., & Aslan, E. (2024). A new way to tune photocatalytic activity, surface morphology, and structural/optical parameters of ZrO2 thin films using different Zr sources along with annealing temperature and film thickness. *Journal of Sol-Gel Science and Technology*, *112*(2), 425-443.

Greene, J. E. (2014). Tracing the 5000-year recorded history of inorganic thin films from 3000 BC to the early 1900s AD. *Applied Physics Review 1*, 041302.

Ghosh, M., Paul, A., Mandal, R. (2024). Comprehensive Materials Processing (Second Edition), Spain, Elsevier.

Jilani A., Abdel-Wahab, M. S., Hammad, A. H. (2017). Advance
deposition techniques for thin film and coating. *Mod Technol Creat Thin Film Syst Coat 2017(2)*. 137-149.

Sönmezoğlu, S., Koç, M., & Akın, S. (2012). Thin film production techniques. *Erciyes Üniversitesi Fen Bilimleri Enstitüsü Dergisi, 28*(5), 389-401.

Pejova, B., & Grozdanov, I. (2006). Structural and optical properties of chemically deposited thin films of quantum-sized bismuth(III) sulfide, *Materials Chemistry and Physics, 99* (1), 39-49.

Rao, M.C., Shekhawat, M. S. (2013). A brief survey on basic properties of thin films for device application. *Int J Mod Phys Conf Ser, 22*, 576-82. World Scientific.

Soonmin, H. (2022). Recent Advances in the Growth and Characterizations of SILAR-Deposited Thin Films. *Appl. Sci,12*, 8184.


BIDGE